The Progenitors of Fast Radio Bursts

Thesis by
Christopher David Bochenek

In Partial Fulfillment of the Requirements for the
Degree of
Doctor of Philosophy in Astrophysics

CALIFORNIA INSTITUTE OF TECHNOLOGY
Pasadena, California

2021
Defended May 18th, 2021

© 2021

Christopher David Bochenek
ORCID: 0000-0003-3875-9568

All rights reserved

ACKNOWLEDGEMENTS

First and foremost, I would like to thank my advisors, Shri Kulkarni and Vikram Ravi. Without their guidance and support, none of this work would have been possible. In particular, I would like to thank Shri for giving me the amazing opportunity to build a radio telescope and the proper resources to succeed. Vikram's guidance has also been invaluable.

Nobody builds an instrument on their own, and STARE2 is no exception. I would like to thank Dan McKenna, Konstantin Belov, Jonathon Kocz, Sandy Weinreb, and David Hodge for their significant contributions to STARE2 and for allowing me the privilege to learn from them. I would also like to thank everyone at the Owens Valley Radio Observatory, including James Lamb, Dave Woody, Morgan Catha, Rick Hobbs, Mark Hodges, Travis Powell, Andres Rizo, and Mike Virgin for all of their help with the project and teaching me how to build telescopes. STARE2 was fortunate to have wonderful shepherds at our sites such as Jeff Lagrange and John Matthews. I have Stephanie Petty, Ulrika Terrones, Priscilla McLean, and Bronagh Glaser the excellent administrative support STARE2 received and my knowledge of how institutions work and project management, in addition to the administrative support from Stephanie Cha-Ramos and Gita Patel.

Thank you to the Caltech astronomy graduate student community for being very welcoming and making this place feel like home for the last 5 years. In addition, thank you to everyone who played on the Cataclysmic Variables soccer team. We may not have won much, but we had a good time! Finally, thank you to my family for their support throughout graduate school.

ABSTRACT

Fast radio bursts (FRBs) are millisecond duration pulses of radio emission that are bright enough to be seen from other galaxies. The nature of the objects that produce fast radio bursts has captivated the interest of astronomers since their discovery in 2007. The durations and energetics of FRBs imply a compact, highly magnetized progenitor, making magnetars a popular progenitor candidate. However, it is difficult to pin down the progenitors of FRBs because they occur so far away. In this thesis, I will present the Survey for Transient Astronomical Radio Emission 2 (STARE2), an experiment designed to detect FRBs in the Milky Way. I will present a formalism through which to interpret the results of this experiment and demonstrate our experiment's effectiveness with the detection of a solar burst. Using STARE2, we discovered the first FRB that originated within the Milky Way, FRB 200428. This FRB was traced back to the Galactic magnetar SGR J1935+2154. The energetics, spectro-temporal properties, host galaxy, environment, and X-ray counterpart are all consistent with the properties of extragalactic FRBs. In addition, the high volumetric rate of these bright radio bursts from magnetars is consistent with the volumetric rate of FRBs, implying that magnetars are the dominant channel of FRB production. I will then develop a novel statistical technique to compare transient host galaxies in order to evaluate whether the hosts of extragalactic FRBs are consistent with a magnetar origin. I will find that the hosts of FRBs are consistent with the hosts of core-collapse supernovae, supporting the hypothesis that magnetars produce FRBs. Finally, I will present two ideas for future observing campaigns to find FRBs from M82 and more extremely bright pulses from Galactic magnetars.

PUBLISHED CONTENT AND CONTRIBUTIONS

Bochenek, Christopher D., Vikram Ravi, and Dillon Dong (Feb. 2021). "Localized Fast Radio Bursts Are Consistent with Magnetar Progenitors Formed in Core-collapse Supernovae". In: *ApJL* 907.2, L31, p. L31. DOI: 10.3847/2041-8213/abd634. arXiv: 2009.13030 [astro-ph.HE].

C.D.B. developed the technique to compare host galaxy samples, performed the analysis on the host galaxy samples, and led the writing of the manuscript.

Bochenek, C. D. et al. (Nov. 2020). "A fast radio burst associated with a Galactic magnetar". In: *Nature* 587.7832, pp. 59–62. DOI: 10.1038/s41586-020-2872-x. arXiv: 2005.10828 [astro-ph.HE].

C.D.B. developed the STARE2 concept and observing strategy, led the construction and initial deployment of STARE2, designed and built the STARE2 subsystems, commissioned and operated STARE2, performed the localisation and transient rate analyses, performed the searches for sub-threshold events and events associated with other SGR flares, and led the writing of the manuscript.

Bochenek, Christopher D., Daniel L. McKenna, et al. (Mar. 2020). "STARE2: Detecting Fast Radio Bursts in the Milky Way". In: *Publications of the Astronomical Society of the Pacific* 132.1009, 034202, p. 034202. DOI: 10.1088/1538-3873/ab63b3. arXiv: 2001.05077 [astro-ph.HE].

C.D.B. developed the STARE2 concept and observing strategy, led the construction and initial deployment of STARE2, designed and built the STARE2 subsystems, commissioned and operated STARE2, developed the formalism through which to interpret STARE2 results, performed the analysis on the solar burst, and led the writing of the manuscript.

TABLE OF CONTENTS

LIST OF ILLUSTRATIONS

LIST OF TABLES

Chapter 1

INTRODUCTION

1.1 What is a fast radio burst?

Fast radio bursts (FRBs) are stupendously bright millisecond-duration flashes of radio light of extragalactic origin. Their progenitors are unknown. The key feature of fast radio bursts is their extragalactic dispersion measure (DM). Plasma, such as the interstellar and intergalactic mediums, have a refractive index that is dependent on both the electron density of the plasma and the frequency of light that travels through it. Because of this, higher frequency light travels faster than lower frequency light in plasma, and the time delay between the arrival of the high and low frequency light at Earth is a probe of the integrated density, or column density, of electrons between the source and Earth. The DM of a source is the column density of electrons between a source and Earth. The DMs of FRBs indicate there are many times more electrons between Earth and the source than exist in the Milky Way, indicating they are extragalactic objects.

FRBs have been seen from 110 MHz–8 GHz (Pleunis et al., 2020; Gajjar et al., 2018) and FRBs have been localized to galaxies ranging from 3.6 Mpc (Bhardwaj et al., 2021) to $z = 0.66$ (V. Ravi et al., 2019). These localizations imply a wide range of isotropic-equivalent energies from $\sim 10^{25}\,\mathrm{erg\,Hz^{-1}}$ to $\sim 10^{34}\,\mathrm{erg\,Hz^{-1}}$ (Bhardwaj et al., 2021; V. Ravi et al., 2019). The event rate is $\sim$ 1600 $\mathrm{FRBs\,sky^{-1}\,day^{-1}}$ with fluences $> 2\,\mathrm{Jy\,ms}$ (S. Bhandari et al., 2018). Despite the fact that FRBs have been seen across a wide range of frequencies, they appear to be a band-limited phenomenon. Simultaneous observations of FRBs at two frequencies separated by at least 1 GHz have yet to produce a detection of the same burst at each frequency (Pearlman et al., 2020; Majid et al., 2020; P. Scholz, Cook, et al., 2020; P. Scholz, Bogdanov, et al., 2017). FRBs are highly linearly polarized, and there are several that are 100% linearly polarized.

The first FRB, known as the Lorimer burst, was discovered serendipitously during a search of archival pulsar survey data of the Small Magellanic Cloud (Lorimer et al., 2007) and is shown in Figure 1.1. However, the study of FRBs was not taken seriously until the discovery of four additional bursts by Thornton et al. (2013). Even then, serious concern about the possibility that FRBs are terrestrial persisted. At

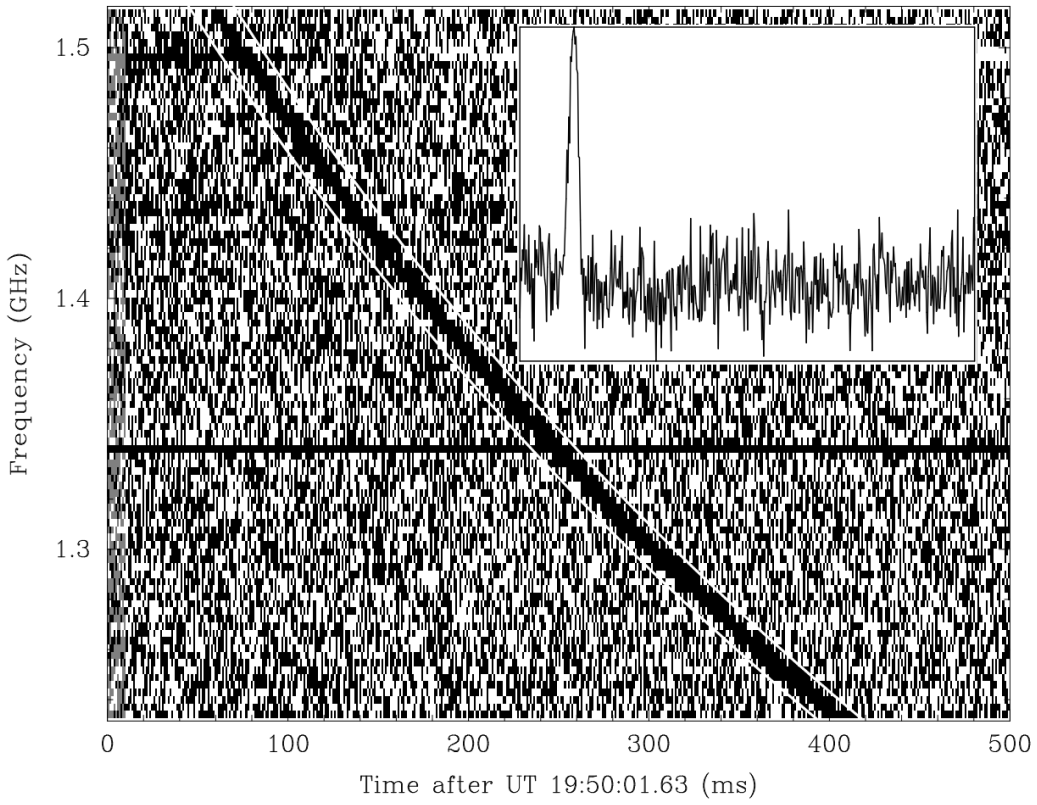

Figure 1.1: Dynamic spectrum of the fast radio burst found by Lorimer et al. (2007). The large time delay between high and low frequencies indicates that this source has an extragalactic origin. Reproduced from Lorimer et al. (2007).

this point, a similar phenomenon known as "perytons" shared many characteristics of FRBs including the extragalactic dispersion measures, but were clearly terrestrial in origin (Burke-Spolaor et al., 2011). It was not until Petroff, E. F. Keane, et al. (2015) identified that perytons are produced by the microwave oven at the Parkes Observatory and that this cannot explain the Lorimer burst that most did not doubt the extraterrestrial nature of FRBs.

Spitler et al. (2016) discovered repeat bursts from FRB 121102. Not only did this rule out cataclysmic progenitors for this source, but it enabled the localization of FRB 121102 to a star-forming metal-poor dwarf galaxy and its association with a persistent radio radio source (S. Chatterjee et al., 2017; Marcote, Paragi, et al., 2017; S. P. Tendulkar et al., 2017). In addition, FRB 121102 has an extremely high rotation measure of 10^5 rad m^{-2}, indicating a highly magnetized environment (Michilli et al., 2018). However, localizations of FRBs not known to repeat revealed massive host galaxies with at most moderate amounts of star formation, no associated persistent radio sources (K. W. Bannister et al., 2019; V. Ravi et al., 2019; J. Xavier Prochaska

et al., 2019). Furthermore, the high rotation measure of FRB 121102 appears anomalous among repeating FRBs and no non-repeating FRB has a comparable rotation measure (Petroff, Barr, et al., 2016).

Another repeating FRB, FRB 180916, was localized to a star-forming region on the outskirts of a spiral galaxy (Marcote, Nimmo, et al., 2020). Furthermore, this FRB was found to have periodic activity cycles (Chime/Frb Collaboration et al., 2020). FRBs are only found in 25% of a 16.35 day activity cycle, possibly indicating the presence of a binary (Lyutikov, Barkov, and Giannios, 2020), a precessing magnetar (Y. Levin, Beloborodov, and Bransgrove, 2020), or ultra-long period magnetar (Beniamini, Wadiasingh, and Metzger, 2020). Later, a period of approximately 160 days with a duty cycle of $\sim$ 50% was proposed for FRB 121102 (Rajwade et al., 2020; Cruces et al., 2021). It remains to be seen whether all repeating FRBs have an underlying periodicity.

There are significant challenges to uncovering more about the nature of FRBs. Despite $\sim$ 1 detectable FRB occurring every minute, it takes $\sim$ 1 month of telescope time Parkes, a 64 m dish with 13 beams, to detect an FRB. This is because there are significant challenges to building instruments with both high sensitivity and a large field of view. Furthermore, the size of the beams on large dishes are $\sim$ 10 arcmin. Within such a large beam, there are $> 10^4$ possible host galaxies, making an association impossible (Gardner and Satyapal, 2000). Without host galaxy associations, progress on the nature of FRBs is difficult, as the environments where FRBs are found hold significant clues about their origins. Although interferometers have been in operation for decades, they are typically made up of large dishes with small fields of view, making the blind detection of an FRB with an old interferometer a rare event. Thus the challenge is two-fold: a large field of view with sufficient sensitivity to detect FRBs and the power to localize FRBs to a host galaxy are required to make progress on the origins of FRBs. There have been two approaches to dealing with this challenge. The first is the development of phased-array feeds, which allows a single-dish telescope to form many different beams simultaneously. This is the approach taken by the Australian Square Kilometer Array Pathfinder (ASKAP) (Johnston et al., 2008), an array of 36 12 m dishes with a field of view of 30 $\deg^2$. The second approach is the development of interferometers with a large number of small dishes, such as the Deep Synoptic Array (Hallinan et al., 2019).

Despite the fact that over a hundred of FRBs have been found (Petroff, Barr, et al., 2016), it remains difficult to characterize the relative abundance of FRBs in

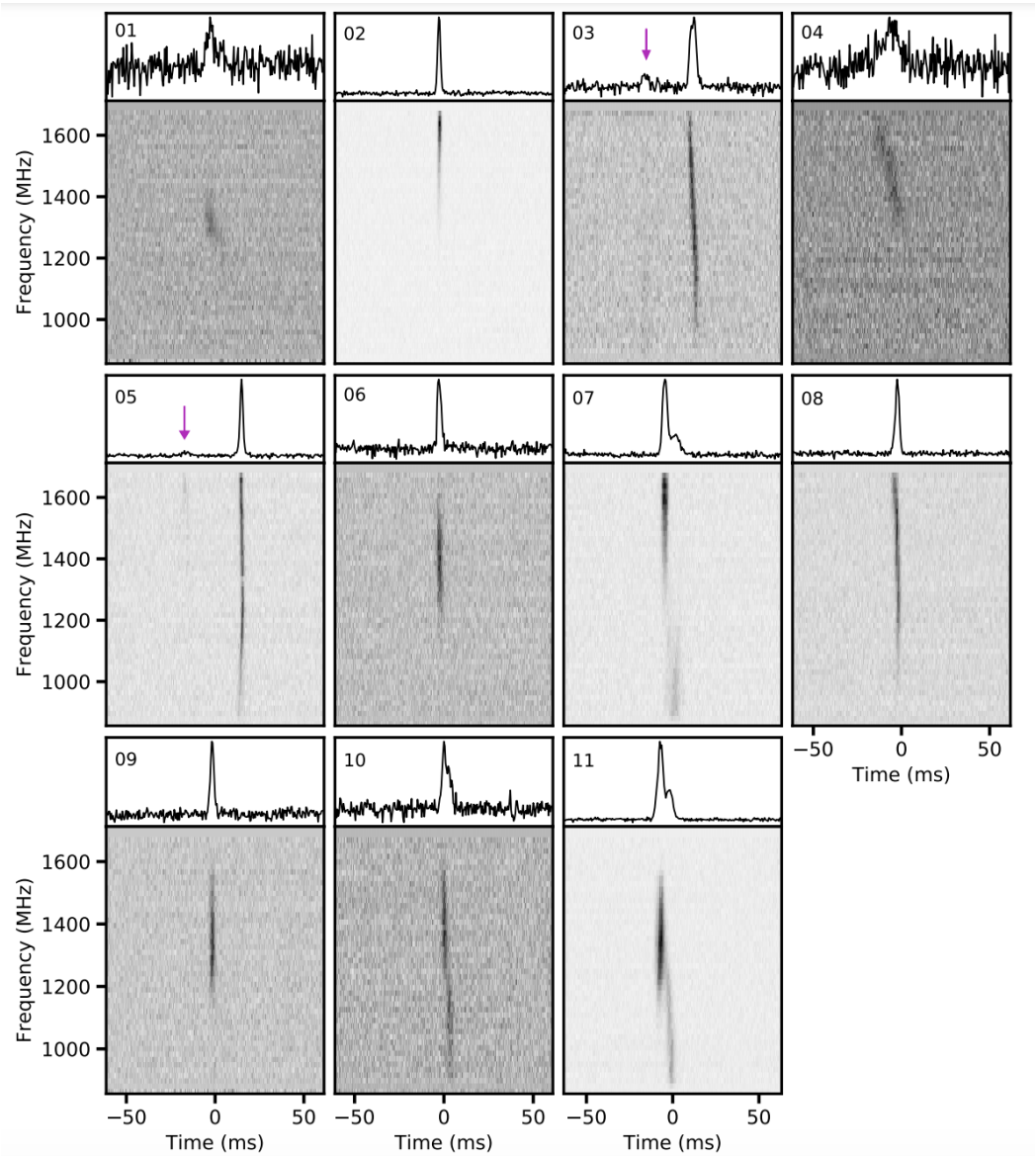

Figure 1.2: A selection of bursts from FRB 121102 detected by MeerKAT. A variety of complicated spectral features are shown. This illustrates that the shape of FRBs in frequency-time space is not always simple. Reproduced from (Caleb et al., 2020).

different parts of the fluence-duration plane. This is due to the fact that their spectra are complex (see Figure 1.2) (Hessels et al., 2019; Caleb et al., 2020), combined with complex effects from the discrete channelization of search data and dedispersion(Connor, 2019). The result of this is that we are not sensitive to FRBs with durations $<\sim 1$ ms and $>\sim 100$ ms. Furthermore, FRBs with high dispersion measures or that are significantly band-limited may also be missed.

There have been a total of 146 FRBs detected, 23 of them repeating FRBs (Petroff, Barr, et al., 2016). However, the number of FRBs is expected to dramatically increase due to their regular detection with CHIME/FRB (CHIME/FRB Collaboration, Amiri, et al., 2018).

1.2 What *is* a fast radio burst?

Up to this point, we have mainly discussed FRBs as an observational classification. However, the question remains: what produces these powerful flashes of radio waves and how? For much of FRB history, there have been more theories about what the origins of FRBs are than there were detected FRBs (Platts et al., 2019).

There are several physical constraints any FRB progenitor theory must satisfy. The first constraint is that the progenitors of FRBs must be compact sources. This is derived from the fact that the duration of FRBs is ~ 1 ms. Because the speed of light is the maximum speed information can travel at, this timescale can be used to set a size limit on the source of FRBs, shown in equation 1.1, where s is the maximum size of the FRB source, t is the duration of FRBs, and γ is the Lorentz factor of the material producing the FRB.

$$s < 300\,\mathrm{km}\frac{t}{1\,\mathrm{ms}}\gamma^2 \tag{1.1}$$

Such small spatial scales are only possible in compact objects such as black holes, neutron stars, and white dwarfs. Furthermore, the brightness temperatures of FRBs are among the brightest in the universe at $\sim 10^{34}$ K (Lorimer et al., 2007). Such high brightness temperatures are impossible for an incoherently emitting object. Beyond $\sim 10^{12}$ K, an incoherently emitting sources will inverse Compton scatter against the material in the emitting region. Therefore, the emission mechanism for FRBs must be coherent.

In addition to these physical constrains, the volumetric rate of FRBs is large. Vikram Ravi (2019b) derive that there must be $> 10^5\,\mathrm{FRBs\,Gpc^{-3}\,yr^{-1}}$. This is significant because this implies that FRBs are more common than core-collapse supernovae,

the most frequent cataclysmic event energetic enough to produce an FRB. Therefore, an FRB progenitor should be able to produce multiple FRBs in its lifespan. This is supported by the lack of FRBs associated with transients in other wavelengths (Chen, Vikram Ravi, and Lu, 2020).

Because of the fact that neutron stars are known to emit coherent radiation with similar brightness temperatures (Jessner et al., 2010), they are a favorite candidate for the progenitors of FRBs. In particular, magnetars, neutron stars with magnetic fields $> 10^{14}$ G (Victoria M. Kaspi and Beloborodov, 2017), are preferred for the large energy reservoir in their magnetic fields. The spin-down luminosity of pulsars is $< 10^{40}\,\mathrm{erg\,s^{-1}}$, significantly less than the luminosity of FRBs of $\sim 10^{42}\,\mathrm{erg\,s^{-1}}$, implying that FRBs cannot be powered from spin-down and, if they originate from neutron stars, must be powered by the neutron star's magnetic fields. Given the magnetic fields must be able to produce $\sim 10^{42}$ erg of energy and the minimum timescale of emission seen in an FRB is 4 µs (Nimmo et al., 2021), the magnetic field of the neutron star must be $> 6 \times 10^{13}$ G. Therefore, a highly magnetized neutron star would be needed to produce FRBs.

This line of reasoning makes magnetars a very appealing candidate for the origins of FRBs. However, there are many different ways that a magnetar could produce an FRB. While these models are not fully prescriptive, they do give us insight into how an FRB may be produced by a magnetar. The main distinction between different magnetar models for FRBs is whether the emission is produced inside of the magnetar's magnetosphere or outside of it. The magnetosphere of a neutron star is the area around the neutron star where its magnetic fields have influence. Its boundary is defined by the light cylinder, the radius of which corresponds to the radius at which co-rotating with the neutron star requires traveling at the speed of light. In the models where the FRB is produced outside of the magnetosphere (e. g. Metzger, Margalit, and Sironi, 2019; Beloborodov, 2017; Yu. Lyubarsky, 2014), the magnetic pressure inside of the magnetar cracks the surface of the magnetar, injecting enough energy in the magnetosphere to break its magnetic field lines, ejecting a relativistic magnetized ball of plasma, or plasmoid, in the process. This plasmoid then shocks the surrounding medium, producing an FRB through a synchrotron maser.

There are a few different of models for FRBs that are produced inside of the magnetosphere. In the model presented by Lu, Pawan Kumar, and B. Zhang (2020), seismic activity caused by magnetic pressure occurs on the surface of the magnetar

produces Alfvén waves in the magnetosphere. Once the Alfén waves on open magnetic field lines propagate to the charge-starvation radius, or the radius at which there is insufficient conductive material to effectively screen out electric fields, a strong electric field forms and accelerates the particles along these magnetic field lines, producing an FRB through curvature radiation.

In "low twist" magnetar models (e. g. Wadiasingh and Timokhin, 2019), the FRB is created on closed magnetic field lines, rather than open ones. When seismic activity caused by magnetic pressure occurs, the configuration of the magnetic field shifts, creating a gap in the magnetosphere. Since the closed magnetic field lines are more abundant than open ones, most of the energy from the seismic activity will involve closed field lines. A strong change in magnetic field, like the change produced by shifting the magnetic field of a magnetar, implies the creation of a strong electric field, unless there is sufficient conducting material present to screen it out. Initially, since there is less material in the newly formed gap in the magnetosphere, a strong electric field could be generated. However, it may be filled fast enough to prevent the growth of a strong electric field if there is sufficient current. This would imply that the magnetar's magnetic field has sufficient $|\nabla \times B|$, or twist, to quickly fill the gap. However, if the magnetic twist of a magnetar is sufficiently low, a strong electric field will be created, starting a pair-cascade and an FRB is produced through a pulsar-like emission mechanism.

1.3 We need to look for FRBs in our own galaxy.

There are three main categories of questions that FRB research aims to solve. The first concerns the progenitors of FRBs. What objects produce FRBs? What is the emission mechanism that produces the FRB? Are there multiple kinds of FRBs (e. g. repeaters and non-repeaters)?

The second category of questions revolves around using FRBs as tools. FRBs probe of ionized gas between and around galaxies, and could possibly be used as standard rulers to measure cosmological parameters. Can gas in the circumgalactic mediums (CGMs) of galaxies explain the total baryon content of the universe? How does the gas in the CGM affect the evolution of galaxies? What is the nature of gas between galaxies and what is its magnetic field?

All of these lines of inquiry require understanding of the progenitors of FRBs. To understand FRBs as probes of ionized gas and cosmology, good understanding of the contributions of different components to the dispersion measure is required. The

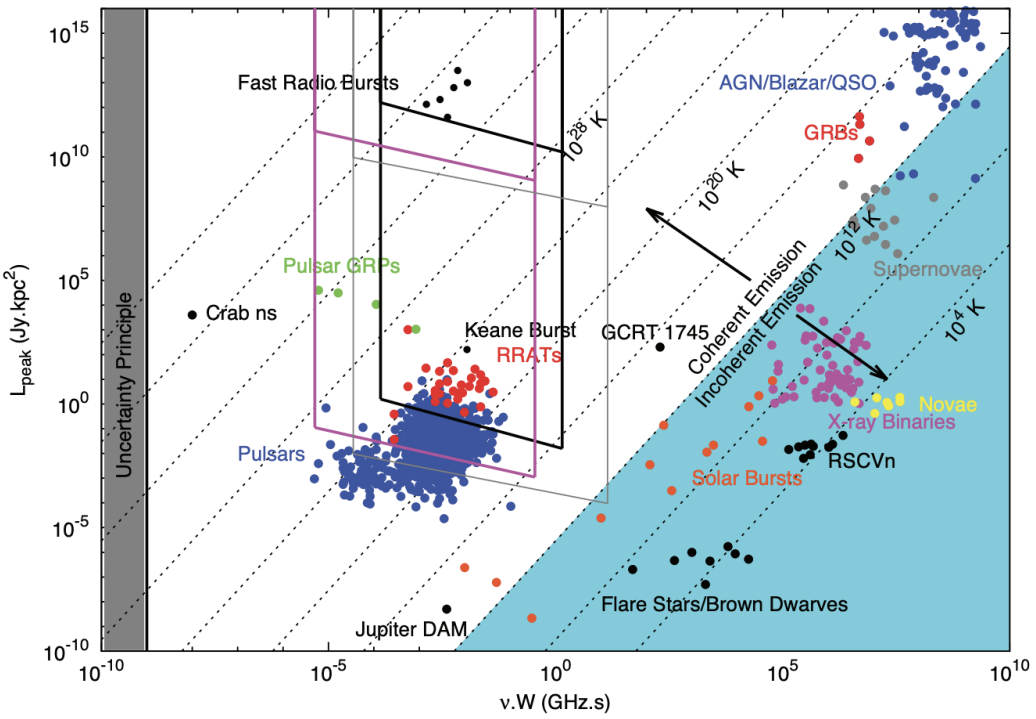

Figure 1.3: Radio transient parameter space of specific luminosity versus the product of observing frequency and transient duration. Overplotted are 1 kpc and 1 Gpc sensitivity curves for Parkes (black), SKA1-LOW (pink) and SKA1-MID (grey). Galactic FRB searches are particularly sensitive to transients in the gap between FRBs and giant pulses from pulsars. Reproduced from J. P. Macquart, E. Keane, et al. (2015).

measured dispersion measure has contributions from the Milky Way's interstellar medium, the halo of the Milky Way, the intergalactic medium, possibly the halos of intervening galaxies, the halo of the host galaxy, and the interstellar medium of the host galaxy. Good understanding of the progenitor will enable good understanding of the systematic effects present in the contribution from the interstellar medium of the host.

However, determining the origin of an extragalactic phenomenon is very difficult. Many different explanations can accommodate the observations of the radio properties of FRBs. If one looks to the galaxies that FRBs reside in, even the telescopes with the highest angular resolution cannot distinguish between two stars in distant galaxies, making it impossible to pin down a distant fast radio burst to a known source. Furthermore, if counterparts in other wavelengths exist, they may be too faint to be seen from extragalactic distances. However, if one were to find an FRB in the Milky Way, all of these difficulties would be eliminated.

Furthermore, searching for FRBs in the Milky Way probes a unique area of the radio transient phase space. Figure 1.3 shows the radio transient phase space. There may be fast radio transients with luminosities higher than giant radio pulses but lower than extragalactic FRBs that we do not currently have access to because they are too faint to be seen from other galaxies, but rare enough that it is unlikely radio telescopes would be looking at the right place at the right time if one were to occur in the Milky Way. Therefore, not only would a search for FRBs in the Milky Way potentially solve a major question in the field, but it would be sensitive to an unexplored area of parameter space where exciting new phenomenon may be hiding.

In this thesis, I will describe the Survey for Transient Astronomical Radio Emission 2 (STARE2), an experiment designed to search for an FRB in the Milky Way. I will develop a formalism to interpret the results for a search for FRBs in the Milky Way and discuss how even a nondetection from a Galactic FRB search will be useful in constraining the luminosity function of FRBs. Furthermore, I will show the area in the radio transient phase space that such a search probes. I will then describe the instrument and present the detection of a solar burst, verifying that STARE2 is capable of detecting Galactic FRBs.

Then, I will present the discovery of the first Galactic FRB with STARE2, FRB 200428. This FRB was traced back to the known Galactic magnetar SGR J1935+2154 and is also the first FRB to have an associated transient in another wavelength, as a particularly hard X-ray burst was produced simultaneously with the FRB. I will argue that this burst is comparable to the extragalactic population of FRBs and further suggest that the rates of these events from SGR J1935+2154 imply that magnetars are responsible for most extragalactic FRBs.

Third, I will test the hypothesis that magnetars produce most FRBs by comparing the host galaxies of FRBs to the host galaxies of other transients thought to be associated with the birth of magnetars, including core-collapse supernovae, hydrogen-poor superluminous supernovae, and long gamma-ray bursts. To make this comparison, I developed a new statistical technique to compare samples of transient host galaxies with different redshifts. I conclude that the population of FRB hosts is consistent with core-collapse supernovae, but not superluminous supernovae or long gamma-ray bursts. This is consistent with the hypothesis that most FRBs originate from magnetars.

Finally, I will propose two FRB surveys that consist of long, targeted observing campaigns. The first is a year long survey of M82 to search for FRBs at 20 GHz.

This survey has the potential to unlock a new hidden population of FRBs at high frequencies and in galaxies with dense and turbulent interstellar mediums. The second survey consists of broadband observations from 1.4 GHz–20 GHz of Galactic magnetars with recent X-ray flares for several months. This survey will help us understand the emission mechanism of FRBs and offer clues as to whether FRBs exist at high frequencies.

Chapter 2

STARE2: DETECTING FAST RADIO BURSTS IN THE MILKY WAY

Bochenek, Christopher D. et al. (Mar. 2020). "STARE2: Detecting Fast Radio Bursts in the Milky Way". In: *Publications of the Astronomical Society of the Pacific* 132.1009, 034202, p. 034202. DOI: 10.1088/1538-3873/ab63b3. arXiv: 2001.05077 [astro-ph.HE].

Christopher D. Bochenek[1], Daniel L. McKenna[1], Konstantin V. Belov[2], Jonathon Kocz[1], S. R. Kulkarni[1], James Lamb[3], Vikram Ravi[1], David Woody[3]

[1]Cahill Center for Astronomy and Astrophysics, California Institute of Technology, Pasadena, CA 91125, USA
[2] Jet Propulsion Laboratory, California Institute of Technology, Pasadena, CA
[3]Owens Valley Radio Observatory, California Institute of Technology, Big Pine, CA

Abstract

There are several unexplored regions of the short-duration radio transient phase space. One such unexplored region is the luminosity gap between giant pulses (from pulsars) and cosmologically located fast radio bursts (FRBs). The Survey for Transient Astronomical Radio Emission 2 (STARE2) is a search for such transients out to 7 Mpc. STARE2 has a field of view of 3.6 steradians and is sensitive to 1 millisecond transients above $\sim$ 300 kJy. With a two-station system we have detected and localized a solar burst, demonstrating that the pilot system is capable of detecting short duration radio transients. We found no convincing transients with duration between 65 μs and 34 ms in 200 days of observing, limiting with 95% confidence the all-sky rate of transients above $\sim$ 300 kJy to $< 40\, sky^{-1}\, year^{-1}$. If the luminosity function of FRBs could be extrapolated down to 300 kJy for a distance of 10 kpc, then one would expect the rate to be $\sim 2\, sky^{-1}\, year^{-1}$.

2.1 Introduction

Just 13 years ago, Lorimer et al. (2007) discovered the first fast radio burst (FRB) that has led to a great amount of activity to find and characterise the population (e. g. Champion et al., 2016; Bailes et al., 2017; Amiri et al., 2018; Kocz et al., 2019; J.-P. Macquart et al., 2010). It is now established that FRBs herald from cosmological

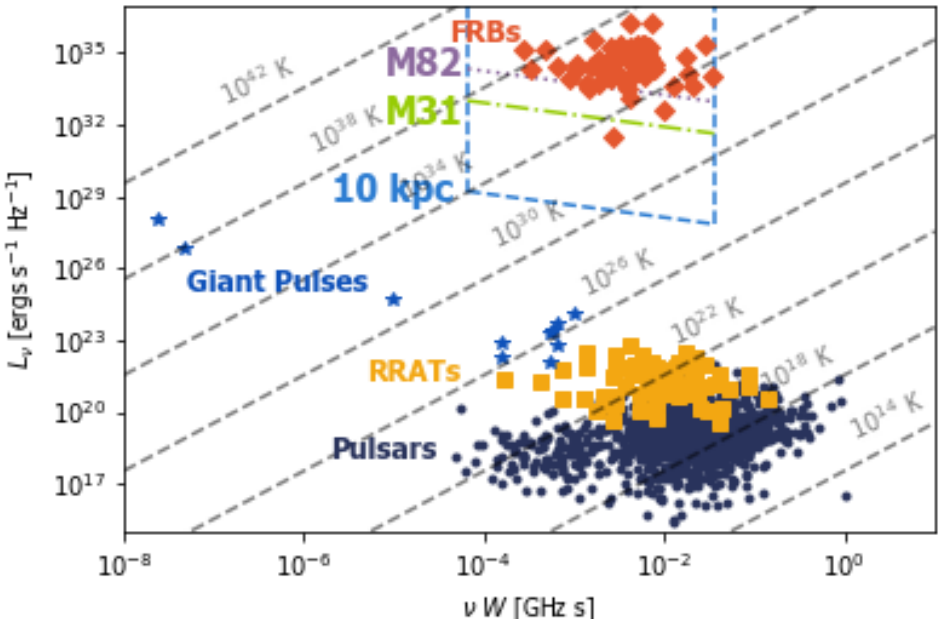

Figure 2.1: Luminosity of radio transients vs. the frequency of the transient times the duration of the transient (Pietka, Fender, and E. F. Keane, 2015). The blue box shows STARE2's sensitivity to transients within 10 kpc, the green dot-dashed line shows STARE2's sensitivity to transients from M31, and the purple dotted line shows STARE2's sensitivity to transients from M82. STARE2 is able to detect transients in the gap between pulsars and FRBs, and most FRBs at the distance of M82.

distances (S. Chatterjee et al., 2017; Vikram Ravi, 2019b; K. W. Bannister et al., 2019; J. Xavier Prochaska et al., 2019) and are of great luminosity.

The existence of FRBs shows that processes in nature can produce brightness temperatures of up to 10^{36} K with long enough duration to be seen at cosmological distances. However, as shown in Figure 2.1, there is unexplored parameter space between giant pulses from pulsars and FRBs, particularly with respect to luminosity.

There have been several surveys for extremely bright fast radio transients that may have been sensitive to events in this luminosity gap. STARE (Katz et al., 2003) was a network of three feeds located throughout the Northeast United States. STARE used a multi-station coincidence approach to filter out radio frequency interference (RFI). Only events seen at all three stations were considered candidates. The experiment ran for 18 months with observations conducted in the 600–613 MHz band with a time resolution of 0.125 s and typical flux density threshold at zenith of 27 kJy.

STARE found 3,898 coincident events and associated all of them with solar radio bursts.

Saint-Hilaire, Benz, and Monstein (2014) conducted a similar experiment at the Bleien Observatory (near Zurich, Switzerland). It consisted of a 70°x110° FWHM log-periodic antenna and a 10° FWHM horn, both operating in the 1170–1740 MHz band and a time resolution of 10 ms and a frequency resolution of 1.02 MHz. They observed for 289 days with the log-periodic antenna, and 609 days using a horn antenna, achieving a sensitivity to events greater than 200 kJy for signals 10 ms in duration. In all, five events were detected. Four happened during the daytime and could have been "perytons" (Petroff, E. F. Keane, et al., 2015) or solar radio bursts. The fifth event happened at night with the full moon in the beam of the antenna. Saint-Hilaire, Benz, and Monstein (2014) speculate that this event could have been a solar radio burst reflected off the moon, as its spectrum is similar to that of solar radio bursts. Furthermore, the pulse did not follow the expected ν^{-2} frequency sweep expected from traveling through the interstellar medium.

Using the fact that they detected no non-solar fast transients, we conclude from their observations with the log-periodic antenna that the all-sky rate of "intermediate luminosity" fast radio transients is $< 15.1\ \mathrm{s}ky^{-1}\ yr^{-1}$ for transients above 400 kJy and longer than 10 ms using the statistical framework of Gehrels (1986).

Current FRB searches will likely find it difficult to detect nearby fast radio transients in this phase space. If a transient in this luminosity gap was to occur within the Milky Way, it would be a tremendously bright event —so bright, that a dish is not needed to see it. Furthermore, if it did occur in the primary beam of a deep single pulse search, it would likely saturate the instrument and be removed as radio frequency interference (RFI). It is possible that a deep single pulse search would detect such an event in a far sidelobe. For a single dish or beamforming search, it would be difficult to identify that the burst occurred in a far sidelobe without some identifying feature, such as it having the same dispersion measure (DM) as a known pulsar. This would make the burst difficult to place in the luminosity gap and is more likely to be interpreted as a single pulse from a galactic pulsar. However, if baseband data is saved, then it would be possible to determine that the pulse came from far outside of the primary beam. For an image-plane search, one would have to ensure that complex structure in the primary beams of the antennas did not impart a significant amount of noise to the phases and the delay beam did not suppress significantly off-axis emission. Even then, it would be difficult to determine the

burst's flux density to even an order of magnitude, as far sidelobes are typically not well characterized. This uncertainty would make it difficult to identify the burst as belonging to this luminosity gap.

Motivated by the considerations discussed above we initiated a similar search called the Survey for Transient Astronomical Radio Emission 2 (STARE2). In a nutshell, STARE2 aims to survey the transient radio sky for millisecond bursts in the 1280–1530 MHz band. The experiment consists of a single feed pointed at zenith at several sites. Temporal coincidence is used to identify and remove RFI. Our basic time and frequency resolution are 65.536 μs and 122 kHz. We are sensitive to signals of 1 ms duration above 300 kJy.

The paper is organized as follows: In Section 2.2, we consider different types of sources that STARE2 might be sensitive to. The instrumentation and data processing of STARE2 is described in Section 2.3. We have commensally detected a solar burst, which is described in Section 2.4. In Section 2.5, we set an upper limit on the all-sky rate of extremely bright fast radio transients and discuss our future plans.

2.2 Extremely Bright Radio Bursts in the Milky Way

Currently, there is no known source of fast transient radio emission beyond the solar system that is bright enough to be seen by STARE2. However, the discovery of fast radio bursts has opened up a vast phase space ranging from Galactic giant radio pulses to cosmologically located FRBs.

There is a wide range in luminosity of the classical FRBs themselves. It is reasonable to hypothesize that there is a population of FRBs that is too faint to be seen at cosmological distances, but more numerous than classical FRBs such that we should expect the Milky Way to host such a source (Vikram Ravi, 2019b). Even a burst of luminosity 10^{29} ergs s^{-1} Hz^{-1}, approximately three orders of magnitude fainter than the lowest luminosity FRB, would be detected at a distance of 10 kpc with flux density 800 kJy. Such FRBs, should they exist, would be detected with could be seen by a simple dipole.

The field of gamma-ray bursts (GRBs) provides another inspiring motivation for the proposed search program (see Kulkarni, 2018). There are actually four distinct bursting sources in the gamma-ray sky: terrestrial lightning, soft gamma-ray repeaters (SGRs; these are seen from sources in our Galaxy and the galaxies within a few Mpc of the Sun), short hard bursts (whose typical red-shift is 0.5; associated with neutron star coalescence) and long duration GRBs (whose typical red-shift is

2; associated with deaths of a certain class of massive stars).

In fact, even just over three decades ago SGRs were not seen as distinct from GRBs (either short or hard). We now know that SGRs, as implied by their name repeat and furthermore have a distinctly different origin than that of short or long GRBs. Furthermore, SGRs have moderate luminosity but have a higher volumetric rate than GRBs, as it is rare for a GRB to occur in any individual galaxy in a given year, whereas it is common for an individual galaxy to host multiple SGRs.

This analogy, if applied to FRBs, would suggest that there may be a class of radio bursts which are not as luminous as FRBs but have a much higher volumetric rate than FRBs. Just as with SGRs, these hypothesized sources would be relatively common in the Milky Way.

Undiscovered Fast Radio Transients

In this section, we connect the observed galactic rate of an unknown transient to the volumetric rate, $\Phi(> E)$, of that transient in order to understand what types of events might be seen by STARE2.

If a radio transient tracks stellar mass, then the rate of that transient for a given galaxy is given by Equation 2.1, where M_{galaxy} is the stellar mass of the galaxy and $\Phi_{\rm M}$ is the volumetric rate of stellar mass. We take $\Phi_{\rm M}$ to be $7.4 \times 10^8\,{\rm M}_\odot\,{\rm Mpc}^{-3}$ (Karachentsev and Telikova, 2018a). Thus, if a radio transient happens once every year in the Milky Way and is detected by STARE2, then its volumetric rate is of order $10^7\,{\rm Gpc}^{-3}\,{\rm yr}^{-1}$ above an energy of $2 \times 10^{28}\,{\rm erg\,s}^{-1}\,{\rm Hz}^{-1}$,

$$R_{galaxy}(> E) = \frac{M_{galaxy}}{\Phi_{\rm M}}\Phi(> E). \tag{2.1}$$

If a radio transient instead tracks star formation instead of stellar mass, then we can similarly relate the volumetric rate of the transient to the star formation rate as shown in Equation 2.2, where Φ_{SFR} is the local volumetric rate of star formation and S is the star formation rate for a particular galaxy,

$$R_{galaxy}(> E) = \frac{S}{\Phi_{SFR}}\Phi(> E). \tag{2.2}$$

The volumetric star formation rate is $1.95 \times 10^{-2}\,{\rm M}_\odot\,{\rm Mpc}^{-3}\,{\rm yr}^{-1}$ (Salim, Rich, et al., 2007). For a transient with an all-sky rate of $1\,{\rm yr}^{-1}$ in the Milky Way, which has a star

formation rate of approximately $1\,M_\odot\,yr^{-1}$, the volumetric rate is $2\times10^7\,Gpc^{-3}\,yr^{-1}$ above $2\times10^{28}\,erg\,s^{-1}\,Hz^{-1}$.

There is approximately $12.5\,M_\odot\,yr^{-1}$ within 3.6 Mpc, mostly from M82, which has a SFR of $10.7\,M_\odot\,yr^{-1}$ Jarrett et al. (2019). This SFR is calculated using the sum of Hα luminosities from all galaxies in Kennicutt et al. (2008) with declinations greater than $-30°$, excepting M82, whose Hα luminosity underestimates the SFR. For a transient that has an all-sky rate of $1sky^{-1}\,yr^{-1}$ at the distance of M82, the volumetric rate of fast transients above $5\times10^{33}\,erg\,s^{-1}\,Hz^{-1}$ is approximately $1.6\times10^6\,Gpc^{-3}\,yr^{-1}$.

From this analysis, we see that while STARE2 is sensitive to transients that are bright (have high flux densities) and rare (have low all-sky rates), any transient seen would be relatively faint (have luminosities significantly lower than FRBs) and common (have a high volumetric rate).

Low Energy Fast Radio Bursts

In addition to finding new classes of fast radio transients, it is possible that STARE2 could see low energy FRBs in the Milky Way if the luminosity function of FRBs extends a few orders of magnitude towards lower energies. It is, however, difficult to make a prediction for the rate of Galactic FRBs given the considerable amount of uncertainty in the FRB luminosity function.

Lu and Piro (2019) analyzed a sample of FRBs and found that the number of FRBs above a given energy, $N_{FRB}(>E)$, follows a power law distribution of index -0.7, with a cutoff above $\sim 10^{34}\,ergs\,Hz^{-1}$. Lu and Piro (2019) also constrained the volumetric rate of FRBs to $> 1.1\times10^3\,Gpc^{-3}\,yr^{-1}$ above $10^{32}\,ergs\,Hz^{-1}$. We note this rate is a lower limit due to incompleteness of the ASKAP sample and contributions to the DM from the host galaxy and circumgalactic medium of the Milky Way that were not taken into account. Luo et al. (2018) analyzed a smaller sample of FRBs and constrained this power law index to between -0.2 and -0.8. Notably, this is the same energy distribution as exhibited by the first repeating event, FRB 121102 (Law et al., 2017). However, Gourdji et al. (2019) analyzed a sample of low energy FRBs from FRB 121102, and found a much steeper slope of -1.8 for energies above 2×10^{37} erg. Gourdji et al. (2019) attempt to explain this discrepancy by pointing to the fact that they may have unavoidably underestimated the burst energies, propagation effects (J. M. Cordes, Wasserman, et al., 2017), and by suggesting that a single power-law may not explain the intrinsic energy function

from FRB 121102.

Current observations are not sensitive to the minimum energy of FRBs. Luo et al. (2018) set an upper limit on the lower cut-off of the FRB luminosity function of 10^{42} erg s^{-1}. However, as shown by Gourdji et al. (2019), the FRB luminosity may not be a simple power law with a cut-off.

Using equations 2.1 and 2.2, assuming a volumetric rate of FRBs of 10^3 Gpc^{-3} yr^{-1} above 10^{35} erg s^{-1} Hz^{-1}, and assuming the luminosity function given by Lu and Piro (2019), we can infer how far down the luminosity function we must extrapolate such that the rate of FRBs in the Milky Way is $\sim$ 1 yr^{-1}. We find that regardless of whether FRBs track stellar mass or star formation, the FRB rate in the Milky Way should be above $\sim$ 1 yr^{-1} for FRBs with energy greater than $\sim 10^{29}\Phi_3^{1.4}$ erg s^{-1} Hz^{-1}, where Φ_3 is $\frac{\Phi_{FRB}(>10^{35}\, ergs\, \mathrm{s}^{-1}\, \mathrm{Hz}^{-1})}{10^4\, Gpc^{-3}\, yr^{-1}}$. This is approximately 5 orders of magnitude fainter than a typical FRB of luminosity 10^{34} erg s^{-1} Hz^{-1}, as defined by Figure 2.1. For a distance of 10 kpc, a luminosity of 4×10^{28} erg s^{-1} Hz^{-1} corresponds to STARE2's sensitivity limit of $\sim$ 300 kJy. If the luminosity function of FRBs could be extrapolated down to this luminosity, then one would expect the galactic rate to be $\sim 2\, year^{-1}$.

In addition to low energy FRBs, there is a small chance of finding an FRB with energy equivalent to those FRBs seen at extragalactic distance. STARE2 will be able to detect 1 ms radio transients above ~300 kJy. Given this, STARE2 could detect an FRB with the same energy as FRB 190523 out to a distance of 191 Mpc (V. Ravi et al., 2019). Figure 2.2 shows STARE2's horizon to FRBs for FRBs of different luminosity, as well as the probability of an FRB detectable to STARE2 occurring in a two year period as a function of horizon. Given the volumetric rate of $\sim 10^3$ Gpc^{-3} yr^{-1} above an energy of 10^{35} erg s^{-1} Hz^{-1} and luminosity function of Lu and Piro (2019) without a cutoff energy, this implies the probability of an FRB detectable to STARE2 occurring within 191 Mpc is $\sim$ 33%.

2.3 STARE2: The Instrument

STARE2 consists of two dual-polarization choke-ring feeds pointed at zenith at the Owens Valley Radio Observatory (OVRO) and the Venus Antenna at the Goldstone Deep Space Communications Complex (GDSCC). The feed from OVRO is shown in Figure 2.3. A block diagram of the signal path for one station is shown in Figure 2.4. The signal enters the feed through and excites two orthogonally polarized linear probes. We measured the beam pattern of the choke feed by radiating tones ranging

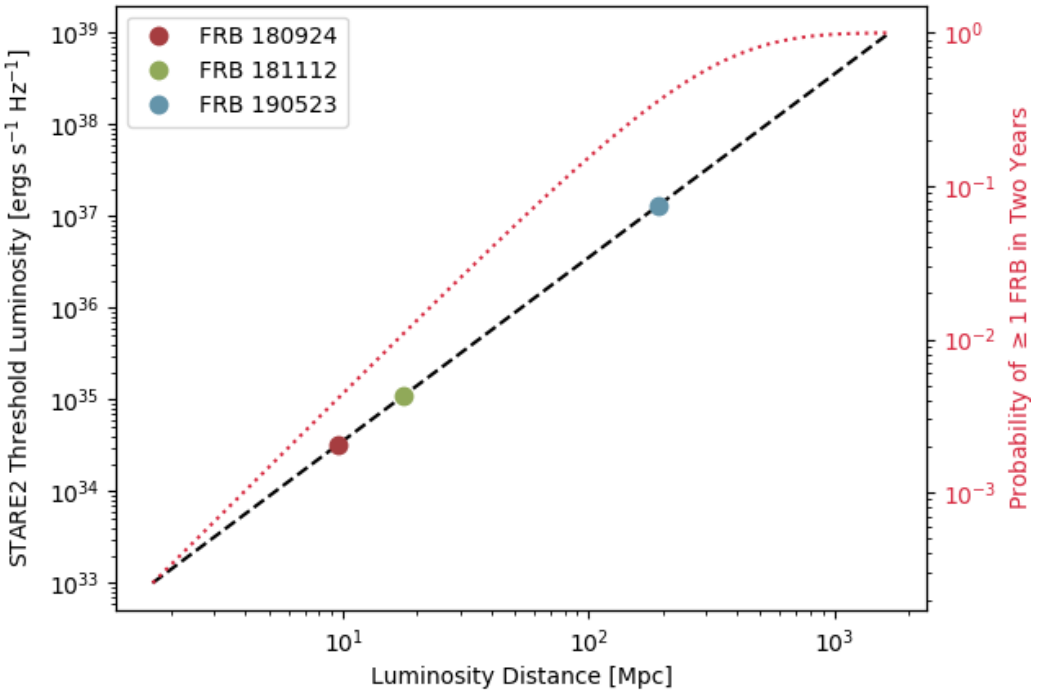

Figure 2.2: The left axis shows the minimum luminosity of a 1 ms FRB that would be above STARE2's detection threshold as a function of luminosity distance. The points show the horizon to non-repeating FRBs of known luminosity. The right hand axis shows the probability of at least one FRB occurring above STARE2's detection threshold in a 2 year period as a function of luminosity distance, calculated using the rate and luminosity function given in Lu and Piro (2019), assuming no maximum energy of FRBs.
(K. W. Bannister et al., 2019; J. Xavier Prochaska et al., 2019; V. Ravi et al., 2019)

from 1165 MHz to 1665 MHz. Each tone was generated with the same amount of power, and the distance between the radiating antenna and our feed kept constant at approximately 10 m. We then measured the power received at each frequency relative to the radiated power with a vector network analyzer. We repeated this measurement for all angles between −180° and +180° at 5° increments. There was a concern about reflections off a low wall near the feed, and we placed absorber along this wall to mitigate this concern. The beam pattern of the feed is shown in Figure 2.5. The FWHM of the beam is 70 ± 5°.

Each polarization is then amplified by 31 dB across the STARE2 passband by separate low noise amplifiers and travels down coax cables to a front end box. The front end box has a bandpass filter that sets the STARE passband from 1280

Figure 2.3: The choke-ring feed located at OVRO. It lies in a 6 m dish which is used as a horizon shield. The 6 m dish blocks up to 25° above the horizon.

MHz–1530 MHz. The signal is then amplified again by 18 dB and is mixed with an infrared laser driver so that the signal can be sent via optical fiber from the field to a server room. When the signal arrives at the back end box in the server room, the infrared laser signal is converted back to an RF signal. Inside the back end box, the signal goes through a 1200 MHz–1600 MHz filter, is amplified again by 46 dB, mixed with a 1030 MHz local oscillator so that the 1280 MHz–1530 MHz signal is downconverted to a 250 MHz–500 MHz intermediate frequency signal. This signal is amplified further and sent to a SNAP board[1] to be digitized, channelized, and integrated to the desired time resolution of 65.536 μs. The SNAP board then sends

[1] https://casper.ssl.berkeley.edu/wiki/SNAP

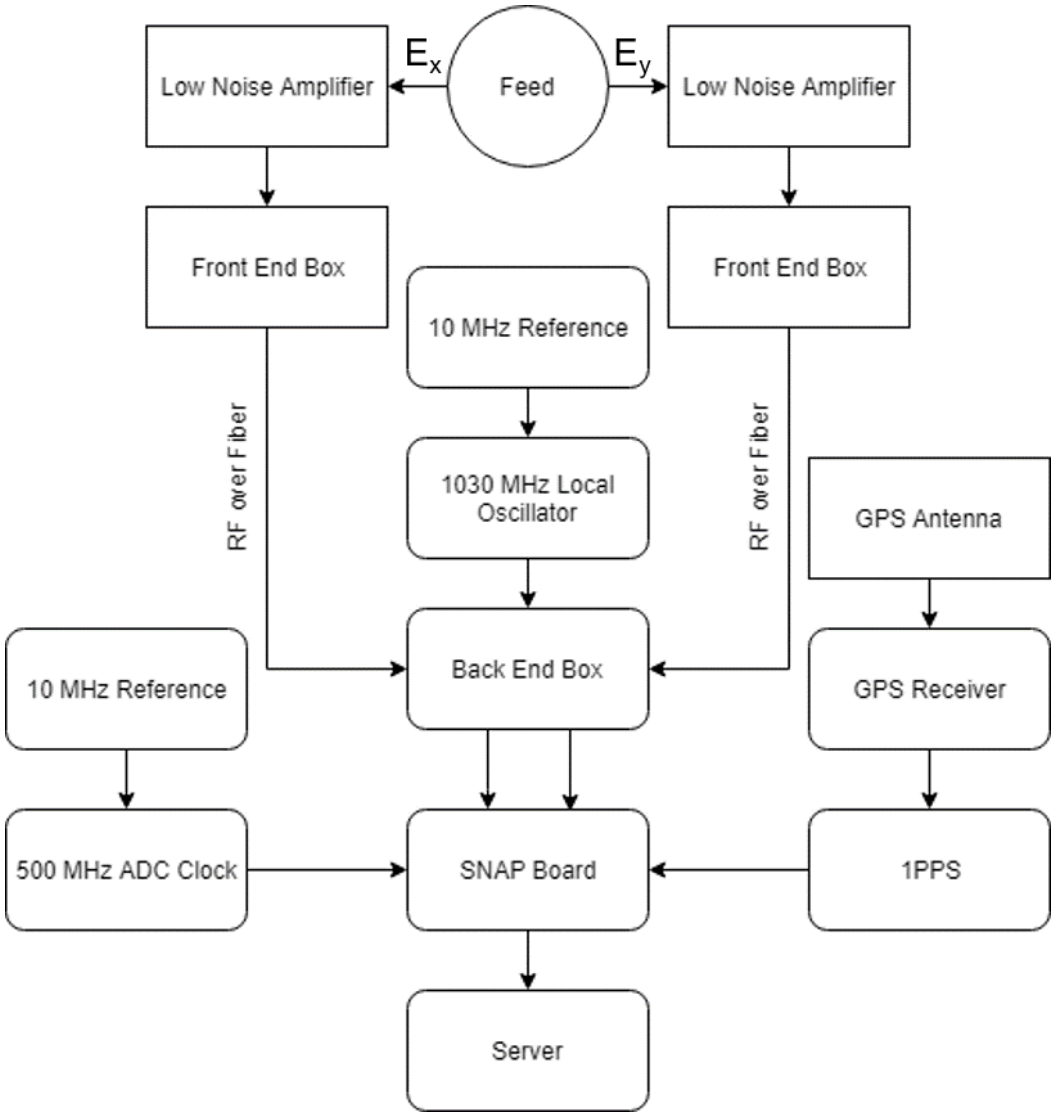

Figure 2.4: Block diagram for STARE2's system. The blocks with sharp edges are outside in the field and the blocks with rounded edges, except for the feed, are indoors. For a description of the front end box and back end box, see (Kocz et al., 2019)

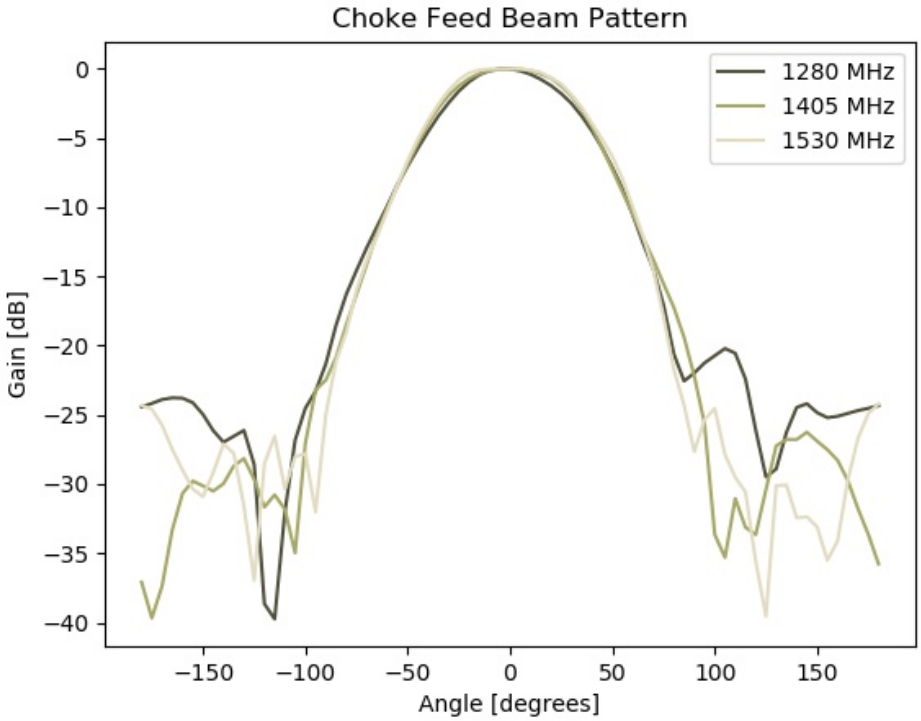

Figure 2.5: Beam pattern measurement for STARE2's choke ring feed. The FWHM of the beam is 70° ± 5°.

a spectrum of 2048 16 bit channels at a frequency resolution of 0.12207 MHz, every 65.536 μs to a server.

The system temperature at each site is 60 ± 5 K. This was measured with the y-factor method by pointing the receiver at zenith and measuring the passband over 10 seconds of recorded data with absorber on and off of the feed. This value represents an average across the band. Given our system temperature, we can compute the system equivalent flux density (SEFD) within the FWHM of the beam pattern. We find the SEFD is 19 ± 2 MJy.

The server receives the data from the SNAP, measures the passband, normalizes the data by the shape of the passband, and filters out RFI. The RFI filtering pipeline replaces single pixels in the dynamic spectrum above an SNR of 20, blocks of width 1.95 MHz and 3.3 ms above an SNR of 20, and spectral channels that change by more than an SNR of 10 over 1.6 s or have significantly higher variance than average with the mean value of all pixels. The threshold for the variance is set empirically to remove no channels under typical RFI conditions and let through a single injected 1 ms long burst with an SNR of 1000. Typically, 25% of the band is unusable due

to RFI. Because a fast radio burst as bright as the ones seen in other galaxies would likely cause the data to meet these criteria, we also enforce that no more than 730 out of 2048 spectral channels will be replaced at any given time so that a broadband burst will not be completely removed from the data.

We use `heimdall`(Barsdell et al., 2012) to search the data out of the RFI pipeline for dispersed signals. `heimdall` dedisperses the data, convolves the data with several matched filters corresponding to different pulse widths, then computes the signal to noise for each time sample, DM, and pulse width, and finally groups high signal to noise candidates of similar times, widths, and DMs together. We search 1546 DMs between 5 pc cm^{-3} and 3000 pc cm^{-3}, with a loss in SNR between DM trials of 25% for a candidate that is one time integration wide (L. Levin, 2012). We search ten logarithmically spaced pulse widths between 65.535 μs and 33.5 ms. We save every candidate above an SNR of 7.3. This threshold was determined empirically to be as low as possible without producing an overwhelming number of candidates. The fact that we require events to be detected independently at multiple sites allows us to use a lower threshold than other experiments. Therefore, for an effective bandwidth of 188 MHz (the average available bandwidth) and pulse width of 1 ms, we are sensitive to events above 314 ± 26 kJy.

To estimate the completeness of our detection pipeline, we injected 5484 broadband pulses with a flat spectral index into data from a single station. We detected 4055 of them. The pulses had log uniformly distributed SNRs ranging from 7.3 to 10^4, log uniformly distributed DMs ranging from 5 pc cm^{-3} to 3000 pc cm^{-3}, and log uniformly distributed durations between 0.066 ms and 45.340 ms. Because we run each station independently, our two station coincidences are approximately 55% complete.

The distance between the two stations is 258 km, corresponding to a light travel time of 0.86 ms between the stations. Each station generates candidate events independently. In addition to our single station RFI removal, RFI is filtered out by enforcing that a candidate was found at each site within one light travel time, 0.86 ms plus the maximum duration of a candidate, 33.554 ms, which gives a window in time for coincident events of 34.414 ms.

In order to successfully detect coincident events at multiple independent sites, keeping accurate absolute time is critical. To time-stamp the start of an observation, we use a GPS receiver that produces one pulse per second (1PPS) at the start of every GPS second. This receiver is locked to a rubidium clock to minimize drift on small

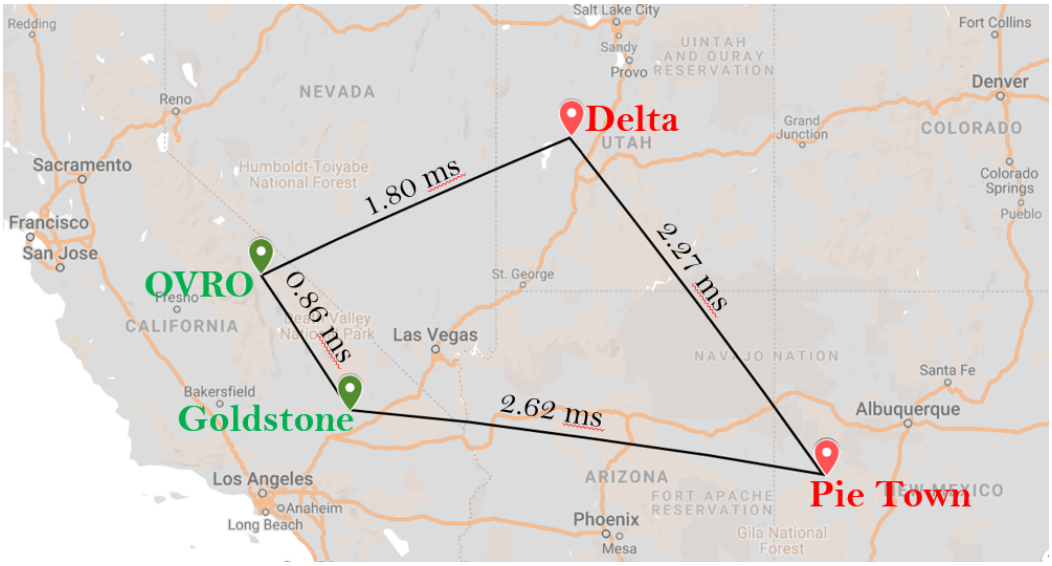

Figure 2.6: Map of STARE2 stations with light travel time delays between the baselines. The OVRO and Goldstone sites in green are operational, while the Delta and Pie Town sites in red are options for additional stations.

timescales. This 1PPS is accurate to within 250 ns. To keep track of time during an observation, we rely on the clock that runs the ADC. This clock is locked to a 10 MHz reference that is good to better than 2 parts in 10^9. We obtain a new 1PPS pulse every 5 hours to reset the system. The difference in cable lengths between the two sites should also impart an offset of no more than 3 μs, with the station at OVRO having longer cables.

The RFI filtering and candidate search pipeline produces a candidate rate of 83 hr^{-1} at OVRO and 270 hr^{-1} at GDSCC. The rate of coincidences is 5 day^{-1}. This rate is consistent with the expected rate of coincidences assuming that the candidates at OVRO are unrelated to the candidates at GDSCC, and while there are correlated events associated with the Sun and RFI, they are a minority of candidates. Real correlated events are distinguished by their dynamic spectra and time delay between the two sites.

2.4 Detection of a Solar Burst

On May 6th, 2019, at UTC 17:47:35.385, we detected a candidate event, ST 190506B, at both OVRO and GDSCC. The naming scheme of the candidates begins with an abbreviation of the instrument, followed by the date, shown as YYMMDD, and a letter or series of letters corresponding to the order of coincidences detected on that day. The dynamic spectrum of this event at each station is shown in Figure

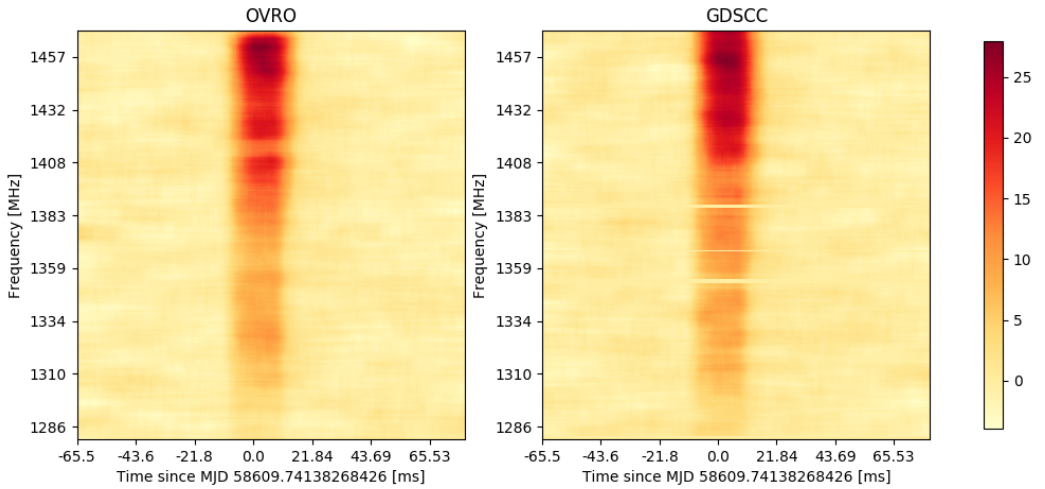

Figure 2.7: Left: The dynamic spectrum of ST 190506B from OVRO. Right: The dynamic spectrum of ST 190506B from GDSCC. The same solar burst is seen from both OVRO and GDSCC. The data have been corrected for the shape of the passband and normalized to unit variance. They have also been averaged to the width of the burst in time and every 7.8 MHz in frequency. Channels with significant RFI have been replaced with zero. The colorbar shows the signal to noise in each pixel after averaging.

2.7.

The measured delay time between OVRO and GDSCC was $394 \pm 68\,\mu$s. The expected delay time for the Sun between the two stations at the time of the burst was $404\,\mu$s. This delay time corresponds to the localization region shown in 2.8, and is consistent with the position of the Sun.

The width of the burst is 19.33 ± 0.06 ms and it has a beam-corrected flux density of 9.1 ± 0.8 MJy. The burst was detected with a DM of $5\,\mathrm{pc\,cm^{-3}}$, however it is consistent with a DM of $0\,\mathrm{pc\,cm^{-3}}$. The burst was also seen during a time of heightened solar activity, and X-ray data from the *GOES* satellite show a significantly higher flux than average at the time of the burst. The burst width, flux density, and solar activity during the time of the burst is consistent with a solar burst (Meléndez et al., 1999; Benz, Bernold, and Dennis, 1983). From this event, we conclude that the system can commensally detect FRB-like events of similar flux density, should they occur.

2.5 Discussion

We have been observing for 200 days and have seen no convincing fast transient events. We can therefore set a 95% confidence upper limit on the all-sky rate of

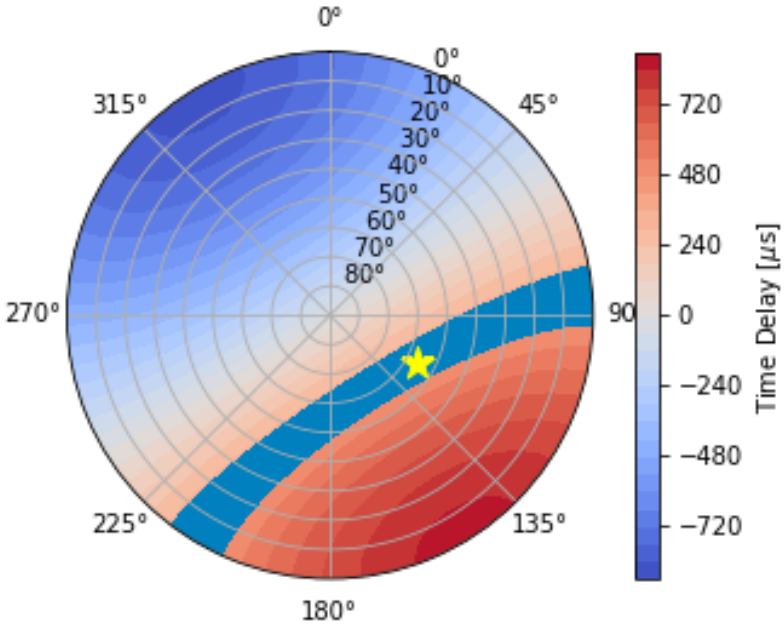

Figure 2.8: Localization region for ST 190506B in altitude and azimuth at OVRO. The colorbar maps a time delay between each station to a part of the sky. The localization region for ST 190506B is shown in blue. The Sun's position at the time of the burst is shown by the yellow star. The time delay expected from the Sun is within the uncertainty of the measured time delay.

extremely bright fast radio transients of 40 $\mathrm{sky}^{-1}\,\mathrm{yr}^{-1}$ above 314 ± 26 kJy.

We plan to expand our network to four stations as shown in 2.9. With four stations, we will be able to localize an event to a patch of sky, rather than a stripe. We will also be able to determine the altitude of a source below approximately 10^3 km, in a manner similar to the Global Positioning System. As shown in Figure 2.9, with the proposed four station system, we would have localized ST 190506B to 15 deg^2. As of November 2019, the station in Delta, Utah is operational.

2.6 Acknowledgements

We would like to thank the then director of OVRO, A. Readhead, for funds (derived from the Alan Moffet Funds) which allowed us to start this project. The Presidential Director's Fund (PDF) allowed us to build the second system at Goldstone. We are thankful to Caltech and the Jet Propulsion Laboratories for the second round of funding. We would also like to thank Sandy Weinreb and David Hodge for building the front end and back end boxes, Jeffrey Lagrange for his support at GDSCC, and the entire OVRO staff for their support. Part of the research was carried out at the

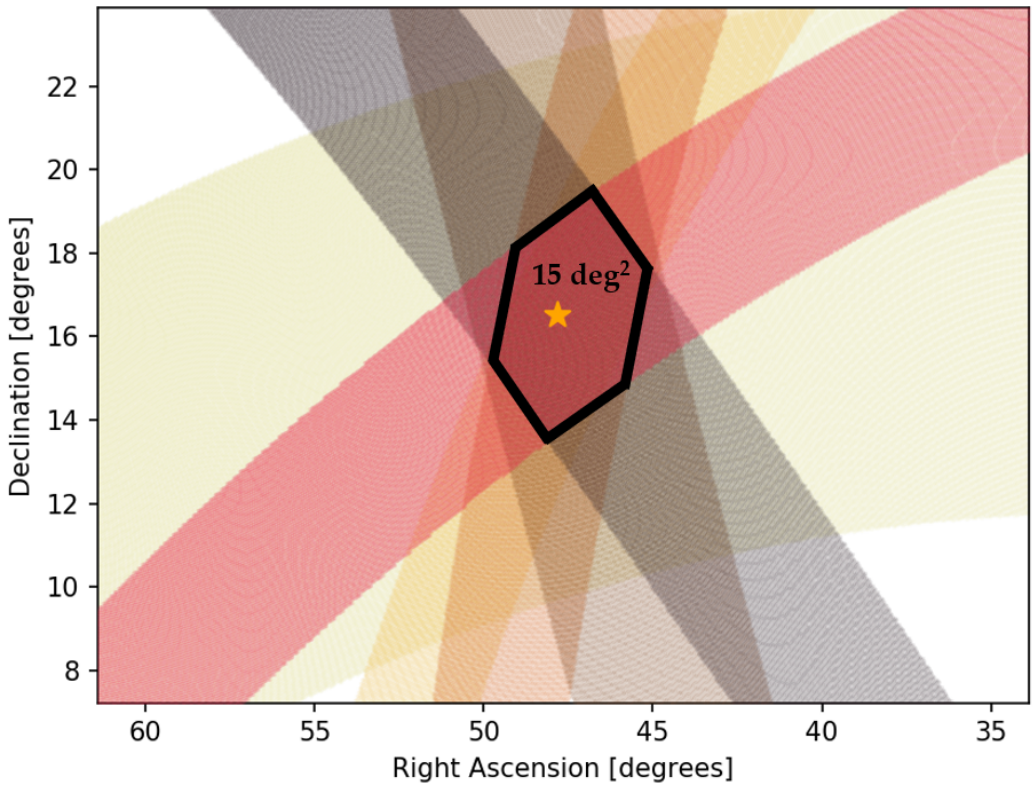

Figure 2.9: Localization region for ST 190506B in right ascension and declination, assuming the four station system in Figure 2.6 and an uncertainty of 68 μs in delay time. The overlap of the localization arcs is 15 deg^2. The overlap of all the localization arcs is marked by a black hexagon.

Jet Propulsion Laboratory, California Institute of Technology, under a contract with the National Aeronautics and Space Administration.

Chapter 3

A FAST RADIO BURST ASSOCIATED WITH A GALACTIC MAGNETAR

Bochenek, C. D. et al. (Nov. 2020). "A fast radio burst associated with a Galactic magnetar". In: *Nature* 587.7832, pp. 59–62. DOI: 10.1038/s41586-020-2872-x. arXiv: 2005.10828 [astro-ph.HE].

Christopher D. Bochenek[1,2], Vikram Ravi[2], Konstantin V. Belov[3], Gregg Hallinan[2], Jonathon Kocz[2,4], S. R. Kulkarni[2], Daniel L. McKenna[5]

[1]Cahill Center for Astronomy and Astrophysics, California Institute of Technology, Pasadena, CA, USA
[2]Owens Valley Radio Observatory, California Institute of Technology, Pasadena, CA
[3]Jet Propulsion Laboratory, California Institute of Technology, Pasadena, CA
[4]Department of Astronomy, University of California, Berkeley, CA, USA.
[5]Caltech Optical Observatories, California Institute of Technology, Pasadena, CA, USA.

Abstract

Since their discovery in 2007 (Lorimer et al., 2007), much effort has been devoted to uncovering the sources of the extragalactic, millisecond-duration fast radio bursts (FRBs) (Petroff, Hessels, and Lorimer, 2019). A class of neutron star known as magnetars is a leading candidate source of FRBs (Yu. Lyubarsky, 2014; Beloborodov, 2017). Magnetars have surface magnetic fields in excess of 10^{14} G, the decay of which powers a range of high-energy phenomena (Victoria M. Kaspi and Beloborodov, 2017). Here we present the discovery of a millisecond-duration radio burst from the Galactic magnetar SGR J1935+2154, with a fluence of 1.5 ± 0.3 Mega-jansky milliseconds. This event, termed ST 200428A(=FRB 200428), was detected on 28 April 2020 by the STARE2 radio array (Christopher D. Bochenek et al., 2020) in the 1281–1468 MHz band. The isotropic-equivalent energy released in FRB 200428 is 4×10^3 times greater than any radio pulse from the Crab pulsar, previously the source of the brightest Galactic radio bursts observed on similar timescales (J. M. Cordes, Bhat, et al., 2004). FRB 200428 is just 30 times less energetic than the weakest extragalactic FRB observed to date (Marcote, Nimmo, et al., 2020), and is drawn from the same population as the observed FRB sample. The coincidence of FRB 200428 with an X-ray burst (Mereghetti et al., 2020; Ridnaia et al., 2020; Li and B. Zhang, 2020) favours emission models developed

for FRBs that describe synchrotron masers or electromagnetic pulses powered by magnetar bursts and giant flares (Yu. Lyubarsky, 2014; Beloborodov, 2017; Metzger, Margalit, and Sironi, 2019; Yuri Lyubarsky, 2020). The discovery of FRB 200428 implies that active magnetars like SGR J1935+2154 can produce FRBs at extragalactic distances.

3.1 Discovery of ST 200428A

Three 1281–1468 MHz radio detectors comprise STARE2 (Christopher D. Bochenek et al., 2020), and are located across the south-western United States. All three detectors were triggered by ST 200428A, henceforth referred to as FRB 200428, at an Earth-centre arrival time at infinite frequency of UTC 28 April 2020 14:34:24.45481(3). Standard errors are reported with the last significant figures in parenthesis. The detected signal-to-noise ratios (S/N) were 21, 15, and 20 (see Methods). The burst had a dispersion measure (DM) of 332.702(8) pc cm^{-3} and and a band-averaged fluence of $1.5(3) \times 10^6$ Jy ms (see Table 3.1). The full-width half-maximum temporal width of the burst, after correcting for propagation and instrumental effects (see Methods), is 0.61(9) ms. Although we model the temporal profile of the burst intrinsic to the source as a Gaussian, it is possible that there is unresolved sub-structure on timescales less than the instrumental resolution of 0.122 ms.

On 27 April 2020, the Swift Burst Alert Telescope reported multiple bursts from the soft γ-ray repeater (SGR) 1935+2154 (Barthelmy et al., 2020). One day later, the CHIME/FRB collaboration reported an approximately 10^3 Jy ms burst in the 400 MHz–800 MHz band from the approximate direction of SGR J1935+2154 (Figure 3.2) (Paul Scholz and Chime/Frb Collaboration, 2020). We expedited our daily inspection of STARE2 triggers and found an event that was detected at approximately the same time and DM as the CHIME event, but with a roughly one thousand times higher fluence. The localisation region of FRB 200428 includes SGR J1935+2154 (Figure 3.2). Shortly thereafter, a constellation of space-borne instruments (Mereghetti et al., 2020; Ridnaia et al., 2020; Li and B. Zhang, 2020) reported a one-second-long X-ray (1–250 keV) burst from the direction of SGR J1935+2154. INTEGRAL determined the burst was coming from within 5.5 arcminutes of the SGR within seconds of the burst. This X-ray burst occurred at precisely the same time as the CHIME bursts and FRB 200428 after accounting for the dispersion delay and different spatial positions of the observatories (Figure 3.1). On 30 April 2020, the Five hundred meter Aperture Spherical Telescope (FAST)

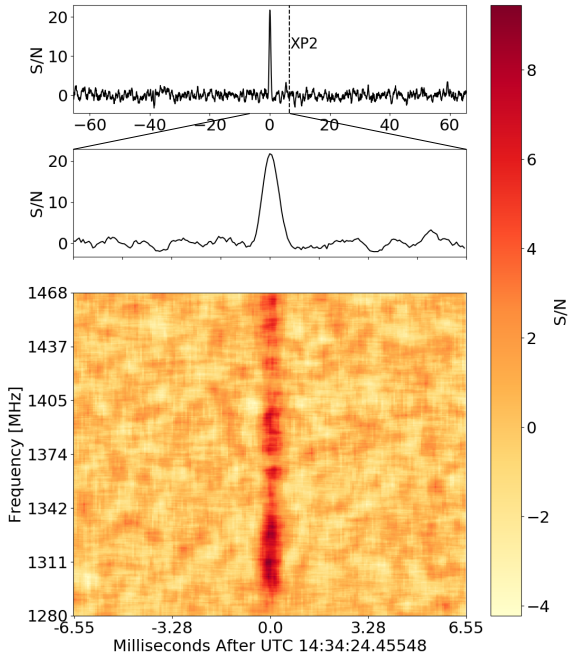

Figure 3.1: Time series and dynamic spectrum of FRB 200428. We show data obtained from the Owens Valley Radio Observatory (OVRO) alone. All data units are signal to noise ratio (S/N). The quoted times are relative to the Earth-centre arrival time of the burst at infinite frequency. For a description of the data processing, see the Methods section. *Top:* De-dispersed time series of all available data on FRB 200428 (see Methods). The original data were de-dispersed at a DM of 332.702 pc cm^{-3}. We detect no other radio bursts within our data, spanning a window of 131.072 ms, the total amount of data stored around this event, centred on the time of FRB 200428. We place an upper limit on bursts with S/N> 5 in this time window of < 400 kJy ms. The relative arrival time of the second, brighter peak in the coincident X-ray burst (XP2) is indicated as a vertical dashed line (Mereghetti et al., 2020; Li and B. Zhang, 2020). The full X-ray burst lasted approximately 1 s centred on UTC 14:34:24.444 (arrival time at the Earth center). *Middle:* Expanded plot of the region surrounding the burst. *Bottom:* Dynamic spectrum of FRB 200428 corrected for the effects of dispersion.

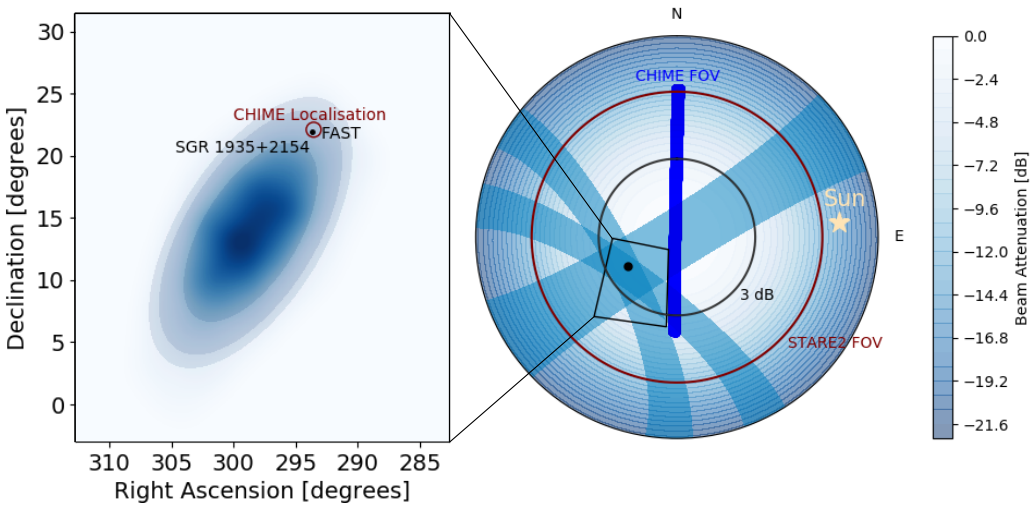

Figure 3.2: STARE2 localisation of FRB 200428. *Right:* An altitude and azimuth view of the sky at the OVRO STARE2 station at the time FRB 200428 was detected. The maroon circle corresponds to the STARE2 field of view (FOV), which is set by the edge of a horizon shield at OVRO (Christopher D. Bochenek et al., 2020). A black circle labelled "3 dB" indicates the zenith angle corresponding to the FWHM of the STARE2 response on the sky. The thick blue line represents the CHIME FOV. The star represents the Sun, which is a common source of STARE2 triggers (Christopher D. Bochenek et al., 2020). The black dot represents the known position of SGR J1935+2154. The three light blue arcs correspond to the 95%-confidence localisations for each individual STARE2 baseline. The black quadrilateral represents the outline of the region shown in the left panel. *Left:* From inside to outside, the ellipses represent the 68.4%, 90%, and 95% confidence STARE2 localisation regions of FRB 200428. The blue gradient corresponds to the probability the burst occurred at that location. The CHIME localisation region (CHIME/FRB Collaboration, Andersen, et al., 2020) corresponds approximately to the maroon circle. The known position of SGR J1935+2154, which is identical to the position of the weak burst detected by FAST (C. F. Zhang et al., 2020), is shown as a black dot.

detected (C. F. Zhang et al., 2020) a weak (0.06 Jy ms) burst in the 1.02–1.48 GHz band and localized it to within 3 arcminutes (the size of FAST's beam) of SGR J1935+2154. The DM links the CHIME, STARE2, and FAST bursts with the best localization proved by FAST. The temporal coincidence of the CHIME, STARE2, and X-ray bursts then link FRB 200428 to SGR J1935+2154.

Table 3.1: Data on FRB 200428. Standard errors in the final significant figures (68% confidence) given in parentheses.
[a] The correction to the infinite-frequency ($\nu = \infty$) arrival time is done using the DM quoted in this table, and assuming a dispersion constant of $\frac{1}{2.41} \times 10^4$ s MHz^2 pc^{-1} cm^3. (R. Manchester and Taylor, 1980)
[b] The full-width half-maximum (FWHM) of the Gaussian used to model the intrinsic burst structure (Methods).
[c] This assumes a distance to SGR J1935+2154 of 9.5 kpc.

Property	Measurement
OVRO arrival time at ν = 1529.267578 MHz (UTC)	28 April 2020 14:34:25.02657(2)
OVRO arrival time at $\nu = \infty$[a] (UTC)	28 April 2020 14:34:24.43627(3)
Earth centre arrival time at $\nu = \infty$[a] (UTC)	28 April 2020
Fluence (MJy ms)	1.5(3)
Dispersion measure (pc cm^{-3})	332.702(8)
Intrinsic burst FWHM[b] (ms)	0.61(9)
Isotropic-equivalent energy release[c] (erg)	$2.2(4) \times 10^{35}$

3.2 Observational classification

The fluence of FRB 200428 is unprecedented for a neutron star. Adopting a distance of 9.5 kpc (see Kothes et al., 2018; P. Zhou, X. Zhou, et al., 2020; Kozlova et al., 2016) we infer an isotropic-equivalent energy release of $2.2(4) \times 10^{35}$ erg, and the spectral energy release was $1.6(3) \times 10^{26}$ erg Hz^{-1} (see Methods). Previously, giant radio pulses (GRPs) from pulsars (Kuzmin, 2007) were the brightest known sources of Galactic radio pulses. GRPS are emitted stochastically amongst regular radio pulses but have sub-microsecond durations, unlike millisecond duration of the observed FRBs including FRB 200428. The brightest and most luminous GRP to date was observed at 430 MHz from the Crab pulsar had a fluence of 3×10^4 Jy ms and an isotropic-equivalent energy release of 6×10^{31} erg[7]. FRB 200428 is therefore a factor of approximately 4×10^3 more energetic than any millisecond radio burst previously observed from a source within the Milky Way.

From Figure 3.3, we see that FRB 200428 is most plausibly related to the fast radio bursts (FRBs) observed at extragalactic distances. FRBs span a wide range of energies, but the least energetic FRB reported to date (from FRB 180916.J0158+65) had an isotropic-equivalent spectral energy of just $5(2) \times 10^{27}$ erg Hz^{-1} at 1.7 GHz[8]. Using the parameters from Table 1, the brightness temperature of FRB 200428 is approximately 1.4×10^{32} K, consistent with those of FRBs (Petroff, Hessels,

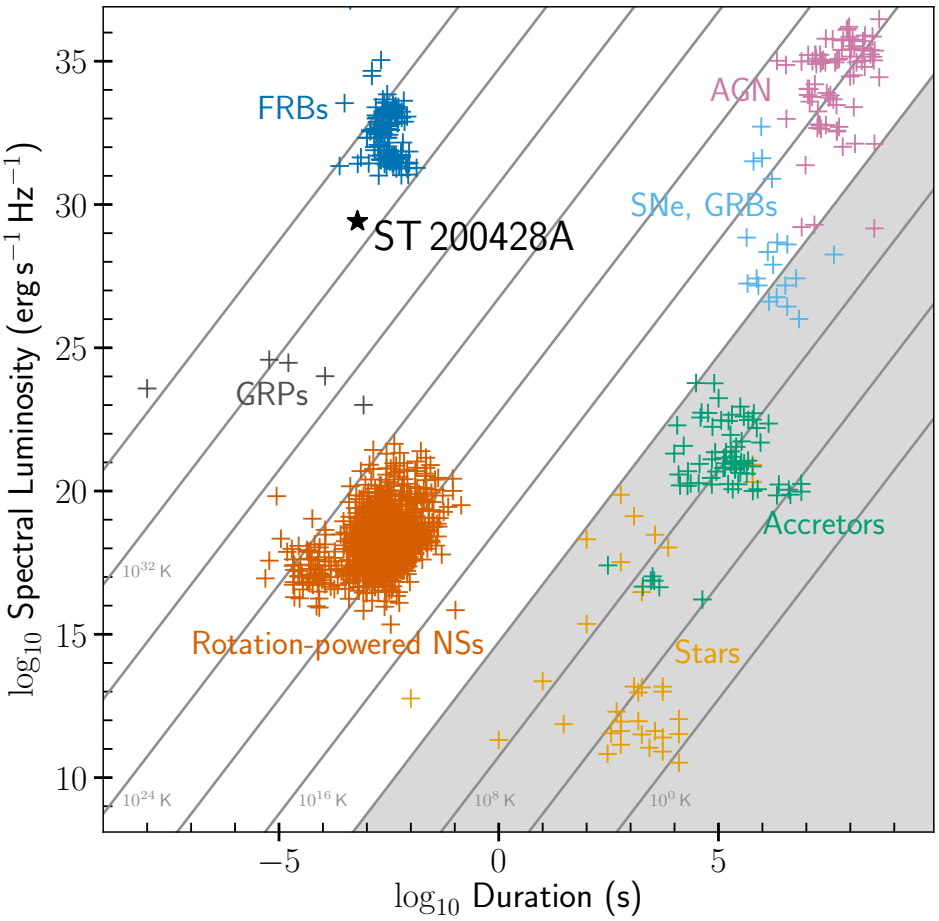

Figure 3.3: Phase space of centimetre-wavelength radio transient events. The vertical extent of the FRB 200428 star corresponds to the uncertainty in the spectral luminosity caused by the uncertain distance to SGR J1935+2154, which ranges between 6.5–12.5 kpc (Kothes et al., 2018; P. Zhou, X. Zhou, et al., 2020; Kozlova et al., 2016). Only isotropic-equivalent spectral luminosities are shown. The FRBs plotted only include bursts detected between 1–2 GHz from sources at known distances. All other data were gathered from E. F. Keane (2018) and Villadsen and Hallinan (2019). "GRPs" refers to giant radio pulses, "Rotation-powered NSs" refers to rotating radio transients and rotation-powered pulsars, "accretors" refers to accreting binary systems in the Milky Way, "SNe" and "GRBs" refers to supernovae and γ-ray bursts at extragalactic distances, and "AGN" refers to accreting supermassive black holes. All radio transients plotted are detections between 1 GHz–2 GHz. Lines of constant brightness temperature at a reference frequency of 1.4 GHz are shown, and the shaded area (representing brightness temperatures less than 10^{12} K) indicates sources that are likely incoherent emitters that are not relativistically boosted. The spectral luminosity of FRB 200428 was derived by dividing the burst spectral energy by the duration.

and Lorimer, 2019). Since the first announcement, the CHIME/FRB collaboration revised the flux and fluence of FRB 200428 (CHIME/FRB Collaboration, Andersen, et al., 2020). The factor of seven disparity, which is likely intrinsic, between the fluence of FRB 200428 and that of the CHIME event is consistent with previous wide-band radio observations of FRBs (Sokolowski et al., 2018).

We have observed no other FRB-like radio bursts besides FRB 200428 during 448 days of observing. STARE2 has a detection threshold of 300 kJy for millisecond duration bursts within a field-of-view of 1.84 steradian, which corresponds to the 3 dB beamwidth (see Methods). We have observed no other radio bursts from SGR J1935+2154 despite the occurrence of 79 X-ray bursts visible to STARE2 (see Methods).

Based on the entirety of the STARE2 observing campaign, we derive a volumetric rate for bursts with energy releases equivalent to or greater than FRB 200428 of $7^{+9}_{-6} \times 10^7\,\mathrm{Gpc^{-3}\,yr^{-1}}$, where 1σ uncertainties are quoted. At 95% confidence, the volumetric rate is $> 4 \times 10^6\,\mathrm{Gpc^{-3}\,yr^{-1}}$. This rate is consistent with an extrapolation of the luminosity function of bright FRBs (see Methods).

SGR J1935+2154 is located approximately 100 pc above the plane of the Milky Way disk and situated at the centre of a known supernova remnant (Kothes et al., 2018). Such a locale is consistent with those of six of the seven accurately localised FRBs within their host galaxies (Marcote, Nimmo, et al., 2020; K. W. Bannister et al., 2019; V. Ravi et al., 2019; J. Xavier Prochaska et al., 2019; J. P. Macquart, J. X. Prochaska, et al., 2020). These six host galaxies are similar to the Milky Way in their masses and star-formation rates. There is no evidence for a significant DM enhancement locally to SGR J1935+2154 (see Methods). The Faraday rotation measure (RM) of the weak radio pulse detected by FAST from SGR J1935+2154 is consistent with the RM of radio emission from the associated supernova remnant at the position of SGR J1935+2154 (Kothes et al., 2018), implying no significant enhancement in the plasma magnetisation immediately surrounding the SGR.

3.3 Implications for FRBs

We have established that FRB 200428 is arguably drawn from the same population as the observed FRB sample. This implies that magnetars like SGR J1935+2154 are viable FRB engines. However, it is puzzling that events like FRB 200428 have not previously been observed from SGR J1935+2154, or from any of the 30 known magnetars in the Milky Way (Victoria M. Kaspi and Beloborodov, 2017),

especially since SGR J1935+2154 is not extraordinary in its spin period or magnetic field compared to other Galactic magnetars. This may be due to the fact that bursts this bright are often flagged as RFI or saturate receivers. Furthermore, the X-ray burst coincident with FRB 200428 (isotropic-equivalent energy release of $8.3(8) \times 10^{39}$ erg) was a typical example of a magnetar burst (Victoria M. Kaspi and Beloborodov, 2017), with perhaps some unusual spectral characteristics (Li and B. Zhang, 2020). So apparently, only a subset of X-ray bursts are accompanied by bright radio emission.

The properties of FRB 200428 and the rarity of similar events provide insight into the emission mechanism of FRBs. The temporal coincidence of FRB 200428 with an X-ray burst is not fully consistent with models in which FRB emission is generated within the magnetospheres of magnetars. If the X-ray burst is emitted through standard mechanisms, magnetospheric FRB emission is predicted to occur immediately prior to the X-ray bursts (Lu and Pawan Kumar, 2018). Indeed, X-ray bursts appear to suppress magnetospheric radio emission from the magnetar-like pulsar PSR J1119-6127 for several tens of seconds (Archibald et al., 2018).

The energetics of FRB 200428 and its coincident X-ray burst are consistent with some models for FRB emission from beyond the magnetospheres of magnetars. Models for FRB emission external to magnetospheres have only been developed for the most energetic X- and γ-ray bursts from magnetars, known as giant flares. An event that manifests as a giant flare is also predicted to result in the ejection of a highly magnetised portion of the magnetar magnetosphere at relativistic speeds, known as a "plasmoid". Although plasmoids are distinct from the observed X- and γ-ray radiation from giant flares, they are expected to contain comparable amounts of energy ($> 10^{44}$ erg) (Yu. Lyubarsky, 2014; Beloborodov, 2017; Metzger, Margalit, and Sironi, 2019). An FRB radiated by the synchrotron maser mechanism may result from a shock driven by the plasmoid into the external medium (Yu. Lyubarsky, 2014; Beloborodov, 2017; Metzger, Margalit, and Sironi, 2019). Alternatively, the plasmoid may trigger an electromagnetic pulse just beyond the magnetosphere, resulting in an FRB (Yuri Lyubarsky, 2020). FRB energies of $10^{-7}E_{\mathrm{p}l}$ to $10^{-4}E_{\mathrm{p}l}$ are predicted by these models. The ratio between the radio energy release of FRB 200428 and the X-ray energy release of the coincident burst is approximately 3×10^{-5}, consistent with these predictions for the energy of the radio burst.

In this scenario, individual X-ray bursts from magnetars would result in radio emission being relativistically beamed in random directions, explaining the rarity

of events like FRB 200428. However, it remains to be seen whether the theory developed for plasmoids launched by giant magnetar flares can be extended to lower-energy events like the 10^{40} erg X-ray burst coincident with FRB 200428. The close coincidence between FRB 200428 and the associated X-ray burst (Figure 3.1) is difficult to explain if the FRB were launched extremely far from the magnetosphere (Beloborodov, 2017), unless the X-ray emission was not associated with the FRB-emitting region.

Our observations suggest that magnetars like those observed in the Milky Way can produce FRBs. We estimate that the volumetric rate of events like FRB 200428 is consistent with a low-energy extrapolation of the FRB volumetric rate (Lu and Piro, 2019). This suggests that we have observed the dominant FRB channel. However, it is by no means proven that magnetars can produce the highest luminosity FRBs. There may be other surprises such as the discovery of FRBs from galaxies lacking star-formation. The link between SGRs and FRBs and the large inferred rate of low-luminosity FRBs implied by the detection of FRB 200428 provide motivations for dedicated radio burst searches from nearby, rapidly star-forming galaxies such as the nearby Messier 82, which has a star-formation rate more than 10 times that of the Milky Way (Jarrett et al., 2019).

3.4 Methods

The STARE2 instrument

STARE2 consists of a set of three radio receivers at locations across the south-western United States. The receivers are located at the Owens Valley Radio Observatory (OVRO), the Goldstone Deep Space Communications Complex (GDSCC), and a site operated by the Telescope Array project[35] near Delta, Utah. Although the STARE2 receivers operate in the 1280 MHz–1530 MHz band, the useful band is limited to 1280.732422 MHz to 1468.232422 MHz by radio-frequency interference. STARE2 is sensitive to fast, dispersed radio transients above a detection threshold of 300 $(\frac{w}{1\,ms})^{\frac{1}{2}}$ kJy, where w is the width of the burst. STARE2 has a time resolution of 65.536 µs and frequency resolution of 122.07 kHz. The instrument and data analysis are further described elsewhere (Christopher D. Bochenek et al., 2020). Since the publication of Christopher D. Bochenek et al. (2020), our station in Delta, Utah commenced operations. With the addition of the third station, we now visually inspect candidate bursts if any pair of stations identifies a candidate event within 100 ms of each other.

STARE2 data consist of (a) candidate dispersed bursts that triggered the automated pipeline software, and (b) spectra recorded every 65.536 µs with 2048 frequency channels between 1280 MHz–1530 MHz. The latter data span the full duration of the dispersion sweep of each candidate burst, with an additional 1000 spectra both before and after the start and end of the dispersion sweep respectively. Such time series of spectra are referred to as dynamic spectra. After de-dispersion, the available time series data on each burst span 131.072 ms, as displayed in Figure 3.1 for FRB 200428.

To produce Figure 3.1, the OVRO dynamic spectrum was smoothed with a 2D boxcar function with a width of 0.524288 ms in time (equivalent 8 bins) and 7.8125 MHz in frequency (equivalent to 64 bins). That is not the width of the pulse. We choose this smoothing timescale so that there is sufficient signal in each pixel to be visible. Data from the other stations were not summed for the purposes of display because of the different instrumental spectral responses, but are shown in Figure 3.4. The data were baselined by subtracting the mean of the off-pulse region. We normalised the time series in each frequency bin by dividing by the standard deviation of the time series in each frequency bin, derived from the off-pulse region. The data were again normalised by the standard deviation of the off-pulse time and frequency bins to measure the signal to noise (S/N) in each time and frequency bin. To produce the time series, we simply took our dynamic spectra, which was processed as described above, and averaged the data in frequency and re-normalised by the standard deviation of the time series in the off-pulse region.

Localisation

To localise FRB 200428, we first measured the relative arrival times of the burst between each station. For this analysis, we used the frequency-averaged 65.536 µs resolution total-intensity time series data. The data were de-dispersed with the dispersion measure (DM) that maximised the signal to noise ratio (S/N) at OVRO. The time series was convolved with the boxcar function that maximised S/N at OVRO. These values are derived differently than the values reported in the main text and thus differ slightly, as it asks a different question of the data than the values that are derived through fitting the pulse profile to a model. The DM quantifies the observed frequency-dependent dispersion delay in terms of a free-electron column density. This DM and boxcar width were 333.3 pc cm^{-3} and 0.524288 ms, respectively. To measure the S/N for this analysis, we take the frequency-averaged time series that has been de-dispersed and convolved with a boxcar function and subtract the mean

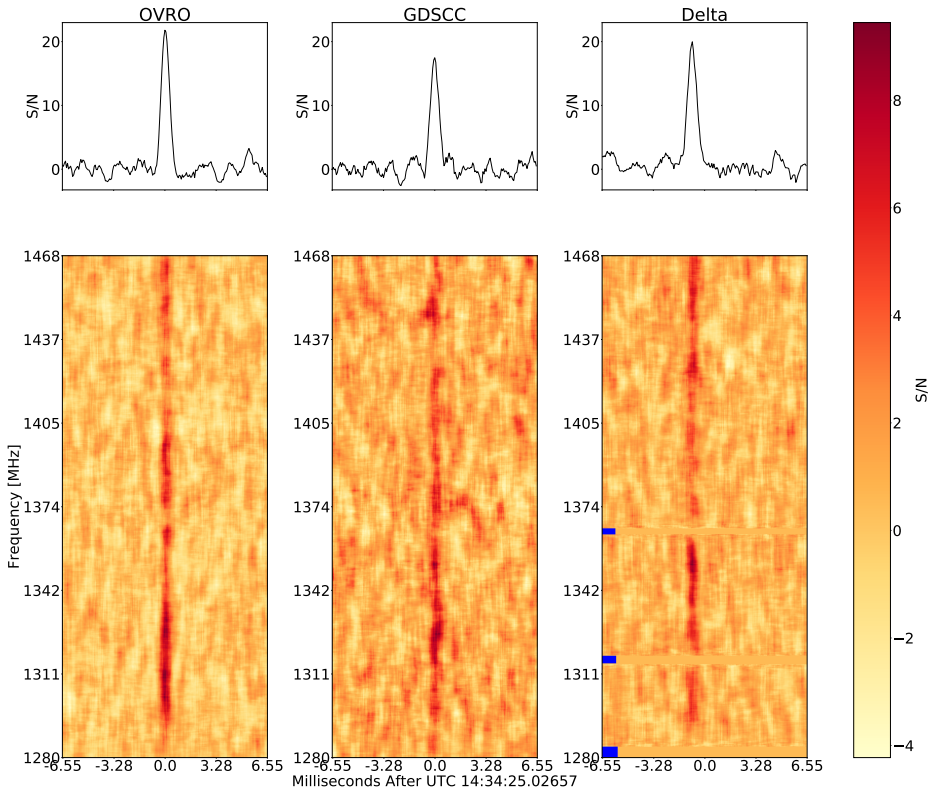

Figure 3.4: Time series and dynamic spectrum of FRB 200428 at each station. *Top panels:* Time series at each station referenced to the arrival time at OVRO at $\nu = 1529.267578$ MHz. *Bottom panels:* Dynamic spectra at each station. In all panels, the data were processed in the same way as those in Figure 3.1. We have not corrected for the spectral response at each station. The blue bars in the Delta dynamic spectrum indicate frequencies affected by radio-frequency interference that were excised from the data.

of the off-pulse region. After this subtraction, the data are divided by the standard deviation of the time series in the off-pulse region. We measure a S/N at OVRO of 21.6, at GDSCC of 15.7, and at Delta of 20.1. Data from each station are shown in Figure 3.4.

After determining the S/N at each station and processing the data as described above, we then cross-correlate the time series from each pair of stations. We fit the peak of the correlation curve with a Lorentzian function. The location of the peak of the Lorentzian corresponds to the time delay between the two stations in the baseline. We find a time delay for OVRO-GDSCC of -7 µs, -884 µs for OVRO-Delta, and -888 µs for GDSCC-Delta. The statistical uncertainty in the time delays is given by the boxcar width divided by the S/N of the station with the lowest S/N. For OVRO-

GDSCC and GDSCC-Delta, this uncertainty is 33 µs and 26 µ s for OVRO-Delta.

To estimate the systematic uncertainty, we take advantage of a test of the Global Positioning System's (GPS) L3 signal at 1381 MHz on 2019 February 28. We recorded data with a time resolution of 131.072 µs during the test. As the data were taken before the Delta station was built, this analysis was done only with OVRO and GDSCC. However, as we use an identical receiver and GPS timing hardware at the Delta station, we expect similar systematics to be present. During testing, the L3 signal turns on and off, allowing for a test of the measured time delay between each station. The intrinsic time delay of the emission of the L3 signal between two satellites is expected to be of order µs, as the GPS satellites are synchronised in transmission. Furthermore, the received signal will be dominated by the satellites closest to zenith. At the time of the signal considered, the satellite expected to dominate the signal had an expected time delay of 46 µs between OVRO and GDSCC. This is less than the time resolution of our data. We measure the time delay as described above, except in this analysis we only consider frequencies corresponding to the L3 signal and do not convolve our time series with a boxcar function. We find a systematic uncertainty of 81 µs, which represents the measured time delay of the GPS L3 signal between OVRO and GDSCC.

To turn the measured time delays for FRB 200428 into a sky position, for each baseline we calculate the expected time delay for a given sky location over a fine grid in azimuth and elevation at a reference location. The reference location is chosen to be OVRO for the OVRO-GDSCC and OVRO-Delta baselines, while GDSCC is chosen for the GDSCC-Delta. We then transform the grid of azimuths and elevations into right ascensions and declinations for the time of the burst. The localisation for one baseline is then those sky positions that are consistent with the measured time delays and uncertainties. This corresponds to an arc across the sky for one baseline.

To combine the baselines, we assign a probability to each sky location for each arc assuming Gaussian statistical and systematic uncertainties, parameterised by the distance from the arc with no uncertainty. The mean of the Gaussian corresponds to the arc with no uncertainty and the standard deviation corresponds to the width of the arc assuming a 1σ uncertainty in the time delay. The probabilities for each arc and sky location were then multiplied together and normalised. We smoothed the probability distribution with a two-dimensional Gaussian of standard deviation 1°. The transformation between local coordinate systems and the celestial coordinate

system produced a sparse array of probabilities that required smoothing to visualise. The smoothing radius is much smaller than the size of the localisation region. This produced the probabilities shown in the right panel of Figure 3.2 as arcs.

With these probabilities, we measured the 95% confidence interval of the STARE2 three-station localisation region by modelling it as an ellipse. The 95% confidence interval corresponds to the smallest ellipse that encloses 95% of the probability distribution. To estimate this ellipse, we first measured the orientation of the ellipse. We measured the angle of the semi-major axis with respect to the declination axis by modelling the sky location probability distribution using a principle component analysis with two components. The angle of the semi-major axis corresponds to the angle of the eigenvector of the principle component with the highest eigenvalue. This angle is 57.88°. We calculated the expectation values of the right ascension and declination directly from their marginalised probability distributions. We find a right ascension of α =19d55m±15° and a declination of δ =14d±19°. The uncertainties contain 95% of the probability in each dimension. We then fit for the semi-major axis and semi-minor axis by minimising the loss function in Equation 3.1 using gradient descent. In Equation 3.1, $p(\alpha', \delta')$ is the probability the event occurred at that sky location, a is the semi-major axis, b is the semi-minor axis, and λ is a regularisation hyperparameter that we set to 2.7×10^{-2}. This regularisation corresponds to the ellipse area contributing approximately equally to the loss as the confidence interval when $|\int_{ellipse} p(\alpha', \delta') d\alpha' d\delta' - 0.95| < 0.001$. We find that $a = 12.3°$ and $b = 5.85°$. To derive the 68.4% and 90% confidence regions, we scale the ratio of the semi-major and semi-minor axis of the 95% confidence ellipse so that the appropriate amount of probability is contained.

$$\mathcal{L}(a, b) = (\int_{ellipse} p(\alpha', \delta') d\alpha' d\delta' - 0.95)^2 + \lambda a b \tag{3.1}$$

Properties of FRB 200428

The dynamic spectrum of FRB 200428 was analysed using methods previously applied to FRBs detected at the Parkes telescope (Vikram Ravi, 2019a). First, the dynamic spectra of FRB 200428 at the native time and frequency resolutions (65.536 µs and 122.07 kHz) obtained from OVRO and GDSCC were summed. No correction for the OVRO-GDSCC geometric arrival-time delay was applied because the correction (−7 µs) is much smaller than the time resolution. Data from Delta were not included in the sum, and in subsequent analysis, because of the increased

presence of RFI at the Delta station (Figure 3.4). No calibrations were applied to the data, as none were available. After excising frequency ranges at the edges of the band that are always affected by radio-frequency interference and are set to zero in the real-time pipeline (1468.232422 MHz–1529.267578 MHz and 1279.267578 MHz–1280.732422 MHz), we formed time series in four evenly spaced sub-bands after de-dispersing at an initial DM of 332.72 pc cm^{-3} (CHIME/FRB Collaboration, Andersen, et al., 2020). The time series in each sub-band were normalised by the rms noise level in 50 ms intervals of data on either side of the burst. As described in Vikram Ravi (2019a), we fit a series of models with increasing complexity, stopping when the Bayes Information Criterion (BIC) does not favour the more complex models. We found that a model combining an intrinsic width in excess of the dispersion-smeared instrumental resolution, convolved with a one-sided exponential function with a characteristic timescale scaling as ν^{-4}, was negligibly preferred according to a change in BIC of 1 unit. Here, ν is the radio frequency. This corresponds to Model 3 of Vikram Ravi (2019b) with $\alpha = 4$. The free parameters of the fit were the intrinsic width of the burst (assumed to be frequency-independent), a reference arrival time at 1529.267578 MHz, a correction to the assumed DM, the $1/e$ timescale of the exponential function, and the burst fluences in each sub-band in data units. The convolution with the exponential is observed in several FRBs and radio pulsars, and is expected due to stochastic multi-path propagation of the burst due to refraction in inhomogeneous interstellar plasma (James M. Cordes and Shami Chatterjee, 2019). This effect is commonly referred to as "scattering". Despite the insignificant evidence favouring the above model over a version of this model with no scattering, we adopt it because scattering was observed in the CHIME-detected event temporally coincident with FRB 200428 (CHIME/FRB Collaboration, Andersen, et al., 2020).

The resulting best-fit burst parameters and the half-widths of their 68% confidence intervals are given in Table 1. The $1/e$ timescale of the scattering, scaled to a frequency of 1 GHz as is common practise in the field (Vikram Ravi, 2019a), was 0.4(1) ms. The model fits in each sub-band are shown in Figure 3.5. The quoted band-averaged fluence (with an effective frequency of 1378 MHz) was derived by averaging the fluences in each sub-band, and by scaling by the noise level according to the measured STARE2 system-equivalent flux density of 19 ± 2 MJy (Christopher D. Bochenek et al., 2020) and the binning in frequency and time. An additional scaling of 1.33 was applied to correct for the location of the burst in the STARE2 primary beam, which was negligibly different at OVRO and GDSCC. The isotropic-

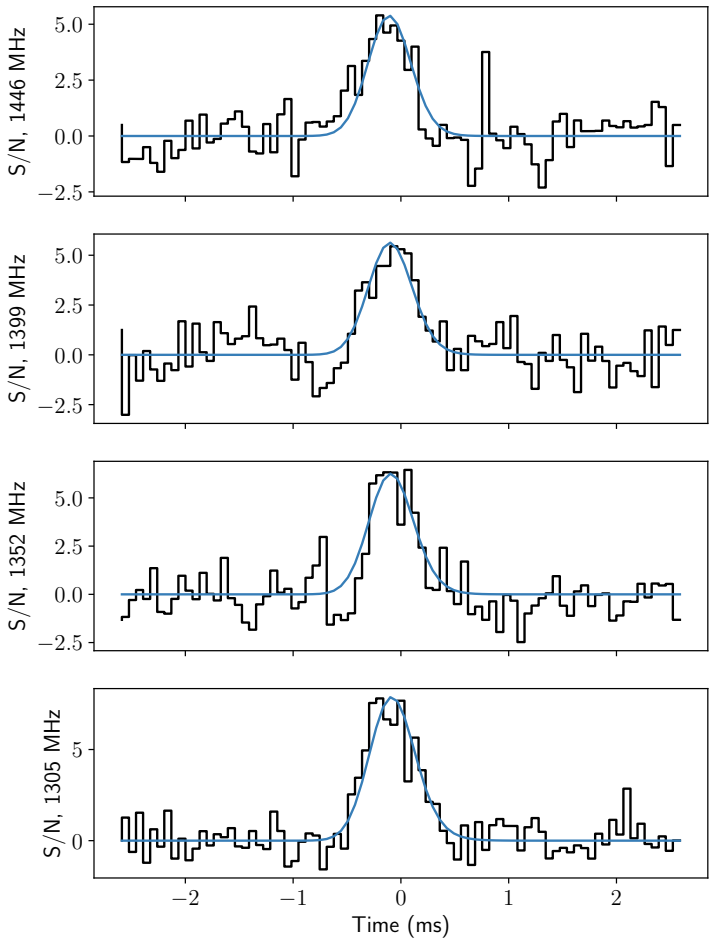

Figure 3.5: Fits to data on ST200428A in four sub bands. The raw data are shown as stepped black lines, and the best-fit model is shown as smooth blue lines. The sub-band centre frequencies are indicated beside each plot.

equivalent energy release of FRB 200428 was calculated by scaling the fluence (in appropriate units) by $4\pi D^2 \nu_0$, where D is the distance to SGR J1935+2154 and $\nu_0 = 1374.482422\,\mathrm{MHz}$ is the midpoint of the STARE2 band. This procedure was consistent throughout the paper.

The burst had an intrinsic width of 0.61(9) ms. As we do not coherently dedisperse our data, it is possible that there is unresolved structure to the burst. However, the intra-channel smearing timescale is 0.122 ms and the scattering timescale at 1.32 GHz is 0.312 ms (Kirsten et al., 2020). This leads us to conclude there is

intrinsic structure throughout the 0.61(9) ms burst.

The adopted distance to SGR J1935+2154 is consistent with the DM of FRB 200428. According to two models for the Galactic distribution of free electrons, this DM corresponds to distances of 6–13 kpc (Yao, R. N. Manchester, and Wang, 2017) and 4–16 kpc (J. M. Cordes and Lazio, 2002). However, the significant uncertainties in these models and in the distance to SGR J1935+2154 make it difficult to numerically constrain any potential DM excess associated with the SGR. The DMs in the two models corresponding to the lowest possible distance (6.6 kpc; P. Zhou, X. Zhou, et al., 2020) to SGR J1935+2154 are approximately 200 pc cm^{-3} (J. M. Cordes and Lazio, 2002) and 190 pc cm^{-3} (Yao, R. N. Manchester, and Wang, 2017). Thus, an approximate upper limit to any potential DM excess associated with SGR J1935+2154 is 140 pc cm^{-3}.

The analysis of the burst dynamic spectrum presented above provides a reference arrival time at 1529.267578 MHz. This refers to the midpoint of the Gaussian function used to model the intrinsic burst structure. We note that it is unlikely that the burst is truly Gaussian in its intrinsic structure, and that the presence of complex structure in the time-frequency plane (as is observed in some FRBs (Hessels et al., 2019)) could bias this result at the approximately 0.1 ms level. The reference arrival time was converted to a UTC arrival time at OVRO using the recorded UTC of the first spectrum in the data set. This time was converted to an arrival time at infinite frequency ($\nu = \infty$) using the fitted DM of 332.702(8) pc cm^{-3}, and a dispersion constant of $\frac{1}{2.41} \times 10^4$ s MHz^2 pc^{-1} cm^3 (R. Manchester and Taylor, 1980). The Earth centre arrival time was then calculated by adding a correction of 0.019210268 s to the OVRO arrival time. This correction was derived using the known position of the OVRO station and the v2.0 astropy software package (Astropy Collaboration et al., 2018).

Searches for sub-threshold events from SGR J1935+2154

We searched the STARE2 data 65.536 ms before and after the burst for sub-threshold pulses at the same DM, and widths ranging from 0.066 ms–4.194 ms at each station. We found no convincing candidates. Assuming we would detect a burst with S/N>5, we place a limit on the fluence of other bursts in this time range of <400 kJy ms. This fluence is obtained by scaling the measured fluence by the median S/N reported by our pipeline (18.3) divided by our sub-threshold search threshold of 5. We choose to use the median S/N reported by our pipeline because we require detections from

2 stations in order to claim that there is evidence for other pulses.

We only detect one component in FRB 200428, whereas the coincident CHIME event (CHIME/FRB Collaboration, Andersen, et al., 2020) consists of two components. We identify the second CHIME burst as the lower-frequency component to the STARE2 burst, as the geocentric arrival time at infinite frequency reported in Table 3.1 is consistent with that reported by the CHIME/FRB collaboration of 2020-04-28 14:34:24.24.45547(2) (CHIME/FRB Collaboration, Andersen, et al., 2020). We place an upper limit on the L-band emission from the first CHIME component of 400 kJy ms.

Rate calculation

STARE2 had been observing for 448 days prior to FRB 200428. For the first 290 days, STARE2 observed only with its stations at OVRO and GDSCC. We observed with all three stations for 158 days before FRB 200428. Throughout this time, in addition to FRB 200428, we detected several solar radio bursts (Christopher D. Bochenek et al., 2020), but no other radio burst above a detection threshold of approximately 300 kJy $\sqrt{\mathrm{m}s}$.

To measure the all-sky rate of fast radio transients above the energy of FRB 200428, we first modelled the population of fast radio transients as a Poisson process. We then calculated our effective observing time for two epochs of observation. The first epoch corresponds to our two-station system, and the second epoch corresponds to our three-station system. We used the single-station completeness reported in Christopher D. Bochenek et al. (2020) and an effective solid angle of 1.84 steradians to convert our observing time into an effective observing time. The single-station completeness gives the two-station system a completeness of 0.56 and the three-station system a completeness of 0.95. The solid angle was chosen such that the median S/N reported by our detection pipeline (18.3) would be at the detection threshold of 7.3 at the edge of the solid angle. This gives the area for which a burst of this fluence would have been detected. Using these parameters, we estimate a total effective observing time of 0.468 years.

We then computed the probability of the all-sky rate for rates ranging from 0 $\mathrm{sky}^{-1}\ \mathrm{yr}^{-1}$ to 40 $\mathrm{sky}^{-1}\ \mathrm{yr}^{-1}$ given that we observed for 0.468 years before we found a burst. We find the all-sky rate of fast radio transients above 1.5 MJy ms is $3.58^{+3.44}_{-2.03}$ $\mathrm{sky}^{-1}\ \mathrm{yr}^{-1}$. The reported uncertainties are 1σ uncertainties.

To estimate the volumetric rate of this type of transient, we use the formalism

developed in Christopher D. Bochenek et al. (2020) which converts the all-sky rate of transients in a particular galaxy into a volumetric rate. The key assumption in this formalism is that the transient linearly tracks star-formation activity. This is justified by the fact that magnetars are young objects, that this object is in the plane of the Milky Way, and is associated with a supernova remnant (Kothes et al., 2018). Using our computed all-sky rate, a star formation rate in the Milky Way of $1.65 \pm 0.19\,\mathrm{M_\odot\,yr^{-1}}$ (Licquia and Newman, 2015), and a volumetric star formation rate of $1.95 \times 10^{-2}\,\mathrm{M_\odot\,Mpc^{-3}yr^{-1}}$, (Salim, Rich, et al., 2007) we find that the volumetric rate of this type of transient is $7.23^{+8.78}_{-6.13} \times 10^7\,\mathrm{Gpc^{-3}\,yr^{-1}}$. This is consistent with the inferred rate making an alternative assumption that transients like FRB 200428 track the stellar mass of their hosts. This volumetric rate is consistent with extrapolating the luminosity function derived from a sample of bright FRBs from the Australian Square Kilometre Array Pathfinder reported in Lu and Piro (2019) down to the energy of this burst. The volumetric rate of this burst along with the FRB luminosity function is shown in Figure 3.6. We note that the uncertainties in the volumetric rate extrapolation are extremely conservative, as they do not take into account the fact that the uncertainties in the parameters in this luminosity function are correlated. For a version of this plot that takes this into account, see Lu, Pawan Kumar, and B. Zhang (2020).

Using our measured volumetric rate, we can compare it to the volumetric rate derived for a sample of ASKAP FRBs (Lu and Piro, 2019). This ASKAP rate is $10^{2.6\pm0.4}\,\mathrm{Gpc^{-3}\,yr^{-1}}$ above $10^{32}\,\mathrm{erg\,Hz^{-1}}$. We fit these two data points to the model given in Equation 3.2, where $\Phi_{FRB}(>E)$ is the volumetric rate of FRBs with energy greater than E, α is the slope of the luminosity function of FRBs, and ϕ_0 is the volumetric rate of FRBs with $E > 10^{32}\,\mathrm{erg\,Hz^{-1}}$.

$$\log_{10}\Phi_{FRB}(>E) = \alpha(\log_{10}E - 32) + \phi_0 \tag{3.2}$$

We assumed a uniform prior for ϕ_0 and α, a Poisson likelihood on the STARE2 rate, and used the posterior distribution from Lu and Piro (2019) as the likelihood of the ASKAP rate. We find that $\alpha = -.91^{+.09}_{-.06}$ and $\phi_0 = 2.76^{+.39}_{-.17}$, where the uncertainties correspond to the 1σ confidence interval.

STARE2 limits on other X-ray bursts from SGR J1935+2154

We looked through our metadata of candidate events triggered by a single station for possible missed triggers coincident with previously reported flares from SGR

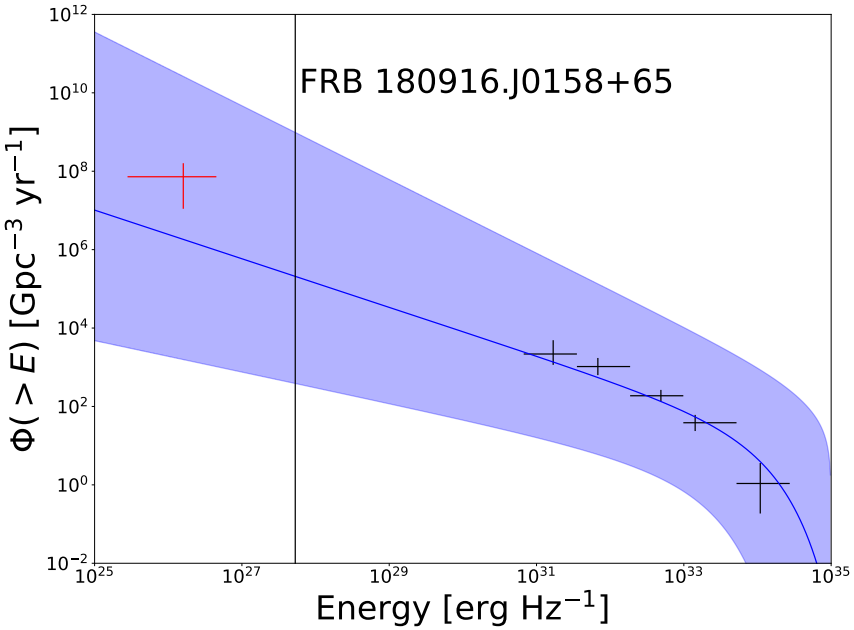

Figure 3.6: Volumetric rates of FRBs. This figure shows the volumetric rate, $\Phi(>E)$, calculated from the radio burst from SGR J1935+2154 (red cross) compared with the extrapolated luminosity function of bright FRBs (Lu and Piro, 2019) (blue shaded region). The black crosses represent the volumetric rate of FRBs determined from the ASKAP Fly's Eye sample (Lu and Piro, 2019). We note that correlated probabilities between the parameters of luminosity function are not taken into account, leading to an overestimate of the uncertainty in the blue shaded region. See Lu, Pawan Kumar, and B. Zhang (2020) for a similar plot where they are taken into account. The volumetric rate was calculated by modelling the population of Galactic fast radio transients as a Poisson process and assuming that these fast radio transients track star formation. The uncertainties on this measurement are 1σ statistical uncertainties in addition to the maximum range of possible distances to SGR J1935+2154 (4–16 kpc) (J. M. Cordes and Lazio, 2002). We also show the energy of the weakest burst detected from FRB 180916.J0158+65, a repeating FRB, for comparison Marcote, Nimmo, et al., 2020. The volumetric rate of Galactic fast radio transients is consistent with extrapolating the luminosity function of bright FRBs to the energy of FRB 200428.

J1935+2154. Our candidate metadata consists of S/N ratios, arrival times, DMs, pulse widths, and number of DM, pulse width, and time trials that are consistent with being from the same candidate. We searched the metadata for candidates within one minute of reported X-ray bursts from SGR J1935+2154 and that had an elevation angle > 25° at OVRO at the time of the burst. We also restricted our search to candidates with DMs between 325 pc cm^{-3} and 340 pc cm^{-3}. We note that SGR J1935+2154 was the only SGR with known X-ray bursts that were visible to STARE2. We find no candidate events other than FRB 200428 that fit this criteria at any of the three STARE2 stations.

Given our single station completeness of 0.74 (Christopher D. Bochenek et al., 2020), our completeness for this analysis is expected to be approximately 0.93 for our two station system and 0.98 for our three station system. Our three station system came online on MJD 58809, and thus only observed the X-ray bursts between MJD 58966–MJD 58987.

We used our measured SEFD, typical observing bandwidth of 188 MHz, and threshold S/N of 7.3 to compute an upper limit on millisecond-duration radio transients for each event. We also apply a beam correction for each upper limit corresponding to the position of SGR J1935+2154 at OVRO. Our limits are shown in Figure 3.7. We include FRB 200428 as a blue dot. We also show our results along with the list of X-ray bursts in Table 3.2.

Table 3.2: STARE2 7.3σ upper limits on reported X-ray bursts from SGR J1935+2154 that occurred in the STARE2 field of view.
[a] The upper limits represent a threshold S/N of 7.3σ.
[b] "GCN" refers to the GRB Circular Network and "ATel" refers to the Astronomers Telegram.

MJD	**OVRO Elevation**	**Limit (MJy $\sqrt{ms}$)**[a]	**Citation**[b]
58791.44753023148	32°	1.65	GCN 26242
58792.257743055554	75°	0.17	GCN 26242
58792.06695601852	29°	1.65	GCN 26171
58791.07959490741	31°	1.65	GCN 26169
58791.44752314815	32°	1.65	GCN 26160
58791.38741898148	49°	0.39	GCN 26160
58791.27361111111	74°	0.17	GCN 26153

Continued on next page

Table 3.2 – continued from previous page

MJD	OVRO Elevation	Limit (MJy $\sqrt{ms}$)[a]	Citation[b]
58760.375621527775	73°	0.17	GCN 25975
58967.77195601852	75°	0.17	GCN 27667
58966.822041064814	71°	0.18	GCN 27667
58966.91622886574	46°	0.53	GCN 27667
58966.98925520833	25°	2.51	GCN 27667
58966.76828703703	74°	0.17	ATel 13675
			GCN 27689
58966.77290509259	74°	0.17	GCN 27664
58966.843981481485	66°	0.21	GCN 27664
58966.77222222222	74°	0.17	GCN 27663
58966.78204861111	75°	0.17	GCN 27663
58966.97083333333	30°	1.65	GCN 27663
58966.83456018518	68°	0.18	GCN 27661
			ATEL 13748
58966.91392361111	47°	0.53	GCN 27661
58966.82204861111	71°	0.18	ATEL 13748
58966.822916666664	70°	0.18	ATEL 13748
58966.83023148148	69°	0.18	ATEL 13748
58966.83445601852	68°	0.18	ATEL 13748
58966.838425925926	67°	0.21	ATEL 13748
58966.84224537037	66°	0.21	ATEL 13748
58966.84280092592	66°	0.21	ATEL 13748
58966.84364583333	66°	0.21	ATEL 13748
58966.87943287037	56°	0.3	ATEL 13748
58966.885243055556	55°	0.3	ATEL 13748
58966.885833333334	55°	0.3	ATEL 13748
58966.88952546296	54°	0.3	ATEL 13748
58966.892372685186	53°	0.3	ATEL 13748
58966.893599537034	52°	0.39	ATEL 13748
58966.903275462966	50°	0.39	ATEL 13748
58966.90493055555	49°	0.39	ATEL 13748
58966.946388888886	37°	1.1	ATEL 13748
58966.94936342593	37°	1.1	ATEL 13748

Continued on next page

Table 3.2 – continued from previous page

MJD	OVRO Elevation	Limit (MJy $\sqrt{ms}$)[a]	Citation[b]
58966.955092592594	35°	1.1	ATEL 13748
58966.960335648146	33°	1.1	ATEL 13748
58966.987974537034	26°	2.51	ATEL 13748
58985.758935185186	72°	0.18	ATEL 13748
58967.59783008102	32°	1.65	ATEL 13729
58967.59789236111	32°	1.65	ATEL 13729
58967.60722395833	35°	1.1	ATEL 13729
58967.71905366898	66°	0.21	ATEL 13729
58967.792013287035	74°	0.17	ATEL 13729
58967.79305381944	74°	0.17	ATEL 13729
58969.58160091435	29°	1.65	ATEL 13729
58969.6540966088	50°	0.39	ATEL 13729
58969.717278206015	66°	0.21	ATEL 13729
58970.629127719905	43°	0.53	ATEL 13729
58970.635658287036	45°	0.53	ATEL 13729
58970.72921851852	70°	0.18	ATEL 13729
58972.70829861111	66°	0.21	ATEL 13729
58972.71731018519	68°	0.18	ATEL 13729
58972.88183449074	51°	0.39	ATEL 13729
58973.90270061343	44°	0.53	ATEL 13729
58975.67770486111	61°	0.24	ATEL 13729
58975.89255034722	46°	0.53	ATEL 13729
58975.950249421294	29°	1.65	ATEL 13729
58976.61089872685	43°	0.53	ATEL 13729
58976.87895075232	49°	0.39	ATEL 13729
58977.662045833335	58°	0.24	ATEL 13729
58977.80805587963	67°	0.21	ATEL 13729
58977.81765358796	65°	0.21	ATEL 13729
58978.61405034722	45°	0.53	ATEL 13729
58978.648174884256	55°	0.3	ATEL 13729
58979.78681759259	70°	0.18	ATEL 13729
58979.84469907408	56°	0.3	ATEL 13729
58979.91060440972	37°	1.1	ATEL 13729

Continued on next page

Table 3.2 – continued from previous page

MJD	OVRO Elevation	Limit (MJy $\sqrt{ms}$)[a]	Citation[b]
58979.922326388885	34°	1.1	ATEL 13729
58980.71925138889	73°	0.17	ATEL 13729
58981.786238113425	69°	0.18	ATEL 13729
58981.90814050926	37°	1.1	ATEL 13729
58982.883207824074	43°	0.53	ATEL 13729
58983.61761574074	50°	0.39	ATEL 13729
58983.810202037035	63°	0.21	ATEL 13729
58985.75893611111	72°	0.18	ATEL 13729

3.5 Acknowledgements

We would like to thank the then director of OVRO, A. Readhead, for funds (derived from the Alan Moffet Funds) which allowed us to start this project. The Caltech and Jet Propulsion Laboratory President's and Director's Fund allowed us to build the second system at Goldstone and third system near Delta, Utah. We are thankful to Caltech and the Jet Propulsion Laboratories for the second round of funding. Christopher Bochenek, a PhD student, was partially supported by the Heising-Simons foundation. We would also like to thank Sandy Weinreb and David Hodge for building the front end and back end boxes, Jeffrey Lagrange for his support at GDSCC, John Matthews and the Telescope Array collaboration for their support at Delta, and the entire OVRO staff for their support, in particular James Lamb, David Woody, and Morgan Catha. We thank Sterl Phinney and Wenbin Lu for comments on the manuscript. A portion of this research was performed at the Jet Propulsion Laboratory, California Institute of Technology, under a contract with the National Aeronautics and Space Administration. This research was additionally supported by the National Science Foundation under grant AST-1836018. This research made use of Astropy, a community-developed core Python package for Astronomy. This research has also made use of the SIMBAD database, operated at CDS, Strasbourg, France.

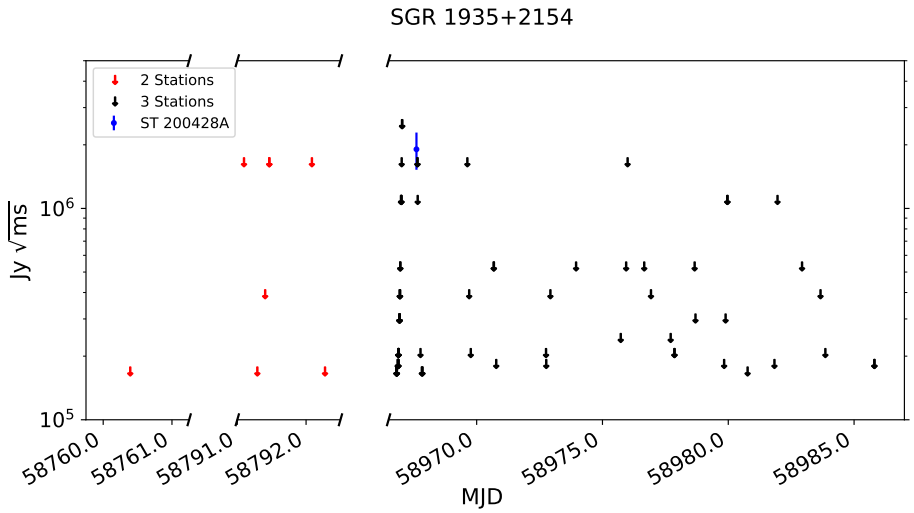

Figure 3.7: Upper limits on fast radio transients from other flares of SGR J1935+2154 observable by STARE2. The ordinate shows the 7.3σ upper limit on a potential burst's fluence in Jy $\sqrt{\text{m}s}$, while the abscissa shows the MJD of reported flares from SGR J1935+2154. The derivation of the upper limits is described in the Methods section. We note that our three station system was observing only during the flares between MJD 58966 and MJD 58987, shown in black. For the other flares, only our stations at OVRO and GDSCC were observing, shown in red. We show FRB 200428 in blue; the error bar represents the standard error in the measured fluence.

Chapter 4

LOCALIZED FRBS ARE CONSISTENT WITH MAGNETAR PROGENITORS FORMED IN CORE-COLLAPSE SUPERNOVAE

Bochenek, Christopher D., Vikram Ravi, and Dillon Dong (Feb. 2021). "Localized Fast Radio Bursts Are Consistent with Magnetar Progenitors Formed in Core-collapse Supernovae". In: *ApJL* 907.2, L31, p. L31. DOI: 10.3847/2041-8213/abd634. arXiv: 2009.13030 [astro-ph.HE].

Christopher D. Bochenek[1], Vikram Ravi[1], Dillon Dong[1]

[1]Cahill Center for Astronomy and Astrophysics, California Institute of Technology, Pasadena, CA, USA

Abstract

With the localization of fast radio bursts (FRBs) to galaxies similar to the Milky Way and the detection of a bright radio burst from SGR J1935+2154 with energy comparable to extragalactic radio bursts, a magnetar origin for FRBs is evident. By studying the environments of FRBs, evidence for magnetar formation mechanisms not observed in the Milky Way may become apparent. In this paper, we use a sample of FRB host galaxies and a complete sample of core-collapse supernova (CCSN) hosts to determine whether FRB progenitors are consistent with a population of magnetars born in CCSNe. We also compare the FRB hosts to the hosts of hydrogen-poor superluminous supernovae (SLSNe-I) and long gamma-ray bursts (LGRBs) to determine whether the population of FRB hosts is compatible with a population of transients that may be connected to millisecond magnetars. After using a novel approach to scale the stellar masses and star-formation rates of each host galaxy to be statistically representative of $z = 0$ galaxies, we find that the CCSN hosts and FRBs are consistent with arising from the same distribution. Furthermore, the FRB host distribution is inconsistent with the distribution of SLSNe-I and LGRB hosts. With the current sample of FRB host galaxies, our analysis shows that FRBs are consistent with a population of magnetars born through the collapse of giant, highly magnetic stars.

4.1 Introduction

The energetics and durations of fast radio bursts (FRBs) imply highly magnetized, compact progenitors. This has led to to magnetars being a leading explanation for the origins of FRBs (Lu and Pawan Kumar, 2018; Beloborodov, 2017; Metzger, Margalit, and Sironi, 2019; Yuri Lyubarsky, 2020; Lyutikov, 2015; Wadiasingh and Timokhin, 2019). The detection of a 1.5 MJy ms radio burst from the Galactic magnetar SGR J1935+2154 is evidence that the extragalactic fast radio bursts (FRBs) originate from magnetars (C. D. Bochenek et al., 2020; The CHIME/FRB Collaboration et al., 2020). This discovery, for the first time, allows us to study magnetars that exist beyond the Milky Way's sphere of influence. It provides us access to magnetars in a wide variety of galactic environments, and opens up the possibility of finding evidence for multiple channels of magnetar formation.

Several different mechanisms for magnetar formation have been proposed in the literature. These include magnetars born in normal core collapse supernovae (CCSNe) (Schneider et al., 2019), engine-driven CCSNe such as Type I superluminous supernovae (SLSNe-I) and long gamma-ray bursts (LGRBs) (Duncan and Thompson, 1992; Woosley, 2010; Kasen and Bildsten, 2010), the accretion induced collapse (AIC) of a white dwarf (Duncan and Thompson, 1992), and the merger of two neutron stars (NS-NS) (Giacomazzo and Perna, 2013; Giacomazzo, Zrake, et al., 2015). Engine-driven SNe, AIC events, and NS-NS mergers are all different transient events expected to form proto-neutron stars with millisecond spin periods, which are hypothesized to create a convective dynamo that amplifies the magnetic field of the newly born neutron star to magnetar strengths. No such millisecond magnetar is required from the CCSNe formation channel (referred to as the "fossil field" channel), as the magnetar simply inherits its large magnetic field through conservation of magnetic flux from its progenitor star. Figure 4.1 shows the sample of FRB hosts in relation to different transient events that may track different magnetar formation channels.

The Milky Way population of magnetars is consistent with being dominated by normal CCSNe and there is not significant evidence for other formation channels in the Milky Way. Of the magnetars and magnetar candidates in the Milky Way (Olausen and V. M. Kaspi, 2014; Esposito et al., 2020; Shriharsh Prakash Tendulkar, 2014), 16 out of 30 are associated with a supernova remnant (SNR), massive star cluster, or star forming region. When restricted to the population of magnetars with a characteristic age < 10 kyr, a population for which a SNR is less likely to

have dissipated and that has not had a significant amount of time to travel far away from its birth location, 12 out of 16 magnetars are associated with these objects. There is no indication that the Galactic magnetars originate from a special type of SN, favoring a "fossil field" origin for their strong magnetic fields (Schneider et al., 2019). In addition, Beniamini, Hotokezaka, et al. (2019) estimate that more than 12% of neutron stars are born as magnetars. In an explosion driven by a millisecond magnetar engine, excess kinetic energy would be injected into the SNR from the spin-down of the magnetar, which would be observable at late times. However, the population of SNRs associated with magnetars does not appear different than the general population of SNRs in the Milky Way (P. Zhou, Vink, et al., 2019). The millisecond magnetar hypothesis also predicts large kick velocities of order $10^3\,\mathrm{km\,s^{-1}}$ (Duncan and Thompson, 1992). However, the distribution of magnetar kick velocities is similar to that of the general NS population (Shriharsh Prakash Tendulkar, 2014; Deller et al., 2012; Ding et al., 2020). In addition, there is evidence that the stellar progenitors of magnetars span a wide range of masses (Muno et al., 2006; Davies et al., 2009; P. Zhou, Vink, et al., 2019), while the progenitors of engine-driven explosions are likely more massive than a typical CCSN (Blanchard et al., 2020).

However, the most promising explanation for the rare SLSN-I explosions is an engine driven explosion powered by a millisecond magnetar (Woosley, 2010; Kasen and Bildsten, 2010), as predicted by Duncan and Thompson (1992). Therefore, there is some evidence that there may be differences between the Galactic population of magnetars and the extragalactic population of magnetar. SLSNe-I are typically found in star forming regions of metal-poor dwarf galaxies, an environment that does not exist in the Milky Way (Lunnan et al., 2015). If a metal-poor environment with many highly massive stars is required to form millisecond magnetars in SLSNe-I, this (together with the low SLSN-I rate; Quimby et al., 2013) would naturally explain them not being found in the Milky Way.

Additionally, the Milky Way magnetar population does not appear to predominantly arise in AIC events or NS-NS mergers. These events track the stellar mass of a galaxy, while CCSNe track the star formation of a galaxy. The fraction of local-universe stellar mass contained in the Milky Way is approximately equal to the fraction of local-universe star formation occurring in the Milky Way (Salim, Rich, et al., 2007; Karachentsev and Telikova, 2018b; Christopher D. Bochenek et al., 2020). Therefore, if AIC or NS-NS mergers were as efficient at making magnetars

as CCSNe, we would expect approximately half the magnetars in the Milky Way to be consistent with originating from AIC or NS-NS mergers. If this were true, due to the high kick velocities and long merger timescales of NS-NS mergers, we would expect to find a population of magnetars that is far away from the Galactic plane. If AIC is an efficient formation channel for magnetars, we would expect a large population of magnetars that are spatially uncorrelated with Galactic star-forming regions. Given that approximately 75% of young Galactic magnetars are associated with star formation, we would expect magnetars born in AIC or NS-NS mergers to make up no more than 25% of the extragalactic magnetar population. Furthermore, given that the volumetric rates of SLSNe-I (Quimby et al., 2013) and NS-NS mergers (Abbott et al., 2017) are much lower than the magnetar birth rate (E. F. Keane and Kramer, 2008), these channels cannot dominate the extragalactic magnetar population.

Giacomazzo and Perna (2013) show that one possible outcome of a NS-NS merger is a stable, more massive NS. Giacomazzo, Zrake, et al. (2015) go on to show that the magnetic field of that stable NS can be amplified through a dynamo driven by internal turbulence. The signature of this population would be extragalactic magnetars with large offsets from their host galaxies and an association of extragalactic magnetars with massive quiescent galaxies. The host galaxies of these magnetars would have similar characteristics to the hosts of short gamma-ray bursts (SGRBs).

The accretion induced collapse of a white dwarf can produce the convective dynamo described in Duncan and Thompson (1992), amplifying the magnetic field of the newly born millisecond neutron star to magnetar strengths. AIC of a white dwarf can occur in several different ways, all of them involving an oxygen/neon white dwarf (ONe WD). An ONe WD can merge with another WD, or it can accrete material from a wide variety of companion stars, including AGB stars, helium giant stars, helium main sequence stars, red giant stars, or main sequence stars. Ruiter et al. (2019) explore the binary evolution of each of these pathways and predict delay time distributions for each of them. The signature of this formation channel would be a population of magnetars roughly consistent with the mass distribution of their host galaxies, and a large fraction would occur in quiescent galaxies. Margalit, Berger, and Metzger (2019) approximate this population by assuming that the host galaxy properties are similar to that of Type Ia SNe. Margalit, Berger, and Metzger (2019) also show that FRB 180924 (K. W. Bannister et al., 2019) is consistent with a magnetar born in a NS-NS merger or AIC event.

To date, there are 12 FRBs with secure host galaxy associations Heintz et al. (2020). In this paper, we use this sample to explore the possibility that there are multiple FRB progenitor channels. To test this possibility, we first need to check if FRB host galaxies are consistent with the expected hosts of the dominant magnetar formation channel in the Milky Way. One compelling way to understand this test, and analyses of FRB host galaxies more generally, is as a search for evidence of alternative magnetar formation channels. In Section 2, we describe our sample of FRB hosts, as well as the sample of CCSN, LGRB, and SLSN-I hosts we compare them to. We also describe a novel technique for comparing different samples of transient host galaxies that corrects for the fact that the underlying distribution of galaxies that different transients are sampled from is evolving with cosmic time. In Section 3, we will compare the population of FRB hosts to the transient hosts to test the hypothesis that other magnetar formation channels are needed to explain the hosts of FRBs. In Section 4, we discuss caveats to this work, and comparable studies, and conclude in Section 5.

4.2 CCSN, SLSNe-I, LGRB, and FRB Host Samples

CCSN Host Sample

We use the sample of CCSNe published in Taggart and D. Perley (2019), henceforth referred to as TP19. This sample contains objects classified as Type II, Type IIP, Type IIb, Type Ib/Ic, Type IIn/Ibn, as well as two Type Ic-BL SNe. This sample of CCSNe is selected from the ASAS-SN supernova sample (Holoien et al., 2019), an unbiased, magnitude limited survey. Given that ASAS-SN is a shallow survey, this sample has a median redshift of 0.014. The fact that this sample is at such low redshift means the host galaxy of every supernova has been identified, regardless of how small it is.

The stellar masses and SFRs of this sample were derived from fitting the spectral energy distribution (SED) from the UV to NIR of each galaxy. If the SED had sufficiently blue colors and a spectrum was available, the luminosities of Hα and [OII] were also included in the fit. The left panel of Figure 4.2 shows the distribution in stellar mass and SFR of the CCSN in TP19 and all CCSNe in the Open Supernova Catalog (Guillochon et al., 2017) with $z < 0.3$ cross-matched with the GWSLC galaxy catalog (Salim, Lee, et al., 2016), which covers 90% of the Sloan Digital Sky Survey (SDSS) footprint. There is a clear bias towards large hosts in the OSC due to the incompleteness of SDSS at low stellar masses, demonstrating the need for the complete sample of TP19.

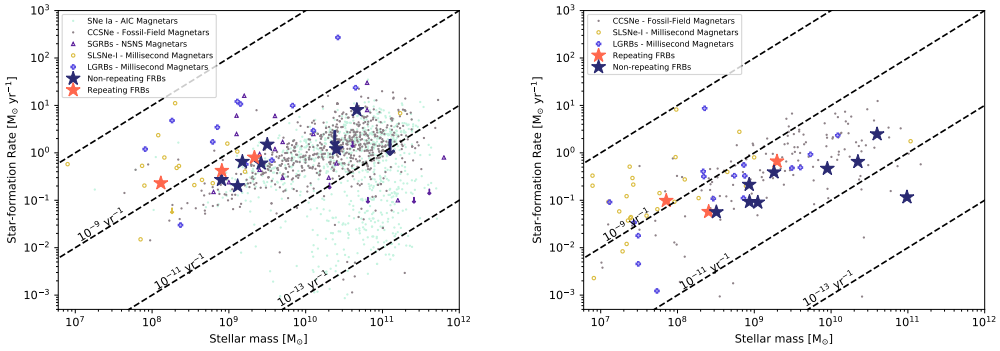

Figure 4.1: **Left:** The star-formation rates and stellar masses of the hosts of a variety of different astrophysical transients that may correspond to evidence of different magnetar formation channels. The dark blue stars represent the nonrepeating FRBs while the orange stars represent the repeating FRBs. The light grey dots represent CCSNe in the GSWLC footprint with $z < 0.3$, while the dark grey dots represent type Ia SNe with the same selection criteria. The CCSNe may track magnetars born through the fossil-field channel, while the Type Ia SNe may track millisecond magnetars born through AIC (Margalit, Berger, and Metzger, 2019). The open yellow circles are SLSNe-I (D. A. Perley et al., 2016), while the open blue crosses represent long gamma-ray bursts (LGRBs) (Levesque et al., 2010). These hosts may be representative of FRBs born as millisecond magnetars in engine-driven SNe. The short gamma-ray bursts are shown as open purple triangles (Berger, 2014) and may track millisecond magnetars born through NS-NS mergers. **Right:** The adjusted star-formation rates and stellar masses relative to the star-forming main sequence of the hosts of transients that track young stellar populations that may correspond to evidence of different magnetar formation channels. The samples shown are the same as used in the analyiss of this paper (Taggart and D. Perley, 2019).

SLSNe-I and LGRB host samples

We use the sample of confirmed SLSNe-I and LGRBs from TP19. This sample is restricted to $z < 0.3$ and contains only LGRBs with associated SNe Ic-BL and LGRBs with deep limits on a SN counterpart. The stellar masses and SFRs of this sample were derived from fitting the spectral energy distribution (SED) from the UV to NIR of each galaxy.

FRB Host Sample

We use the twelve published FRBs with host galaxies as our sample of FRB hosts (Bassa et al., 2017; K. W. Bannister et al., 2019; J. Xavier Prochaska et al., 2019; V. Ravi et al., 2019; Marcote, Nimmo, et al., 2020; J. P. Macquart, J. X. Prochaska, et al., 2020; Heintz et al., 2020; Shivani Bhandari, Sadler, et al., 2020). The redshifts of these FRBs range from $z = 0.034$ to $z = 0.66$. Each of these galaxies has a

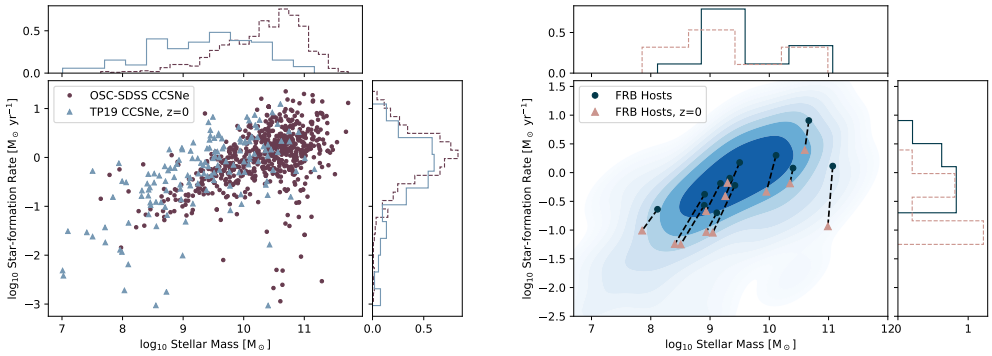

Figure 4.2: **Left**: The distribution of two different samples of CCSN hosts in SFR and stellar mass. The maroon dots correspond to CCSNe in the Open Supernova Catalog cross-matched with GSWLC galaxies, representing an incomplete sample of CCSN hosts. The blue triangles correspond to the hosts of the complete sample of CCSN hosts in TP19 that have been scaled to be representative of $z = 0$ galaxies. **Right:** The dark blue dots correspond to the stellar masses and SFRs of FRB hosts without scaling them to be representative of $z = 0$ galaxies, while the brown triangles correspond to the same FRB hosts scaled to be representative of $z = 0$ galaxies. A dashed line connects each FRB in one sample to itself in the other sample. The blue contour plot is the kernel density estimate of the distribution of TP19 CCSN hosts, where the contours are logarithmically spaced across two orders of magnitude in probability.

published stellar mass and star-formation rate (SFR), however there is no spectrum of the entire host of FRB 180916.J0158+65 (Marcote, Nimmo, et al., 2020), making it difficult to estimate a star-formation rate. Pending a more detailed analysis, we use the star-formation surface density reported in Marcote, Nimmo, et al. (2020) to integrate over the area of the galaxy and estimate a SFR of 0.8 $M_\odot$ yr^{-1} for the host of FRB 180916.J0158+65.

Two of the FRB hosts only report upper limits on the SFR (K. W. Bannister et al., 2019; V. Ravi et al., 2019) due to contamination of Hα from an ionizing continuum that is harder than typical star-forming galaxies. These upper limits are consistent with the SFRs inferred from their Hα luminosity and [OII] luminosity for FRB 180924 and FRB 190523, respectively. We choose to treat these upper limits on the SFR as the true value, as this contamination is unlikely to be recognized in the CCSN sample, given that most of the CCSN hosts do not have spectra (TP19)[1].

[1]We do not use the revised SFR for the FRB 190523 host from Heintz et al. (2020). The photometry of the FRB 190523 host was fitted by V. Ravi et al. (2019) to a stellar population synthesis model that yielded an SFR measurement consistent with the reported upper limit from spectroscopy. Additionally, Heintz et al. (2020) did not account for dust extinction of the Hβ line.

We note that this sample includes three FRBs that are known to repeat (Bassa et al., 2017; Marcote, Nimmo, et al., 2020; Pravir Kumar et al., 2020) and nine FRBs that were localized as one-off events and are not known to repeat (K. W. Bannister et al., 2019; V. Ravi et al., 2019; J. Xavier Prochaska et al., 2019; J. P. Macquart, J. X. Prochaska, et al., 2020; Heintz et al., 2020). It is possible that if repeating and nonrepeating FRBs are two distinct classes, the fact that two different localization strategies were used could introduce bias in the FRB host distribution. However, in the absence of evidence that these two FRB populations represent different progenitor classes (Vikram Ravi, 2019b), we combine both the repeating FRBs and nonrepeating FRBs into one sample.

Correcting for an evolving galaxy distribution

When determining whether two populations of transient host galaxies are consistent with each other, it is important to keep in mind that the underlying distribution of galaxies and the location of star formation in the universe is evolving. A sample of star-forming galaxies at high redshift will preferentially have higher SFRs and masses than a sample of star-forming galaxies at $z = 0$. When searching for evidence of alternate magnetar formation channels using events at a variety of redshifts, one is interested not in SFRs and stellar masses of FRB hosts themselves, but rather where they lie in relation to the distribution of star-formation at these different redshifts. We refer to the location of a sample of transient hosts in relation to the distribution of star formation as the sampling function. Without taking the evolution of the star-formation distribution into account, it is possible to mistake the bias towards higher SFRs at higher redshifts for an intrinsic difference in the hosts of FRBs and CCSNe.

For each sample of host galaxies, we correct for the evolution of star formation with cosmic time by scaling the masses and SFRs of each transient so that the statistical properties of each sample is representative of galaxies at $z = 0$. To do this, we conserve the p-values in both stellar mass and SFR relative to the distribution of star-forming galaxies at the redshift of the transient and $z = 0$. The distribution of star-formation as a function of stellar mass at a particular redshift is given in Equation 4.1, where $\frac{dn(z)}{dM}$ is the mass function of star-forming galaxies, $S_0(M_*, z)$ is the median SFR as a function of M_* and z (known as the star-forming main sequence), and k is a normalization factor such that $\int p_z(M_*)dM_* = 1$. Given that star-forming galaxies are log-normally distributed about $S_0(M_*, z)$ and the scatter is constant with stellar mass (Speagle et al., 2014), this normalization also accounts

for the difference between the median and mean of a log-normal distribution.

$$p_z(M_*) = k\frac{dn(M_*, z)}{dM}S_0(M_*, z) \tag{4.1}$$

First, we need to account for the fact that at lower redshifts, sampling functions that simply track star formation are more likely at lower redshifts to produce transients in smaller galaxies than higher redshifts. We adjust the stellar mass of each galaxy so that $\int_0^{M_0} p_{z=0}(M_*)dM_* = \int_0^{M_{z_t}} p_{z=z_t}(M_*)dM_*$, where $p_z(M_*)$ is given by Equation 4.1, M_0 is the mass of that galaxy at $z = 0$, z_t is the redshift of the transient, and M_z is the mass of that galaxy at the redshift of the transient. This adjusted mass represents the equivalent mass at $z = 0$ that is selected by the sampling function at $z = z_t$. Moustakas et al. (2013) show there is no significant evolution in the number density of star-forming galaxies between $z = 0$ and $z = 0.65$, the redshift range of interest, so we ignore this redshift dependence. To find $\frac{dn(M_*,z)}{dM}$, we fit the Schechter function in Equation 4.2, where M_c is the cutoff stellar mass, ϕ_0 is the normalization, and Γ is the power-law index, to the number densities of star-forming galaxies between $z = 0.2$ and $z = 0.3$ reported in Moustakas et al. (2013).

$$\log_{10}\frac{dn(M_*, z)}{dM_*} = \phi_0 - M_c + \Gamma(M_* - M_c)) - 10^{M_* - M_c}\log_{10}(e) \tag{4.2}$$

To perform the fitting, we drew 10^3 realizations of the data assuming a split Gaussian uncertainty. We find the median parameters and 1σ distributions of the fit are $M_0 = 10.6 \pm 0.2$, $\phi_0 = 8.34^{+.03}_{-.05}$, and $\Gamma = -0.1^{+.09}_{-.25}$. For S_0, we used the "preferred fit" SFR-stellar mass relationship at redshift z published in Speagle et al. (2014). We compute $p_z(M_*)$ between $10^{6.5}\,\mathrm{M}_\odot$ and $10^{12}\,\mathrm{M}_\odot$.

Once we have determined the equivalent stellar mass of the galaxy at $z = 0$, we then utilize the fact that star-forming galaxies are log-normally distributed about the star-forming main sequence and the scatter about the star-forming main sequence does not evolve with redshift (Speagle et al., 2014). To scale the SFRs to be representative of $z = 0$ galaxies, we ensure that the host of the transient is the same number of standard deviations away from the star-forming main sequence at $z = z_t$ for $M_* = M_z$ as at $z = 0$ for $M_* = M_0$. The right panel of Figure 4.2 shows the corrections made to each FRB host galaxy. By applying both of these corrections, each transient is corrected for the effects of how the distribution of star-formation changes with cosmic time, allowing direct comparison between two samples of transient host galaxies at various redshifts.

	M_* p-value	SFR p-value	sSFR p-value	KDE p-value	2D KS Test p-value
CCSN–FRB	>.25	**.035**	.14	.546	>0.2
LGRB–FRB	**.022**	>.25	**.027**	.054	**0.018**
SLSNe-I–FRB	**<0.001**	>.25	**<0.001**	**<.0001**	**<.0001**

Table 4.1: This table shows the results of the various statistical tests performed to determine if two host galaxy samples are consistent with each other. We report Anderson-Darling p-values of the cumulative distributions in stellar mass, SFR, and sSFR between the samples, the p-value corresponding to the likelihood of randomly drawing a less probable sample than the FRB hosts from the kernel density estimate of the type of the hosts of the transient being compared to FRBs, and the p-value of the 2D KS test on 1000 bootstrap samples. Significant results are highlighted in bold.

4.3 Are FRB Hosts Similar to CCSN/LGRB/SLSN-I Hosts?

After we scale the distributions of FRB, CCSN, LGRB, and SLSN-I hosts to be statistically representative of $z = 0$ galaxies, we compare each cumulative distribution in stellar mass, SFR, and specific star-formation rate (sSFR) to the FRB hosts. These distributions are shown in Figure 4.3. We use the k-sample Anderson-Darling test (F. W. Scholz and Stephens, 1987) to compare these distributions. Table 4.1 shows the results of each test. While the FRB host and CCSN host stellar mass and sSFR distributions are not significantly different, the SFRs of CCSN appear systematically higher. The FRB host distribution is inconsistent with the SLSNe-I host distribution with high confidence. Furthermore, the FRB host distribution has significantly higher masses and lower sSFRs that the LGRB host distribution.

We use a kernel density estimator with Gaussian kernels of widths determined by Scott's rule (Scott, 1992) on the logarithmic distribution of stellar masses and SFRs of the CCSN sample to estimate the distribution of these hosts in the stellar mass-SFR plane. We then compute the likelihood of the FRB sample from this distribution and compare this to the likelihood of 10^4 random samples from this distribution. The random samples of this distribution resulted in a lower likelihood than the FRB hosts 54.6% of the time. Therefore, even though the SFRs of FRB hosts and CCSN hosts are significantly different (Figure 4.3; Table 4.1), we contend that FRB hosts and CCSN hosts are nonetheless consistent with being drawn from the same distribution. As demonstrated above, the sSFRs of FRB hosts and CCSN hosts are consistent, and the two-dimensional test better captures the available information. We repeat this procedure, comparing the LGRB hosts and SLSNe-I hosts to the FRB

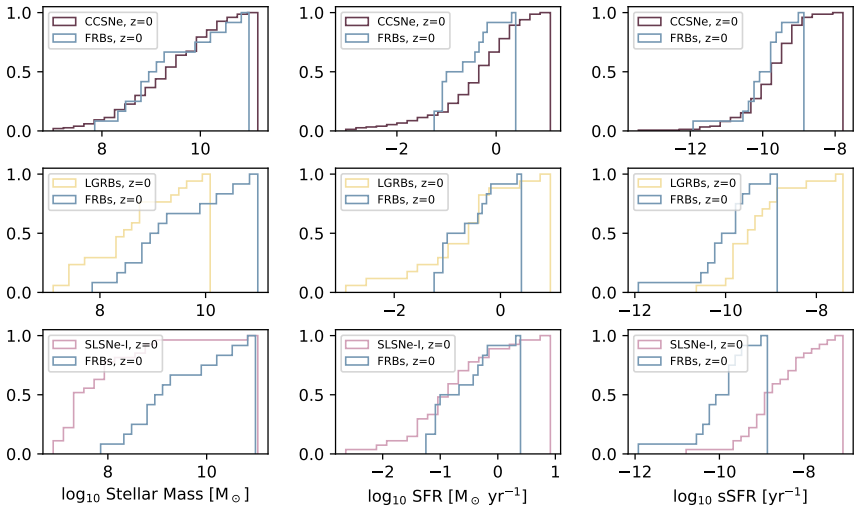

Figure 4.3: **Left:** The cumulative distributions of stellar masses of CCSNe, LGRB, SLSNe-I, and FRB hosts that have all been scaled to be representative of $z = 0$ galaxies and FRB hosts that have been scaled to be representative of $z = 0$ galaxies. **Middle:** The cumulative distributions of SFRs of CCSNe, LGRB, SLSNe-I, and FRB hosts that have all been scaled to be representative of $z = 0$ galaxies and FRB hosts that have been scaled to be representative of $z = 0$ galaxies. **Right:** The cumulative distributions of sSFRs of CCSNe, LGRB, SLSNe-I, and FRB hosts that have all been scaled to be representative of $z = 0$ galaxies and FRB hosts that have been scaled to be representative of $z = 0$ galaxies.

sample. A sample of galaxies drawn from the LGRB and SLSNe-I distributions have likelihoods smaller than the likelihood of the FRB host distribution 5.4% and <0.01% of the time, respectively. These results are also summarized in Table 4.1.

To verify these results, we performed a 2D KS test with 1000 bootstrap samples comparing the CCSN, LGRB, and SLSN-I hosts to the FRB hosts. We confirm our results of the kernel density estimator analysis, although the p-value of this test for the LGRB and FRB host samples dropped to 0.018, which is inconsistent with the null hypothesis, as opposed to marginally consistent with the null hypothesis. These results are summarized in Table 4.1. Therefore, the hosts of FRBs are consistent with the CCSN host sample and inconsistent with the LGRB hosts and SLSN-I hosts.

4.4 Implications for FRB Progenitors and Magnetar Formation

We have compared the host galaxies of FRBs to those of CCSNe, LGRBs, and SLSNe-I. Specifically, we considered the distributions of stellar masses and SFRs

relative to the star-forming main sequence. We were motivated by the possibility of directly determining the origin and formation channels of FRB progenitors. We find that the host galaxies of FRBs are consistent with the host galaxies of CCSNe, but not with the hosts of LGRBs and SLSNe-I. This is consistent with the results of similar studies (Li and B. Zhang, 2020; Heintz et al., 2020; Shivani Bhandari, Sadler, et al., 2020)

The short durations and energetics of FRBs imply that they must originate from highly magnetized compact objects. The hosts of FRBs span a wide variety of galaxies, from dwarf galaxies with high sSFRs (Bassa et al., 2017), to massive starbursts (Heintz et al., 2020), to massive galaxies with SFRs below the star-forming main sequence (V. Ravi et al., 2019). A Galactic magnetar has also produced an FRB (C. D. Bochenek et al., 2020; The CHIME/FRB Collaboration et al., 2020).

All of these facts motivate the hypothesis that FRBs originate from magnetars like those found in the Milky Way. This origin is consistent with our results that the hosts of FRBs are consistent with being drawn from the same selection function as CCSNe, and inconsistent with the SLSN-I and LGRB hosts. Magnetars born in CCSNe that do not have central engines dominate the population of Milky Way magnetars. Therefore, if magnetars are the dominant FRB progenitor, and the Milky Way magnetar population is representative, their host galaxies should be consistent with the hosts of CCSNe.

However, we caution that there may be systematic biases in the FRB population. Massive galaxies with high SFRs often have all of their star formation concentrated in a small region with an incredibly dense interstellar medium. For example, M82 is a nearby massive starburst galaxy which has a central starburst of diameter 700 pc that contains nearly all the star formation, and thus magnetars formed through corresponding channels. Using the H53α flux in this region (Puxley et al., 1989), the volume-averaged electron density of this region is $\sim 30\,\mathrm{cm}^{-3}$. An FRB from M82 could have a dispersion measure of $10^4\,\mathrm{pc\,cm}^{-3}$, likely also implying scatter-broadening orders of magnitude larger than 1 ms, making an M82 FRB impossible to detect in most FRB surveys. Indeed, it may not be a coincidence that FRB 191001, which is in a galaxy of similar mass and SFR as M82, is located on the outskirts of its host (Heintz et al., 2020; Shivani Bhandari, Keith W. Bannister, et al., 2020). This bias away from galaxies with high SFRs may help explain the apparent discrepancy in SFR, but consistency in sSFR, between the CCSN hosts and FRB hosts.

With a sample of only twelve FRBs, we are only sensitive to dominant populations.

It is possible that magnetars born in AIC events are a sub-dominant contributor to the population. Evidence for this channel would be an overabundance of FRBs in massive, quiescent galaxies. Furthermore, it is possible that one magnetar formation channel is significantly more likely to produce an FRB-emitting magnetar, as magnetars whose magnetic fields are formed in different ways may also dissipate that magnetic energy in different ways. Indeed, the host of FRB 121102 is very similar to the hosts of SLSNe-I (Li and B. Zhang, 2020). Furthermore, the repetition rate of FRBs from SGR 1935+2154 is substantially lower than that of extragalactic repeating FRBs, which Margalit, Beniamini, et al. (2020) and Lu, Pawan Kumar, and B. Zhang (2020) suggest indicates the presence of a rare type of magnetar. Beniamini, Wadiasingh, and Metzger (2020) hypothesize that FRBs like the periodically repeating FRB 180916 could originate from a rare magnetar born with strong enough magnetic fields to spin down to ultra-long periods. It is not clear that such magnetars would trace CCSNe, as given the right combination of initial spin period and magnetic field to inject additional energy into the supernova, such millisecond magnetars are hypothesized to explain atypical supernova like a SLSN-I (Woosley, 2010; Kasen and Bildsten, 2010). These atypical supernovae also occur in star-forming metal-poor dwarf galaxies, which are not typical CCSN hosts. Evidence for this hypothesis would be that repeating FRBs prefer galaxies with stellar masses $< 10^9$ $M_\odot$ with high sSFRs, and low metallicities. The data would prefer a second FRB progenitor if, for example, a larger sample of FRB hosts requires that most magnetars are born through AIC events, the birth-rate of magnetars born in engine-driven SNe is much larger than the SLSNe-I/LGRB volumetric rate, or a significant fraction of FRBs are offset from their hosts.

In this paper, we have also demonstrated that it is necessary to use complete samples of transients to compare to FRB hosts due to significant biases induced by the completeness of galaxy catalogs. This often implies using only transients with relatively low redshifts. We have also developed a novel technique for comparing FRB host galaxy samples to samples of transients at lower redshifts by correcting for the evolution of how star formation is distributed with cosmic time. The advantages of this approach are that it makes it possible to directly compare host galaxy samples that have different redshift distributions to ensure that any differences between populations are representative of the nature of the transient event, rather than galaxy evolution. However, more work is required to compare the FRB host galaxy sample to transient host samples that do not track star formation, such as Type Ia SNe and NS-NS mergers. To do this analysis, it is necessary to incorporate the evolution of

the quiescent galaxy population as well. Furthermore, this approach does not allow for determination the FRB delay-time distribution, another crucial piece of the FRB progenitor puzzle.

In a similar study, Safarzadeh et al. (2020) compare the host-galaxy stellar masses, SFRs, and projected offset distributions of the Heintz et al. (2020) FRBs with a population synthesis model for magnetars. The model links all magnetars to ongoing star-formation, consistent with a CCSN progenitor channel. Safarzadeh et al. (2020) conclude that the FRB hosts do not track star-formation activity, and hence are inconsistent with a magnetar origin, although this conclusion is not supported by the offset distribution. Although our conclusions are similar regarding star-formation alone, we come to a different conclusion regarding the overall consistency between FRB hosts and CCSN hosts. We argue that our results are more robust because: (*i*) we directly compare FRB hosts with a complete, observational sample of CCSN hosts, thus obviating the need to rely on untested population synthesis models; and (*ii*) we account for the two-dimensional distribution of host galaxies in star formation and stellar mass when reaching our final conclusion.

4.5 Conclusions

Using a novel approach for comparing two samples of transient host galaxies, we have determined that the current sample of FRB hosts is consistent with the hosts of CCSNe, and inconsistent with the hosts of SLSNe-I and LGRBs. This result is expected if magnetars similar to those in the Milky Way are responsible for the bulk of the FRB population. However, this result is limited by the current sample of FRB host galaxies. A larger sample of FRB hosts may turn up evidence for alternate magnetar formation channels or necessitate second progenitor for FRBs.

This research was supported by the National Science Foundation under grant AST-1836018. This work made use of `Astropy` (Astropy Collaboration et al., 2018).

Chapter 5

FUTURE LONG, TARGETED FRB CAMPAIGNS WITH A 25 METER CLASS TELESCOPE

With the discovery of a 1.5 MJy ms radio burst from the Galactic magnetar SGR J1935+2154 (C. D. Bochenek et al., 2020; CHIME/FRB Collaboration, Andersen, et al., 2020), we have shown that it is likely that most FRBs originate from magnetars. Magnetars are relatively short-lived objects, meaning if a galaxy is forming stars at a high rate, it will also have a high rate of magnetars which may produce FRBs. Meaning, if it took $\sim$ 1.5 years of observing time to find an FRB in the Milky Way, it may take significantly less time to find an FRB in a galaxy with a higher star-formation rate. It would be interesting to undertake a 1 year observing campaign of highly star-forming galaxies with a 25 m class telescope.

Such an observing campaign would inform how we should interpret large samples of FRB host galaxy localizations. Currently, there is no evidence that ionised gas in the host galaxies of FRBs contribute substantially to their dispersion measures (J. P. Macquart, J. X. Prochaska, et al., 2020). However, if magnetars produce FRBs, one would expect galaxies like M82 to produce a large number of FRBs. M82 is located 3.6 Mpc away. Most FRBs are likely found $\sim$ 1 Gpc away, so a large telescope is not required to see FRB-like bursts from M82. M82 also has a star-formation rate of $10.52\,\mathrm{M_\odot\,yr^{-1}}$ and stellar mass of $1.3\times10^{10}\,\mathrm{M_\odot}$ (Jarrett et al., 2019). Nearly all the star formation in M82 occurs in the central 700 pc of the galaxy (de Grijs, 2001). Therefore, we would expect nearly all the magnetars in M82 to live in this region. Using the flux of H53α from this region, the volume-averaged electron density is $30\,\mathrm{cm^{-3}}$ (Puxley et al., 1989). Given the size of the central starburst, it is easy to imagine an FRB with a dispersion measure of $10^4\,\mathrm{pc\,cm^{-3}}$. Figure 5.1 shows the expected extragalactic DM of FRBs from M82 compared to a sample of localised FRBs.

Many FRB searches do not search out to such high DMs (Christopher D. Bochenek et al., 2020; Champion et al., 2016; J.-P. Macquart et al., 2010; Kocz et al., 2019). In addition, such FRBs would be difficult to detect at 1.4 GHz as large DMs are associated with large scattering timescales in the Milky Way. Using the DM-scattering relationship in J. M. Cordes, Wharton, et al. (2016) and scaling the

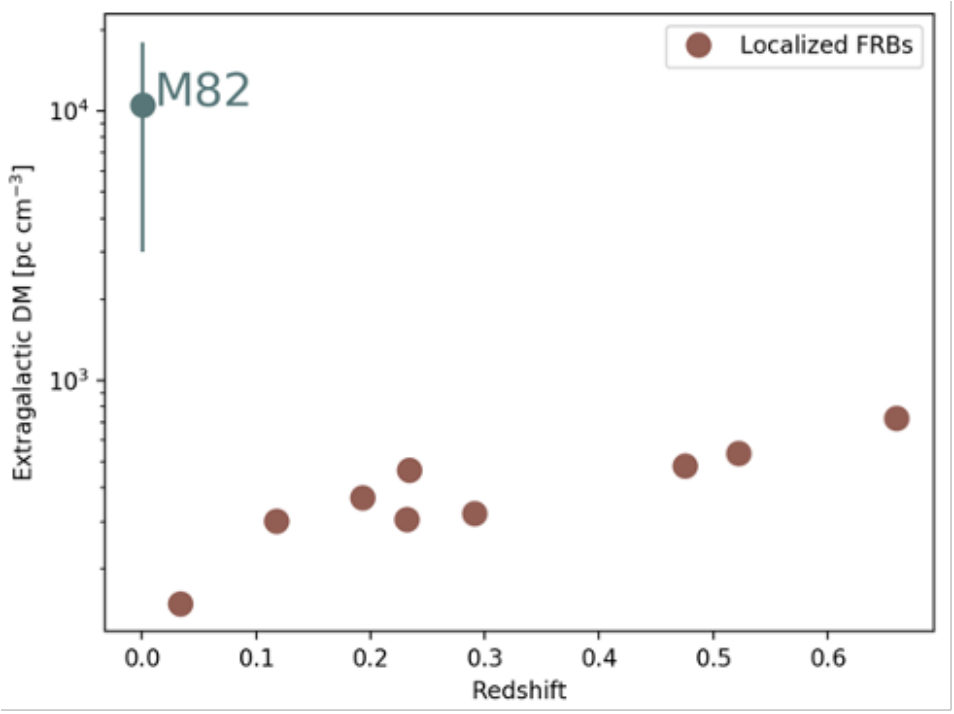

Figure 5.1: Macquart relationship for FRBs, plotted alongside the expected extragalactic DM from M82, assuming the line-of-sight goes through between 100 pc—600 pc of the central star-forming region.

scattering timescale in frequency as ν^{-4}, one needs to observe above 15 GHz to be sensitive to 1 ms FRBs from M82. Despite this expectation of a large amount of scattering, the scattering properties of extragalactic sources is very sightline dependent and difficult to predict. Furthermore, no FRB has been detected above 8 GHz (Gajjar et al., 2018). However, due to the small beams of radio telescopes at frequencies above a few GHz, blind surveys at high frequency have traditionally been unable to succeed. There is also no reason to expect the spectrum of FRBs cuts off sharply above 10 GHz. The FRB searches at 8 GHz have succeeded only when pointed at a well-localised repeating FRB. This high frequency FRB survey is the most likely to succeed at detecting a non-repeater because it targets a small region that fits within the beam of a single-dish telescope with lots of star formation, where we expect there to be an abundance of FRB sources, for a large amount of time.

If extragalactic FRB surveys are missing FRBs in galaxies like M82, then FRB searches are strongly biased against finding FRBs in Galactic center-like environments where the DM, and possibly scattering at low frequencies, are extreme. If this observational bias is not understood, it could lead to incorrect conclusions about the nature of FRB progenitors and prevalence of different magnetar formation channels,

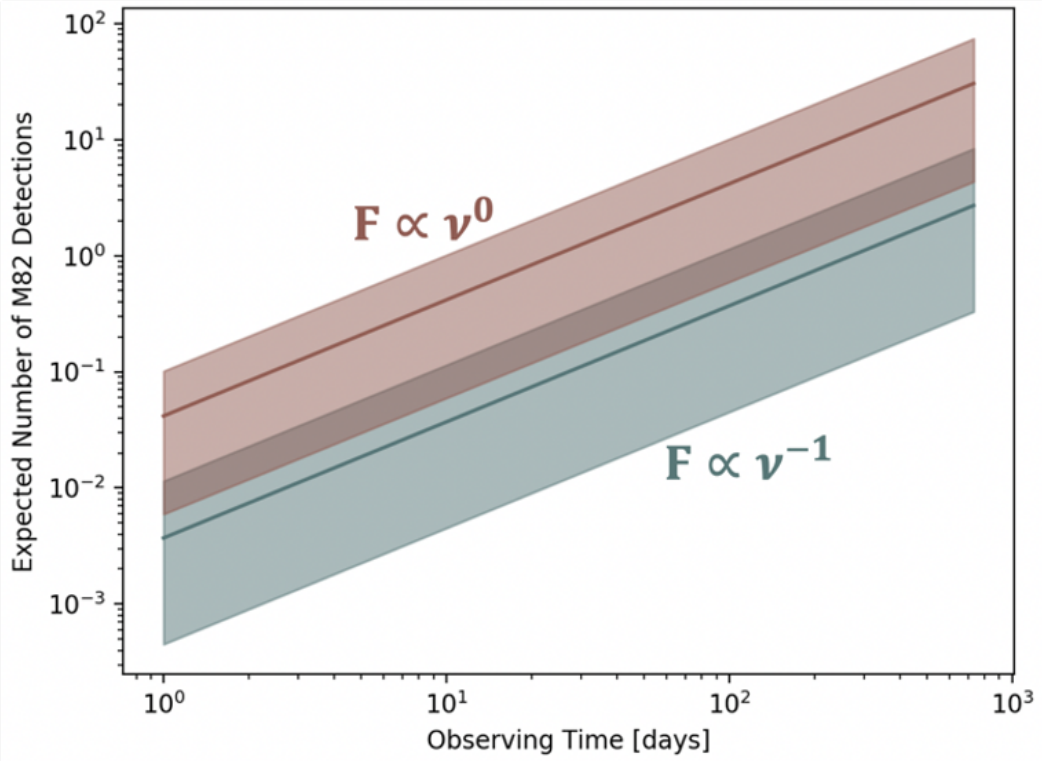

Figure 5.2: Expected detection rate of FRBs at 20 GHz from M82. The different colors correspond to different average spectral indices between 1.4 GHz and 20 GHz. The solid line represents the most probable number of detections while the shaded region represents the 1σ uncertainties. In one year of observing time, a detection is probable, even with an average spectral index as steep as -1.

such as an over-abundance of magnetars born in the accretion induced collapse of a white dwarf.

A one-year observing campaign for FRBs in M82 at 20 GHz would test the hypothesis that there are many FRBs produced in M82 and that they are highly scattered. Furthermore, since no FRB has been detected above 8 GHz (Gajjar et al., 2018), so a detection above 8 GHz would represent a significant advance in our understanding of the physics required to make FRBs. Figure 5.2 shows the expected number of detections as a function of observing time under the assumptions of a flat and steep spectral index. An SEFD of 1000 Jy, bandwidth of 128 MHz, S/N of 10, are assumed as well as the rate and luminosity function published in (C. D. Bochenek et al., 2020). Even if the average spectral index is as steep as -1, a detection is still probable. Because of the small field of view of radio dishes at high frequency, a long, targeted survey such as this has the greatest chance to detect an FRB at high frequencies.

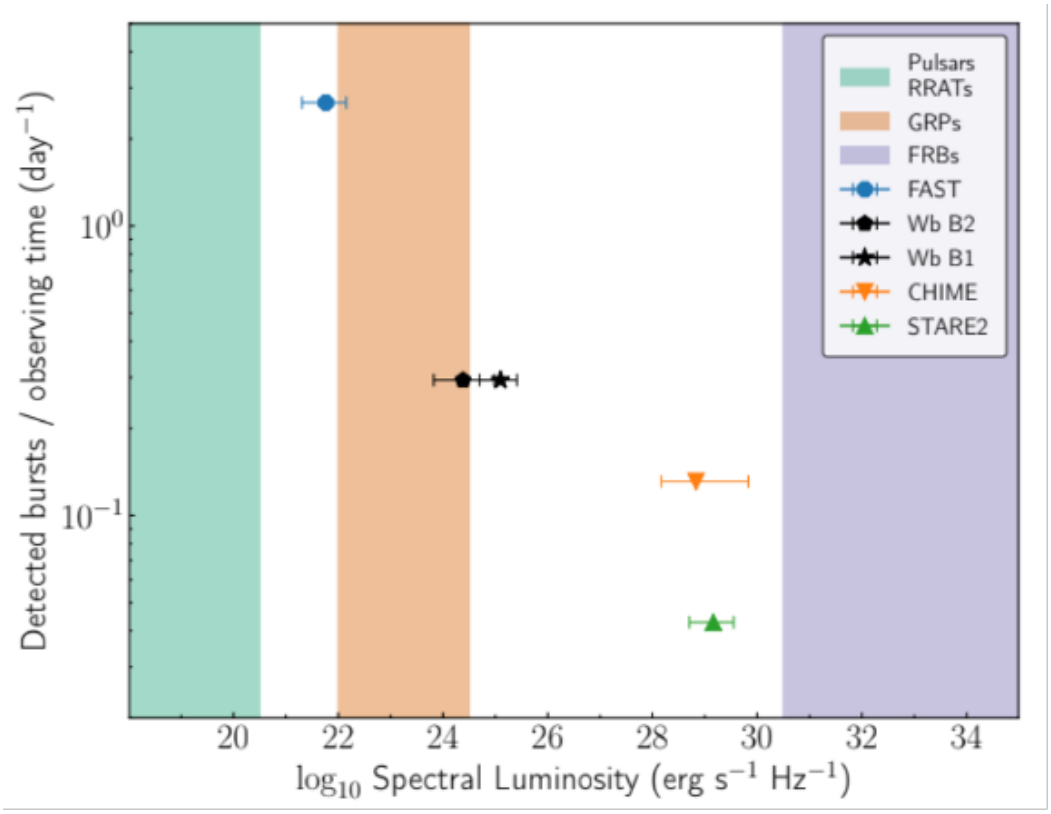

Figure 5.3: The burst rate as a function of spectral luminosity for various short duration radio bursts seen from SGR J1935+2154 during its April 2020 – May 2020 period of activity. The two bursts seen by a European VLBI Network dish are in black. The green, orange, and purple shaded regions show the typical spectral luminosities of pulsars and rotating radio transients (RRATs), giant radio pulses from pulsars (GRPs), and FRBs, respectively. Reproduced from Kirsten et al. (2020).

In addition to this survey, to learn about the emission mechanism of FRBs, a broadband observing campaign of Galactic magnetars, including SGR J1935+2154, at frequencies ranging from 1.4 GHz to 20 GHz would be interesting. Because FRB 200428 was associated with a period of heightened activity from SGR J1935+2154, observing at radio wavelengths for several months after an observed X-ray flare offers the best chance of success. Between August 2019 and August 2020, four different magnetars produced bright X-ray flares, including multiple periods of activity from two sources (SGR J1935+2154 and Swift J1818-1607). The detection of two $\sim$ 100 Jy ms pulses within 1.4 seconds of each other in an observing campaign of hundreds of hours at 1.4 GHz from SGR J1935+2154 from its April 2020 activity period shows that magnetars emit bright single pulses across seven orders of magnitude in luminosity (Kirsten et al., 2020). Figure 5.3 puts these detections in the context of other radio pulses seen from SGR J1935+2154 during its April

2020 – May 2020 period of activity. In this instance, hundreds of hours on smaller telescopes was more rewarding than tens of hours on the world's biggest radio telescopes. However, it is unclear whether the same emission mechanism operates across this entire range of luminosities. The low frequency observations can be used to establish a radio-active period and determine if the repetition statistics are similar to repeating FRBs. If magnetars do emit bright single pulses at 20 GHz (as opposed to their more regular pulsations), that would give credibility to the hypothesis that FRBs also exist at high frequency.

Such observations are important for determining the physics behind the FRB emission mechanism, as well as exploring the diversity of Galactic single pulses. Baseband data with full polarization information would be most useful for such a study. Baseband data gives us access to the minimum timescale of emission and enables us to study the evolution of burst width with frequency. Combined with the wide spectral coverage, this will allow study into how magnetars produce these bright single pulses. Is the emission produced within the magnetosphere or outside of the magnetosphere (Lu, Pawan Kumar, and B. Zhang, 2020; Margalit, Beniamini, et al., 2020; Wadiasingh and Timokhin, 2019)? Due to the steep spectral index of a synchrotron maser, it would be difficult for emission outside of the magnetosphere to regularly produce bright single pulses above 10 GHz. However, a plasma maser within the magnetosphere may emit most of its energy at frequencies above 10 GHz (Lu and Pawan Kumar, 2018). Furthermore, emission outside of the magnetosphere cannot produce emission on timescales less than a few microseconds, while the models inside of the magnetosphere can, making baseband observations of bright pulses from magnetars important for distinguishing between the two. Given these direct constraints we can place on radio emission models from magnetars, high-frequency surveys with baseband information for FRBs from M82 and high-frequency searches for bright single-pulses from magnetars will be able to shed light on these questions.

Furthermore, studying Galactic magnetars informs the diversity of their behavior. By studying bright single-pulses from magnetars, we can compare their spectro-temporal structure to those of FRBs and search for similar phenomenology, such as the "sad trombone" (Hessels et al., 2019) and band-limited or patchy spectra. By further exploring the properties of Galactic magnetars, we better characterize the types and behaviors of FRB sources in the universe.

Chapter 6

SUMMARY AND CONCLUSIONS

In this thesis, I have described STARE2, an experiment to search for FRBs in the Milky Way and local universe. I discussed how this survey is particularly sensitive to fast radio transients with luminosities between those of giant pulses from pulsars and extragalactic fast radio bursts. STARE2 is therefore useful for putting constraints on the low end of the FRB luminosity function, luminosities that are not available to extragalactic FRB surveys. Furthermore, it is uniquely sensitive to fast radio transients of origins different to those of extragalactic FRBs. I was able to estimate that if an FRB was to be detected with STARE2, it would likely have a specific energy of $\sim 10^{26}\,\mathrm{erg\,Hz^{-1}}$.

STARE2 is a network of three antennas located at the Owens Valley Radio Observatory, the Goldstone Deep Space Communications Complex, and Delta, Utah. It observes between 1.28 GHz and 1.53 GHz and is sensitive to 1 ms radio pulses brighter than 300 kJy. Using the stations at the Owens Valley Radio Observatory and Goldstone Deep Space Communications Complex, we were able to demonstrate the system's effectiveness by detecting a solar burst at each site.

I then described the discovery of FRB 200428 with STARE2, which originated from the Galactic magnetar SGR J1935+2154. FRB 200428 had a fluence of $1.5(3) \times 10^6$ Jy ms. It is the first FRB to have an associated transient, as the radio burst occurred simultaneously with a hard X-ray burst. STARE2's localization of this event is consistent with the location of SGR J1935+2154. This event is just 30 times weaker than the faintest FRB discovered and has a comparable brightness temperature to FRBs. The non-detection of counterparts at other wavelengths of FRBs is consistent with this event, as well as the factor of seven disparity in fluence between the 600 MHz band and 1.4 GHz band. The Milky Way is not a surprising host galaxy for an FRB and the lack large contributions to the dispersion measure and rotation measure are consistent with extragalactic FRBs. FRB 200428's isotropic-equivalent energy of $1.6(3) \times 10^{26}\,\mathrm{erg\,Hz^{-1}}$ also matches the energy we predicted a Galactic FRB would have. Furthermore, the inferred volumetric rate of events like FRB 200428 matches the FRB volumetric rate. Because of all this, I conclude that magnetars are the dominant channel that produces FRBs.

To test the hypothesis that magnetars are the dominant FRB channel, I then studied the host galaxies of extragalactic FRBs. Magnetars are thought to be born in typical core-collapse supernovae and may be formed in rare core-collapse supernovae such as those associated with long gamma-ray bursts and hydrogen-poor superluminous supernovae. Magnetars also do not live for a sufficiently long time for their host galaxy to significantly evolve in their lifetimes. Therefore, if magnetars are the dominant FRB progenitor channel, the host galaxies of FRBs should be similar to the host galaxies of core-collapse supernovae. I developed a novel technique to correct for the evolution of galaxies across cosmic time when comparing samples of transient host galaxies and used this technique to compare the FRB host galaxy sample with complete samples of host galaxies of core-collapse supernovae, long gamma-ray bursts, and hydrogen-poor superluminous supernovae. I find that the FRB host galaxy population is consistent with the core-collapse supernovae population and inconsistent with the host galaxies of long gamma-ray bursts and hydrogen-poor superluminous supernovae. This is consistent with the hypothesis that magnetars are the dominant FRB progenitor channel.

Finally, I presented two paths forward to study FRBs that utilize large amounts of available time on 25 m class telescopes. The first is a year long campaign of M82 at 20 GHz. This campaign has to potential to unlock a hidden population of FRBs located in extremely dense and turbulent environments. Understanding the observational biases present in our extragalactic FRB samples will be key to understanding the full picture of the objects that produce FRBs. The second are months-long searches for bright radio pulses from flaring Galactic magnetars between 1.4 GHz and 20 GHz. This campaign will help us understand the emission mechanism behind FRBs and further probe the link between magnetars and extragalactic FRBs.

These results have provided the first concrete evidence that magnetars are responsible for producing FRBs, providing at least a partial answer to one of the primary questions in the field. By using FRBs as tracers of extragalactic magnetars, this discovery will enable new investigations into the deaths of massive stars and rare channels of magnetar formation. In addition, new studies into bright Galactic radio pulses enabled by this discovery will provide insight into the processes that result in coherent radio emission. Furthermore, this knowledge of the progenitors of FRBs will inform their use as probes of ionized gas and cosmology, enabling discoveries about how galaxies grow and evolve as well as the evolution of the universe.

The future of FRB research is bright. Currently, there are roughly a dozen FRBs that

are localized sufficiently well to identify their host galaxies. However, experiments such as the DSA-110, ASKAP, and CHIME Outriggers are poised to make the localization of FRBs to host galaxies a routine procedure, flooding the community with rich datasets. With these data, we will be able to challenge the hypothesis that magnetars are responsible for the bulk of FRBs and look for other FRB progenitors. Furthermore, large numbers of FRBs found by CHIME will nail down our knowledge of the properties of FRBs and find many more repeating FRBs that can be studied in detail by the community.

The history of FRBs is rich in wonderful surprises, from their initial discovery, to the detection of the first repeating FRB to this discovery of a Galactic FRB. The future is likely to be no different. The astronomical community's great effort into studying this phenomenon will surely produce more. Our understanding of FRBs will continue to rapidly evolve and this thesis will likely be outdated within a few years. This rapid pace of discovery makes it an exciting field to work in and I look forward to seeing how our understanding of FRBs evolves.

BIBLIOGRAPHY

Abbott, B. P. et al. (Oct. 2017). "GW170817: Observation of Gravitational Waves from a Binary Neutron Star Inspiral". In: *Phys. Rev. Lett.* 119.16, 161101, p. 161101. DOI: 10.1103/PhysRevLett.119.161101. arXiv: 1710.05832 [gr-qc].

Amiri, M. et al. (Aug. 2018). "The CHIME Fast Radio Burst Project: System Overview". In: *ApJ* 863.1, 48, p. 48. DOI: 10.3847/1538-4357/aad188. arXiv: 1803.11235 [astro-ph.IM].

Archibald, R. F. et al. (Dec. 2018). "The 2016 Outburst of PSR J1119-6127: Cooling and a Spin-down-dominated Glitch". In: *ApJ* 869.2, 180, p. 180. DOI: 10.3847/1538-4357/aaee73. arXiv: 1806.01414 [astro-ph.HE].

Astropy Collaboration et al. (Sept. 2018). "The Astropy Project: Building an Open-science Project and Status of the v2.0 Core Package". In: *AJ* 156.3, 123, p. 123. DOI: 10.3847/1538-3881/aabc4f. arXiv: 1801.02634 [astro-ph.IM].

Bailes, M. et al. (Oct. 2017). "The UTMOST: A Hybrid Digital Signal Processor Transforms the Molonglo Observatory Synthesis Telescope". In: *PASA* 34, e045, e045. DOI: 10.1017/pasa.2017.39. arXiv: 1708.09619 [astro-ph.IM].

Bannister, K. W. et al. (Aug. 2019). "A single fast radio burst localized to a massive galaxy at cosmological distance". In: *Science* 365.6453, pp. 565–570. DOI: 10.1126/science.aaw5903. arXiv: 1906.11476 [astro-ph.HE].

Barsdell, B. R. et al. (Sept. 2012). "Spotting Radio Transients with the Help of GPUs". In: *Astronomical Data Analysis Software and Systems XXI*. Ed. by P. Ballester, D. Egret, and N. P. F. Lorente. Vol. 461. Astronomical Society of the Pacific Conference Series, p. 37. arXiv: 1112.0065 [astro-ph.IM].

Barthelmy, S. D. et al. (Apr. 2020). "Swift detection of multiple bursts from SGR 1935+2154". In: *GRB Coordinates Network* 27657, p. 1.

Bassa, C. G. et al. (July 2017). "FRB 121102 Is Coincident with a Star-forming Region in Its Host Galaxy". In: *ApJ* 843.1, L8, p. L8. DOI: 10.3847/2041-8213/aa7a0c. arXiv: 1705.07698 [astro-ph.HE].

Beloborodov, Andrei M. (July 2017). "A Flaring Magnetar in FRB 121102?" In: *ApJL* 843.2, L26, p. L26. DOI: 10.3847/2041-8213/aa78f3. arXiv: 1702.08644 [astro-ph.HE].

Beniamini, Paz, Kenta Hotokezaka, et al. (July 2019). "Formation rates and evolution histories of magnetars". In: *MNRAS* 487.1, pp. 1426–1438. DOI: 10.1093/mnras/stz1391. arXiv: 1903.06718 [astro-ph.HE].

Beniamini, Paz, Zorawar Wadiasingh, and Brian D. Metzger (June 2020). "Periodicity in recurrent fast radio bursts and the origin of ultralong period magnetars". In: *MNRAS* 496.3, pp. 3390–3401. DOI: 10.1093/mnras/staa1783. arXiv: 2003.12509 [astro-ph.HE].

Benz, A. O., T. E. X. Bernold, and B. R. Dennis (Aug. 1983). "Radio blips and hard X-rays in solar flares". In: *ApJ* 271, pp. 355–366. DOI: 10.1086/161201.

Berger, Edo (Aug. 2014). "Short-Duration Gamma-Ray Bursts". In: *ARA&A* 52, pp. 43–105. DOI: 10.1146/annurev-astro-081913-035926. arXiv: 1311.2603 [astro-ph.HE].

Bhandari, S. et al. (Apr. 2018). "The SUrvey for Pulsars and Extragalactic Radio Bursts - II. New FRB discoveries and their follow-up". In: *MNRAS* 475.2, pp. 1427–1446. DOI: 10.1093/mnras/stx3074. arXiv: 1711.08110 [astro-ph.HE].

Bhandari, Shivani, Keith W. Bannister, et al. (Oct. 2020). "Limits on Precursor and Afterglow Radio Emission from a Fast Radio Burst in a Star-forming Galaxy". In: *ApJL* 901.2, L20, p. L20. DOI: 10.3847/2041-8213/abb462. arXiv: 2008.12488 [astro-ph.HE].

Bhandari, Shivani, Elaine M. Sadler, et al. (June 2020). "The Host Galaxies and Progenitors of Fast Radio Bursts Localized with the Australian Square Kilometre Array Pathfinder". In: *ApJL* 895.2, L37, p. L37. DOI: 10.3847/2041-8213/ab672e. arXiv: 2005.13160 [astro-ph.GA].

Bhardwaj, M. et al. (Mar. 2021). "A nearby repeating fast radio burst in the direction of M81". In: *arXiv e-prints*, arXiv:2103.01295, arXiv:2103.01295. arXiv: 2103.01295 [astro-ph.HE].

Blanchard, Peter K. et al. (July 2020). "The Pre-explosion Mass Distribution of Hydrogen-poor Superluminous Supernova Progenitors and New Evidence for a Mass-Spin Correlation". In: *ApJ* 897.2, 114, p. 114. DOI: 10.3847/1538-4357/ab9638. arXiv: 2002.09508 [astro-ph.HE].

Bochenek, C. D. et al. (Nov. 2020). "A fast radio burst associated with a Galactic magnetar". In: *Nature* 587.7832, pp. 59–62. DOI: 10.1038/s41586-020-2872-x. arXiv: 2005.10828 [astro-ph.HE].

Bochenek, Christopher D. et al. (Mar. 2020). "STARE2: Detecting Fast Radio Bursts in the Milky Way". In: *Publications of the Astronomical Society of the Pacific* 132.1009, 034202, p. 034202. DOI: 10.1088/1538-3873/ab63b3. arXiv: 2001.05077 [astro-ph.HE].

Burke-Spolaor, S. et al. (Jan. 2011). "Radio Bursts with Extragalactic Spectral Characteristics Show Terrestrial Origins". In: *ApJ* 727.1, 18, p. 18. DOI: 10.1088/0004-637X/727/1/18. arXiv: 1009.5392 [astro-ph.CO].

Caleb, M. et al. (Aug. 2020). "Simultaneous multi-telescope observations of FRB 121102". In: *MNRAS* 496.4, pp. 4565–4573. DOI: 10.1093/mnras/staa1791. arXiv: 2006.08662 [astro-ph.HE].

Champion, D. J. et al. (July 2016). "Five new fast radio bursts from the HTRU high-latitude survey at Parkes: first evidence for two-component bursts". In: *MNRAS* 460.1, pp. L30–L34. DOI: 10.1093/mnrasl/slw069. arXiv: 1511.07746 [astro-ph.HE].

Chatterjee, S. et al. (Jan. 2017). "A direct localization of a fast radio burst and its host". In: *Nature* 541.7635, pp. 58–61. DOI: 10.1038/nature20797. arXiv: 1701.01098 [astro-ph.HE].

Chen, Ge, Vikram Ravi, and Wenbin Lu (July 2020). "The Multiwavelength Counterparts of Fast Radio Bursts". In: *ApJ* 897.2, 146, p. 146. DOI: 10.3847/1538-4357/ab982b. arXiv: 2004.10787 [astro-ph.HE].

CHIME/FRB Collaboration, M. Amiri, et al. (Aug. 2018). "The CHIME Fast Radio Burst Project: System Overview". In: *ApJ* 863.1, 48, p. 48. DOI: 10.3847/1538-4357/aad188. arXiv: 1803.11235 [astro-ph.IM].

CHIME/FRB Collaboration, B. C. Andersen, et al. (Nov. 2020). "A bright millisecond-duration radio burst from a Galactic magnetar". In: *Nature* 587.7832, pp. 54–58. DOI: 10.1038/s41586-020-2863-y. arXiv: 2005.10324 [astro-ph.HE].

Chime/Frb Collaboration et al. (June 2020). "Periodic activity from a fast radio burst source". In: *Nature* 582.7812, pp. 351–355. DOI: 10.1038/s41586-020-2398-2. arXiv: 2001.10275 [astro-ph.HE].

Connor, Liam (Aug. 2019). "Interpreting the distributions of FRB observables". In: *MNRAS* 487.4, pp. 5753–5763. DOI: 10.1093/mnras/stz1666. arXiv: 1905.00755 [astro-ph.HE].

Cordes, J. M., N. D. R. Bhat, et al. (Sept. 2004). "The Brightest Pulses in the Universe: Multifrequency Observations of the Crab Pulsar's Giant Pulses". In: *ApJ* 612.1, pp. 375–388. DOI: 10.1086/422495. arXiv: astro-ph/0304495 [astro-ph].

Cordes, J. M. and T. J. W. Lazio (July 2002). "NE2001.I. A New Model for the Galactic Distribution of Free Electrons and its Fluctuations". In: *arXiv e-prints*, astro-ph/0207156, astro–ph/0207156. arXiv: astro-ph/0207156 [astro-ph].

Cordes, J. M., I. Wasserman, et al. (June 2017). "Lensing of Fast Radio Bursts by Plasma Structures in Host Galaxies". In: *ApJ* 842.1, 35, p. 35. DOI: 10.3847/1538-4357/aa74da. arXiv: 1703.06580 [astro-ph.HE].

Cordes, J. M., R. S. Wharton, et al. (May 2016). "Radio Wave Propagation and the Provenance of Fast Radio Bursts". In: *arXiv e-prints*, arXiv:1605.05890, arXiv:1605.05890. arXiv: 1605.05890 [astro-ph.HE].

Cordes, James M. and Shami Chatterjee (Aug. 2019). "Fast Radio Bursts: An Extragalactic Enigma". In: *Annual Reviews of Astronomy and Astrophysics* 57, pp. 417–465. DOI: 10.1146/annurev-astro-091918-104501. arXiv: 1906.05878 [astro-ph.HE].

Cruces, M. et al. (Jan. 2021). "Repeating behaviour of FRB 121102: periodicity, waiting times, and energy distribution". In: *MNRAS* 500.1, pp. 448–463. DOI: 10.1093/mnras/staa3223. arXiv: 2008.03461 [astro-ph.HE].

Davies, Ben et al. (Dec. 2009). "The Progenitor Mass of the Magnetar SGR1900+14". In: *ApJ* 707.1, pp. 844–851. DOI: 10.1088/0004-637X/707/1/844. arXiv: 0910.4859 [astro-ph.SR].

de Grijs, Richard (Aug. 2001). "Starbirth: Star formation timescales in M82". In: *Astronomy and Geophysics* 42.4, pp. 4.12–4.18. DOI: 10.1046/j.1468-4004.2001.0420044.12.x.

Deller, A. T. et al. (Mar. 2012). "The Proper Motion of PSR J1550-5418 Measured with VLBI: A Second Magnetar Velocity Measurement". In: *ApJL* 748.1, L1, p. L1. DOI: 10.1088/2041-8205/748/1/L1. arXiv: 1201.4684 [astro-ph.SR].

Ding, H. et al. (Aug. 2020). "A magnetar parallax". In: *MNRAS*. DOI: 10.1093/mnras/staa2531. arXiv: 2008.06438 [astro-ph.IM].

Duncan, Robert C. and Christopher Thompson (June 1992). "Formation of Very Strongly Magnetized Neutron Stars: Implications for Gamma-Ray Bursts". In: *ApJL* 392, p. L9. DOI: 10.1086/186413.

Esposito, P. et al. (June 2020). "A Very Young Radio-loud Magnetar". In: *ApJL* 896.2, L30, p. L30. DOI: 10.3847/2041-8213/ab9742. arXiv: 2004.04083 [astro-ph.HE].

Gajjar, V. et al. (Aug. 2018). "Highest Frequency Detection of FRB 121102 at 4-8 GHz Using the Breakthrough Listen Digital Backend at the Green Bank Telescope". In: *ApJ* 863, 2, p. 2. DOI: 10.3847/1538-4357/aad005. arXiv: 1804.04101 [astro-ph.HE].

Gardner, Jonathan P. and Shobita Satyapal (June 2000). "Counts and Sizes of Galaxies in the Hubble Deep Field South: Implications for the Next Generation Space Telescope". In: *AJ* 119.6, pp. 2589–2597. DOI: 10.1086/301368. arXiv: astro-ph/0003133 [astro-ph].

Gehrels, N. (Apr. 1986). "Confidence Limits for Small Numbers of Events in Astrophysical Data". In: *ApJ* 303, p. 336. DOI: 10.1086/164079.

Giacomazzo, Bruno and Rosalba Perna (July 2013). "Formation of Stable Magnetars from Binary Neutron Star Mergers". In: *ApJL* 771.2, L26, p. L26. DOI: 10.1088/2041-8205/771/2/L26. arXiv: 1306.1608 [astro-ph.HE].

Giacomazzo, Bruno, Jonathan Zrake, et al. (Aug. 2015). "Producing Magnetar Magnetic Fields in the Merger of Binary Neutron Stars". In: *ApJ* 809.1, 39, p. 39. DOI: 10.1088/0004-637X/809/1/39. arXiv: 1410.0013 [astro-ph.HE].

Gourdji, K. et al. (Mar. 2019). "A sample of low energy bursts from FRB 121102". In: *arXiv e-prints*, arXiv:1903.02249, arXiv:1903.02249. arXiv: 1903.02249 [astro-ph.HE].

Guillochon, James et al. (Jan. 2017). "An Open Catalog for Supernova Data". In: *ApJ* 835.1, 64, p. 64. DOI: 10.3847/1538-4357/835/1/64. arXiv: 1605.01054 [astro-ph.SR].

Hallinan, Gregg et al. (Sept. 2019). "The DSA-2000 — A Radio Survey Camera". In: *Bulletin of the American Astronomical Society*. Vol. 51, p. 255. arXiv: 1907.07648 [astro-ph.IM].

Heintz, Kasper E. et al. (Sept. 2020). "Host Galaxy Properties and Offset Distributions of Fast Radio Bursts: Implications for their Progenitors". In: *arXiv e-prints*, arXiv:2009.10747, arXiv:2009.10747. arXiv: 2009.10747 [astro-ph.GA].

Hessels, J. W. T. et al. (May 2019). "FRB 121102 Bursts Show Complex Time-Frequency Structure". In: *ApJL* 876.2, L23, p. L23. DOI: 10.3847/2041-8213/ab13ae. arXiv: 1811.10748 [astro-ph.HE].

Holoien, T. W. -S. et al. (Apr. 2019). "The ASAS-SN bright supernova catalogue - IV. 2017". In: *MNRAS* 484.2, pp. 1899–1911. DOI: 10.1093/mnras/stz073. arXiv: 1811.08904 [astro-ph.HE].

Jarrett, T. H. et al. (Dec. 2019). "The WISE Extended Source Catalog (WXSC). I. The 100 Largest Galaxies". In: *The Astrophysical Journal Supplement Series* 245.2, 25, p. 25. DOI: 10.3847/1538-4365/ab521a. arXiv: 1910.11793 [astro-ph.GA].

Jessner, A. et al. (Dec. 2010). "Giant pulses with nanosecond time resolution detected from the Crab pulsar at 8.5 and 15.1 GHz". In: 524, A60, A60. DOI: 10.1051/0004-6361/201014806. arXiv: 1008.3992 [astro-ph.HE].

Johnston, S. et al. (Dec. 2008). "Science with ASKAP. The Australian square-kilometre-array pathfinder". In: *Experimental Astronomy* 22.3, pp. 151–273. DOI: 10.1007/s10686-008-9124-7. arXiv: 0810.5187 [astro-ph].

Karachentsev, I. D. and K. N. Telikova (Aug. 2018a). "Stellar and dark matter density in the Local Universe". In: *Astronomische Nachrichten* 339.615, pp. 615–622. DOI: 10.1002/asna.201813520. arXiv: 1810.06326 [astro-ph.GA].

– (Aug. 2018b). "Stellar and dark matter density in the Local Universe". In: *Astronomische Nachrichten* 339.615, pp. 615–622. DOI: 10.1002/asna.201813520. arXiv: 1810.06326 [astro-ph.GA].

Kasen, Daniel and Lars Bildsten (July 2010). "Supernova Light Curves Powered by Young Magnetars". In: *ApJ* 717.1, pp. 245–249. DOI: 10.1088/0004-637X/717/1/245. arXiv: 0911.0680 [astro-ph.HE].

Kaspi, Victoria M. and Andrei M. Beloborodov (Aug. 2017). "Magnetars". In: *Annual Reviews of Astronomy and Astrophysics* 55.1, pp. 261–301. DOI: 10.1146/annurev-astro-081915-023329. arXiv: 1703.00068 [astro-ph.HE].

Katz, C. A. et al. (June 2003). "A Survey for Transient Astronomical Radio Emission at 611 MHz". In: *Publications of the Astronomical Society of the Pacific* 115, pp. 675–687. DOI: 10.1086/375568. arXiv: astro-ph/0304260 [astro-ph].

Keane, E. F. (Oct. 2018). "The future of fast radio burst science". In: *Nature Astronomy* 2, pp. 865–872. DOI: 10.1038/s41550-018-0603-0. arXiv: 1811.00899 [astro-ph.HE].

Keane, E. F. and M. Kramer (Dec. 2008). "On the birthrates of Galactic neutron stars". In: *MNRAS* 391.4, pp. 2009–2016. DOI: 10.1111/j.1365-2966.2008.14045.x. arXiv: 0810.1512 [astro-ph].

Kennicutt Jr., R. C. et al. (Oct. 2008). "An Hα Imaging Survey of Galaxies in the Local 11 Mpc Volume". In: *The Astrophysical Journal Supplement Series* 178, pp. 247–279. DOI: 10.1086/590058. arXiv: 0807.2035.

Kirsten, F. et al. (Nov. 2020). "Detection of two bright radio bursts from magnetar SGR 1935 + 2154". In: *Nature Astronomy*. DOI: 10.1038/s41550-020-01246-3. arXiv: 2007.05101 [astro-ph.HE].

Kocz, J. et al. (Aug. 2019). "DSA-10: A Prototype Array for Localizing Fast Radio Bursts". In: *MNRAS*, p. 2146. DOI: 10.1093/mnras/stz2219. arXiv: 1906.08699 [astro-ph.IM].

Kothes, R. et al. (Jan. 2018). "A Radio Continuum and Polarization Study of SNR G57.2+0.8 Associated with Magnetar SGR 1935+2154". In: *ApJ* 852.1, 54, p. 54. DOI: 10.3847/1538-4357/aa9e89. arXiv: 1711.11146 [astro-ph.HE].

Kozlova, A. V. et al. (Aug. 2016). "The first observation of an intermediate flare from SGR 1935+2154". In: *MNRAS* 460.2, pp. 2008–2014. DOI: 10.1093/mnras/stw1109. arXiv: 1605.02993 [astro-ph.HE].

Kulkarni, S. R. (Oct. 2018). "From gamma-ray bursts to fast radio bursts". In: *Nature Astronomy* 2, pp. 832–835. DOI: 10.1038/s41550-018-0621-y. arXiv: 1811.00448 [astro-ph.HE].

Kumar, Pravir et al. (Sept. 2020). "Extremely band-limited repetition from a fast radio burst source". In: *arXiv e-prints*, arXiv:2009.01214, arXiv:2009.01214. arXiv: 2009.01214 [astro-ph.HE].

Kuzmin, A. D. (Apr. 2007). "Giant pulses of pulsar radio emission". In: *The Astrophysical Journal Supplement Series* 308.1-4, pp. 563–567. DOI: 10.1007/s10509-007-9347-5. arXiv: astro-ph/0701193 [astro-ph].

Law, C. J. et al. (Nov. 2017). "A Multi-telescope Campaign on FRB 121102: Implications for the FRB Population". In: *ApJ* 850, 76, p. 76. DOI: 10.3847/1538-4357/aa9700. arXiv: 1705.07553 [astro-ph.HE].

Levesque, Emily M. et al. (Nov. 2010). "The Host Galaxies of Gamma-ray Bursts. II. A Mass-metallicity Relation for Long-duration Gamma-ray Burst Host Galaxies". In: *AJ* 140.5, pp. 1557–1566. DOI: 10.1088/0004-6256/140/5/1557. arXiv: 1006.3560 [astro-ph.GA].

Levin, L. (June 2012). "A search for radio pulsars: from millisecond pulsars to magnetars". PhD thesis. Swinburne University of Technology.

Levin, Yuri, Andrei M. Beloborodov, and Ashley Bransgrove (June 2020). "Precessing Flaring Magnetar as a Source of Repeating FRB 180916.J0158+65". In: *ApJL* 895.2, L30, p. L30. DOI: 10.3847/2041-8213/ab8c4c. arXiv: 2002.04595 [astro-ph.HE].

Li, Ye and Bing Zhang (Aug. 2020). "A Comparative Study of Host Galaxy Properties between Fast Radio Bursts and Stellar Transients". In: *ApJL* 899.1, L6, p. L6. DOI: 10.3847/2041-8213/aba907. arXiv: 2005.02371 [astro-ph.HE].

Licquia, Timothy C. and Jeffrey A. Newman (June 2015). "Improved Estimates of the Milky Way's Stellar Mass and Star Formation Rate from Hierarchical Bayesian Meta-Analysis". In: *ApJ* 806.1, 96, p. 96. DOI: 10.1088/0004-637X/806/1/96. arXiv: 1407.1078 [astro-ph.GA].

Lorimer, D. R. et al. (Nov. 2007). "A Bright Millisecond Radio Burst of Extragalactic Origin". In: *Science* 318, p. 777. DOI: 10.1126/science.1147532. arXiv: 0709.4301 [astro-ph].

Lu, Wenbin and Pawan Kumar (June 2018). "On the radiation mechanism of repeating fast radio bursts". In: *MNRAS* 477.2, pp. 2470–2493. DOI: 10.1093/mnras/sty716. arXiv: 1710.10270 [astro-ph.HE].

Lu, Wenbin, Pawan Kumar, and Bing Zhang (Aug. 2020). "A unified picture of Galactic and cosmological fast radio bursts". In: *MNRAS* 498.1, pp. 1397–1405. DOI: 10.1093/mnras/staa2450. arXiv: 2005.06736 [astro-ph.HE].

Lu, Wenbin and Anthony L. Piro (Sept. 2019). "Implications from ASKAP Fast Radio Burst Statistics". In: *ApJ* 883.1, 40, p. 40. DOI: 10.3847/1538-4357/ab3796. arXiv: 1903.00014 [astro-ph.HE].

Lunnan, R. et al. (May 2015). "Zooming In on the Progenitors of Superluminous Supernovae With the HST". In: *ApJ* 804.2, 90, p. 90. DOI: 10.1088/0004-637X/804/2/90. arXiv: 1411.1060 [astro-ph.HE].

Luo, Rui et al. (Dec. 2018). "On the normalized FRB luminosity function". In: *MNRAS* 481, pp. 2320–2337. DOI: 10.1093/mnras/sty2364. arXiv: 1808.09929 [astro-ph.HE].

Lyubarsky, Yu. (July 2014). "A model for fast extragalactic radio bursts." In: *MNRAS* 442, pp. L9–L13. DOI: 10.1093/mnrasl/slu046. arXiv: 1401.6674 [astro-ph.HE].

Lyubarsky, Yuri (July 2020). "Fast Radio Bursts from Reconnection in a Magnetar Magnetosphere". In: *ApJ* 897.1, 1, p. 1. DOI: 10.3847/1538-4357/ab97b5. arXiv: 2001.02007 [astro-ph.HE].

Lyutikov, Maxim (Feb. 2015). "Magnetar activity mediated by plastic deformations of neutron star crust". In: *MNRAS* 447.2, pp. 1407–1417. DOI: 10.1093/mnras/stu2413. arXiv: 1407.5881 [astro-ph.HE].

Lyutikov, Maxim, Maxim V. Barkov, and Dimitrios Giannios (Apr. 2020). "FRB Periodicity: Mild Pulsars in Tight O/B-star Binaries". In: *ApJL* 893.2, L39, p. L39. DOI: 10.3847/2041-8213/ab87a4. arXiv: 2002.01920 [astro-ph.HE].

Macquart, J. P., E. Keane, et al. (Apr. 2015). "Fast Transients at Cosmological Distances with the SKA". In: *Advancing Astrophysics with the Square Kilometre Array (AASKA14)*, p. 55. arXiv: 1501.07535 [astro-ph.HE].

Macquart, J. P., J. X. Prochaska, et al. (May 2020). "A census of baryons in the Universe from localized fast radio bursts". In: *Nature* 581.7809, pp. 391–395. DOI: 10.1038/s41586-020-2300-2. arXiv: 2005.13161 [astro-ph.CO].

Macquart, Jean-Pierre et al. (June 2010). "The Commensal Real-Time ASKAP Fast-Transients (CRAFT) Survey". In: *PASA* 27.3, pp. 272–282. DOI: 10.1071/AS09082. arXiv: 1001.2958 [astro-ph.HE].

Majid, Walid A. et al. (July 2020). "A Dual-band Radio Observation of FRB 121102 with the Deep Space Network and the Detection of Multiple Bursts". In: *ApJL* 897.1, L4, p. L4. DOI: 10.3847/2041-8213/ab9a4a. arXiv: 2004.06845 [astro-ph.HE].

Manchester, R. and J. Taylor (1980). *Pulsars.*

Marcote, B., K. Nimmo, et al. (Jan. 2020). "A repeating fast radio burst source localized to a nearby spiral galaxy". In: *Nature* 577.7789, pp. 190–194. DOI: 10.1038/s41586-019-1866-z. arXiv: 2001.02222 [astro-ph.HE].

Marcote, B., Z. Paragi, et al. (Jan. 2017). "The Repeating Fast Radio Burst FRB 121102 as Seen on Milliarcsecond Angular Scales". In: *ApJ* 834.2, L8, p. L8. DOI: 10.3847/2041-8213/834/2/L8. arXiv: 1701.01099 [astro-ph.HE].

Margalit, Ben, Paz Beniamini, et al. (Aug. 2020). "Implications of a Fast Radio Burst from a Galactic Magnetar". In: *ApJL* 899.2, L27, p. L27. DOI: 10.3847/2041-8213/abac57. arXiv: 2005.05283 [astro-ph.HE].

Margalit, Ben, Edo Berger, and Brian D. Metzger (Dec. 2019). "Fast Radio Bursts from Magnetars Born in Binary Neutron Star Mergers and Accretion Induced Collapse". In: *ApJ* 886.2, 110, p. 110. DOI: 10.3847/1538-4357/ab4c31. arXiv: 1907.00016 [astro-ph.HE].

Meléndez, J. L. et al. (June 1999). "Statistical analysis of high-frequency decimetric type III bursts". In: *Solar Physics* 187, pp. 77–88. DOI: 10.1023/A:1005110111620.

Mereghetti, S. et al. (Aug. 2020). "INTEGRAL Discovery of a Burst with Associated Radio Emission from the Magnetar SGR 1935+2154". In: *ApJL* 898.2, L29, p. L29. DOI: 10.3847/2041-8213/aba2cf. arXiv: 2005.06335 [astro-ph.HE].

Metzger, Brian D., Ben Margalit, and Lorenzo Sironi (May 2019). "Fast radio bursts as synchrotron maser emission from decelerating relativistic blast waves". In: *MNRAS* 485.3, pp. 4091–4106. DOI: 10.1093/mnras/stz700. arXiv: 1902.01866 [astro-ph.HE].

Michilli, D. et al. (Jan. 2018). "An extreme magneto-ionic environment associated with the fast radio burst source FRB 121102". In: *Nature* 553.7687, pp. 182–185. DOI: 10.1038/nature25149. arXiv: 1801.03965 [astro-ph.HE].

Moustakas, John et al. (Apr. 2013). "PRIMUS: Constraints on Star Formation Quenching and Galaxy Merging, and the Evolution of the Stellar Mass Function from z = 0-1". In: *ApJ* 767.1, 50, p. 50. DOI: 10.1088/0004-637X/767/1/50. arXiv: 1301.1688 [astro-ph.CO].

Muno, Michael P. et al. (Jan. 2006). "A Neutron Star with a Massive Progenitor in Westerlund 1". In: *ApJL* 636.1, pp. L41–L44. DOI: 10.1086/499776. arXiv: astro-ph/0509408 [astro-ph].

Nimmo, K. et al. (Mar. 2021). "Highly polarized microstructure from the repeating FRB 20180916B". In: *Nature Astronomy*. DOI: 10.1038/s41550-021-01321-3. arXiv: 2010.05800 [astro-ph.HE].

Olausen, S. A. and V. M. Kaspi (May 2014). "The McGill Magnetar Catalog". In: *ApJs* 212.1, 6, p. 6. DOI: 10.1088/0067-0049/212/1/6. arXiv: 1309.4167 [astro-ph.HE].

Pearlman, Aaron B. et al. (Dec. 2020). "Multiwavelength Radio Observations of Two Repeating Fast Radio Burst Sources: FRB 121102 and FRB 180916.J0158+65". In: *ApJL* 905.2, L27, p. L27. DOI: 10.3847/2041-8213/abca31. arXiv: 2009.13559 [astro-ph.HE].

Perley, D. A. et al. (Oct. 2016). "Host-galaxy Properties of 32 Low-redshift Superluminous Supernovae from the Palomar Transient Factory". In: *ApJ* 830.1, 13, p. 13. DOI: 10.3847/0004-637X/830/1/13. arXiv: 1604.08207 [astro-ph.HE].

Petroff, E., E. D. Barr, et al. (Sept. 2016). "FRBCAT: The Fast Radio Burst Catalogue". In: *PASA* 33, e045, e045. DOI: 10.1017/pasa.2016.35. arXiv: 1601.03547 [astro-ph.HE].

Petroff, E., J. W. T. Hessels, and D. R. Lorimer (May 2019). "Fast radio bursts". In: *Astronomy and Astrophysics Reviews* 27.1, 4, p. 4. DOI: 10.1007/s00159-019-0116-6. arXiv: 1904.07947 [astro-ph.HE].

Petroff, E., E. F. Keane, et al. (Aug. 2015). "Identifying the source of perytons at the Parkes radio telescope". In: *MNRAS* 451, pp. 3933–3940. DOI: 10.1093/mnras/stv1242. arXiv: 1504.02165 [astro-ph.IM].

Pietka, M., R. P. Fender, and E. F. Keane (Feb. 2015). "The variability time-scales and brightness temperatures of radio flares from stars to supermassive black holes". In: *MNRAS* 446, pp. 3687–3696. DOI: 10.1093/mnras/stu2335. arXiv: 1411.1067 [astro-ph.HE].

Platts, E. et al. (Aug. 2019). "A living theory catalogue for fast radio bursts". In: *Phys. Rep.* 821, pp. 1–27. DOI: 10.1016/j.physrep.2019.06.003. arXiv: 1810.05836 [astro-ph.HE].

Pleunis, Z. et al. (Dec. 2020). "LOFAR Detection of 110-188 MHz Emission and Frequency-Dependent Activity from FRB 20180916B". In: *arXiv e-prints*, arXiv:2012.08372, arXiv:2012.08372. arXiv: 2012.08372 [astro-ph.HE].

Prochaska, J. Xavier et al. (Sept. 2019). "The low density and magnetization of a massive galaxy halo exposed by a fast radio burst". In: *arXiv e-prints*, arXiv:1909.11681, arXiv:1909.11681. arXiv: 1909.11681 [astro-ph.GA].

Puxley, P. J. et al. (Oct. 1989). "Detection of H53 alpha Emission from M82: A Reliable Measure of the Ionization Rate and Its Implications". In: *ApJ* 345, p. 163. DOI: 10.1086/167891.

Quimby, Robert M. et al. (May 2013). "Rates of superluminous supernovae at z $\sim$ 0.2". In: *MNRAS* 431.1, pp. 912–922. DOI: 10.1093/mnras/stt213. arXiv: 1302.0911 [astro-ph.CO].

Rajwade, K. M. et al. (July 2020). "Possible periodic activity in the repeating FRB 121102". In: *MNRAS* 495.4, pp. 3551–3558. DOI: 10.1093/mnras/staa1237. arXiv: 2003.03596 [astro-ph.HE].

Ravi, V. et al. (July 2019). "A fast radio burst localized to a massive galaxy". In: *Nature* 572.7769, pp. 352–354. DOI: 10.1038/s41586-019-1389-7.

Ravi, Vikram (Jan. 2019a). "The observed properties of fast radio bursts". In: *MNRAS* 482.2, pp. 1966–1978. DOI: 10.1093/mnras/sty1551. arXiv: 1710.08026 [astro-ph.HE].

– (July 2019b). "The prevalence of repeating fast radio bursts". In: *arXiv e-prints*, arXiv:1907.06619, arXiv:1907.06619. arXiv: 1907.06619 [astro-ph.HE].

Ridnaia, A. et al. (May 2020). "A peculiar hard X-ray counterpart of a Galactic fast radio burst". In: *arXiv e-prints*, arXiv:2005.11178, arXiv:2005.11178. arXiv: 2005.11178 [astro-ph.HE].

Ruiter, A. J. et al. (Mar. 2019). "On the formation of neutron stars via accretion-induced collapse in binaries". In: *MNRAS* 484.1, pp. 698–711. DOI: 10.1093/mnras/stz001. arXiv: 1802.02437 [astro-ph.SR].

Safarzadeh, Mohammadtaher et al. (Sept. 2020). "Confronting the Magnetar Interpretation of Fast Radio Bursts Through Their Host Galaxy Demographics". In: *arXiv e-prints*, arXiv:2009.11735, arXiv:2009.11735. arXiv: 2009.11735 [astro-ph.HE].

Saint-Hilaire, P., A. O. Benz, and C. Monstein (Nov. 2014). "Short-duration Radio Bursts with Apparent Extragalactic Dispersion". In: *ApJ* 795, 19, p. 19. DOI: 10.1088/0004-637X/795/1/19. arXiv: 1402.0664 [astro-ph.HE].

Salim, Samir, Janice C. Lee, et al. (Nov. 2016). "GALEX-SDSS-WISE Legacy Catalog (GSWLC): Star Formation Rates, Stellar Masses, and Dust Attenuations of 700,000 Low-redshift Galaxies". In: *ApJs* 227.1, 2, p. 2. DOI: 10.3847/0067-0049/227/1/2. arXiv: 1610.00712 [astro-ph.GA].

Salim, Samir, R. Michael Rich, et al. (Dec. 2007). "UV Star Formation Rates in the Local Universe". In: *The Astrophysical Journal Supplement Series* 173, pp. 267–292. DOI: 10.1086/519218. arXiv: 0704.3611 [astro-ph].

Schneider, Fabian R. N. et al. (Oct. 2019). "Stellar mergers as the origin of magnetic massive stars". In: *Nature* 574.7777, pp. 211–214. DOI: 10.1038/s41586-019-1621-5. arXiv: 1910.14058 [astro-ph.SR].

Scholz, F. W. and M. A. Stephens (1987). "K-Sample Anderson-Darling Tests". In: *JASA* 82, pp. 918–924.

Scholz, P., S. Bogdanov, et al. (Sept. 2017). "Simultaneous X-Ray, Gamma-Ray, and Radio Observations of the Repeating Fast Radio Burst FRB 121102". In: *ApJ* 846.1, 80, p. 80. DOI: 10.3847/1538-4357/aa8456. arXiv: 1705.07824 [astro-ph.HE].

Scholz, P., A. Cook, et al. (Oct. 2020). "Simultaneous X-Ray and Radio Observations of the Repeating Fast Radio Burst FRB ∼ 180916.J0158+65". In: *ApJ* 901.2, 165, p. 165. DOI: 10.3847/1538-4357/abb1a8. arXiv: 2004.06082 [astro-ph.HE].

Scholz, Paul and Chime/Frb Collaboration (Apr. 2020). "A bright millisecond-timescale radio burst from the direction of the Galactic magnetar SGR 1935+2154". In: *The Astronomer's Telegram* 13681, p. 1.

Scott, D. W. (1992). *Multivariate Density Estimation: Theory, Practice, and Visualization*. New York, Chicester: John Wiley & Sons.

Sokolowski, M. et al. (Nov. 2018). "No Low-frequency Emission from Extremely Bright Fast Radio Bursts". In: *ApJL* 867.1, L12, p. L12. DOI: 10.3847/2041-8213/aae58d. arXiv: 1810.04355 [astro-ph.HE].

Speagle, J. S. et al. (Oct. 2014). "A Highly Consistent Framework for the Evolution of the Star-Forming "Main Sequence" from z ∼0-6". In: *ApJs* 214.2, 15, p. 15. DOI: 10.1088/0067-0049/214/2/15. arXiv: 1405.2041 [astro-ph.GA].

Spitler, L. G. et al. (Mar. 2016). "A repeating fast radio burst". In: *Nature* 531.7593, pp. 202–205. DOI: 10.1038/nature17168. arXiv: 1603.00581 [astro-ph.HE].

Taggart, Kirsty and Daniel Perley (Nov. 2019). "Core-collapse, superluminous, and gamma-ray burst supernova host galaxy populations at low redshift: the importance of dwarf and starbursting galaxies". In: *arXiv e-prints*, arXiv:1911.09112, arXiv:1911.09112. arXiv: 1911.09112 [astro-ph.HE].

Tendulkar, S. P. et al. (Jan. 2017). "The Host Galaxy and Redshift of the Repeating Fast Radio Burst FRB 121102". In: *ApJ* 834.2, L7, p. L7. DOI: 10.3847/2041-8213/834/2/L7. arXiv: 1701.01100 [astro-ph.HE].

Tendulkar, Shriharsh Prakash (Jan. 2014). "Beyond the Blur: Construction and Characterization of the First Autonomous AO System, and, An AO Survey of Magnetar Proper Motions". PhD thesis. California Institute of Technology.

The CHIME/FRB Collaboration et al. (May 2020). "A bright millisecond-duration radio burst from a Galactic magnetar". In: *arXiv e-prints*, arXiv:2005.10324, arXiv:2005.10324. arXiv: 2005.10324 [astro-ph.HE].

Thornton, D. et al. (July 2013). "A Population of Fast Radio Bursts at Cosmological Distances". In: *Science* 341.6141, pp. 53–56. DOI: 10.1126/science.1236789. arXiv: 1307.1628 [astro-ph.HE].

Villadsen, Jackie and Gregg Hallinan (Feb. 2019). "Ultra-wideband Detection of 22 Coherent Radio Bursts on M Dwarfs". In: *ApJ* 871.2, 214, p. 214. DOI: 10.3847/1538-4357/aaf88e. arXiv: 1810.00855 [astro-ph.SR].

Wadiasingh, Zorawar and Andrey Timokhin (July 2019). "Repeating Fast Radio Bursts from Magnetars with Low Magnetospheric Twist". In: *ApJ* 879.1, 4, p. 4. DOI: 10.3847/1538-4357/ab2240. arXiv: 1904.12036 [astro-ph.HE].

Woosley, S. E. (Aug. 2010). "Bright Supernovae from Magnetar Birth". In: *ApJL* 719.2, pp. L204–L207. DOI: 10.1088/2041-8205/719/2/L204. arXiv: 0911.0698 [astro-ph.HE].

Yao, J. M., R. N. Manchester, and N. Wang (Jan. 2017). "A New Electron-density Model for Estimation of Pulsar and FRB Distances". In: *ApJ* 835.1, 29, p. 29. DOI: 10.3847/1538-4357/835/1/29. arXiv: 1610.09448 [astro-ph.GA].

Zhang, C. F. et al. (May 2020). "A highly polarised radio burst detected from SGR 1935+2154 by FAST". In: *The Astronomer's Telegram* 13699, p. 1.

Zhou, Ping, Jacco Vink, et al. (Sept. 2019). "Spatially resolved X-ray study of supernova remnants that host magnetars: Implication of their fossil field origin". In: *A&A* 629, A51, A51. DOI: 10.1051/0004-6361/201936002. arXiv: 1909.01922 [astro-ph.HE].

Zhou, Ping, Xin Zhou, et al. (Dec. 2020). "Revisiting the Distance, Environment, and Supernova Properties of SNR G57.2+0.8 that Hosts SGR 1935+2154". In: *ApJ* 905.2, 99, p. 99. DOI: 10.3847/1538-4357/abc34a. arXiv: 2005.03517 [astro-ph.HE].